



Delft University of Technology

## Slightly-destructive tests on cores: method validation and correlations

Jafari, Samira; Licciardello, Lucia; Esposito, Rita

**Publication date**  
2017

**Document Version**  
Final published version

**Citation (APA)**  
Jafari, S., Licciardello, L., & Esposito, R. (2017). *Slightly-destructive tests on cores: method validation and correlations*. Delft University of Technology.

**Important note**  
To cite this publication, please use the final published version (if applicable).  
Please check the document version above.

**Copyright**  
Other than for strictly personal use, it is not permitted to download, forward or distribute the text or part of it, without the consent of the author(s) and/or copyright holder(s), unless the work is under an open content license such as Creative Commons.

**Takedown policy**  
Please contact us and provide details if you believe this document breaches copyrights.  
We will remove access to the work immediately and investigate your claim.

*This work is downloaded from Delft University of Technology.  
For technical reasons the number of authors shown on this cover page is limited to a maximum of 10.*

<i>Project number</i>	C31B67
<i>File reference</i>	C31B67WP1-13
<i>Date</i>	December 25, 2017
<i>Corresponding author</i>	Samira Jafari ( <a href="mailto:s.jafari@tudelft.nl">s.jafari@tudelft.nl</a> )

*TU Delft Large-Scale Testing Campaign 2016*

## **SLIGHTLY-DESTRUCTIVE TESTS ON CORES: METHOD VALIDATION AND CORRELATIONS**

*Authors: Samira Jafari, Lucia Licciardello, Rita Esposito*

*Lab collaborator: Elena Casprini*

**Cite as:** Jafari, S., Licciardello, L., Esposito, R. *Slightly-destructive tests on cores: method validation and correlations. Report No. C31B67WP1-13, 25 December 2017. Delft University of Technology.*

**This document is made available via the website 'Structural Response to Earthquakes' and the TU Delft repository. While citing, please verify if there are recent updates of this research in the form of scientific papers.**

All rights reserved. No part of this publication may be reproduced, stored in a retrieval system of any nature, or transmitted, in any form or by any means, electronic, mechanical, photocopying, recording or otherwise, without the prior written permission of TU Delft.

TU Delft and those who have contributed to this publication did exercise the greatest care in putting together this publication. This report will be available as-is, and TU Delft makes no representations of warranties of any kind concerning this Report. This includes, without limitation, fitness for a particular purpose, non-infringement, absence of latent or other defects, accuracy, or the presence or absence of errors, whether or not discoverable. Except to the extent required by applicable law, in no event will TU Delft be liable for on any legal theory for any special, incidental consequential, punitive or exemplary damages arising out of the use of this report.

This research work was funded by NAM Structural Upgrading stream

## Table of Contents

1	Introduction.....	3
2	Nomenclature .....	5
2.1	Symbols.....	5
2.2	Abbreviations.....	6
3	Construction of the samples .....	7
4	Compression strength of masonry unit .....	8
4.1	Testing procedure.....	8
4.2	Experimental results.....	8
5	Flexural and compressive strength of mortar.....	10
5.1	Testing procedure.....	10
5.2	Experimental results.....	10
6	Compression strength of masonry.....	14
6.1	Testing procedure.....	14
6.2	Experimental results.....	16
7	Bond strength of masonry .....	22
7.1	Testing procedure.....	22
7.2	Experimental results.....	22
8	Shear strength of masonry .....	26
8.1	Testing procedure.....	26
8.2	Experimental results.....	27
9	Summary and properties overview .....	32
	References .....	34
	Appendix A.....	35

# 1 Introduction

To characterise the mechanical properties of existing masonry, non/slightly destructive tests (NDT/SDT) can be performed in-situ or masonry samples can be collected to perform destructive tests (DT) in the laboratory. The in-situ tests aim to provide a quick-identification method for existing masonry, while laboratory tests are conducted to have a complete overview of the material behaviour (e.g. stress-strain relationships).

In order to provide reliable data, the pre-qualification of the companies to perform in-situ testing activities is of importance. Consequently a project, developed within the work package WP1a of the NAM Structural Upgrading project, has been set in cooperation with ARUP and EUCentre. The main aim of this work package is to qualify the companies. Additionally, the study of the correlation between DT and NDT/SDT results is investigated. NDT/SDT were performed by firms in the controlled laboratory environment on the calcium silicate brick masonry walls, built at TU Delft laboratory. Companion DT were performed by TU Delft. An overview of the material properties which can be achieved with the DT methods (in the scope of this project) is provided in Table 1. These obtained properties will be used to further investigate the correlation between NDT and SDT. Table 2 shows the correlation between the results obtained by NDT/SDT and DT methods.

All the tests were performed on replicated calcium silicate brick masonry. This masonry type was previously used in the large-scale testing campaign 2015, in which a complete material characterisation was made [1]. During the previous campaign two different construction phases took place:

- The first phase of construction took place in April and May 2015, with the aim of characterising the material properties as well as studying the behaviour of large-scale walls subject to quasi-static cyclic in-plane and out-of-plane tests.
- The second phase of construction took place in September 2015, with the aim of studying the behaviour of full-scale assemblage subject to quasi-static cyclic pushover test. As a result, companion samples for the compression and bond wrench tests were constructed.

In this report the results of the destructive material tests performed as companion material tests for the NDT/SDT are reported. These results are compared with the ones obtained in the large-scale testing campaign 2015 [1]. If comparison with previous test result is made, the results obtained in this project are named as third construction phase.

Table 1 – Destructive material tests for the characterisation of masonry.

Type of test			Material property
Masonry	Compression	Vertical	Compressive strength Young's modulus Fracture energy in compression Poisson ratio Stress-strain relationship in compression (pre- and post-peak)
	Shear test	Standard triplets	Initial and residual shear strength Initial and residual shear friction coefficient
		Modified triplets with head joints	Mode-II fracture energy Shear stress vs. shear displacement relationship (pre- and post-peak)
	Bond wrench		Flexural bond strength
Masonry unit	Compression	Single unit	Compressive strength of brick Stress-strain relationship in compression
Mortar	Mortar bar	Compression	Compressive strength of masonry mortar
		Bending	Flexural strength of masonry mortar



Table 2 – Correlation between the results of NDT/SDT and DT.

Type of test			Laboratory destructive test			
			Tests on brick	Tests on mortar	Compression test on masonry	Shear test on triplets
In-situ test	Non-destructive	Rebound hammer				
		Penetrometric				
		Ultrasonic				
	Slightly destructive	Single flat jack				
		Double flat jack				
		Shove test				

## 2 Nomenclature

### 2.1 Symbols

This report adopts mainly the nomenclature used in Eurocode 6 [2]. In addition, symbols used in the codes for testing are adopted.

$\alpha$	Masonry (bed joint) angle of internal friction
$\alpha_{res}$	Masonry (bed joint) residual angle of internal friction
$\nu$	Poisson ratio of masonry
$\mu$	Masonry (bed joint) coefficient of friction
$\mu_{res}$	Masonry (bed joint) residual coefficient of friction
$d_1$	Distance between bearing supports
$f_b$	Normalised compressive strength of masonry unit
$f_b^*$	Compressive strength of masonry unit
$f_m$	Compressive strength of masonry mortar
$f_{mt}$	Flexural strength of masonry mortar
$f_m'$	Compressive strength of masonry in the direction perpendicular to the bed joints
$f_p$	Applied lateral pre-compression stress
$f_{v0}$	Masonry (bed joint) initial shear strength for standard triplet
$f_{v0}^*$	Masonry (bed joint) initial shear strength for modified triplet
$f_{v0,res}$	Masonry (bed joint) residual shear strength for standard triplet
$f_{v0,res}^*$	Masonry (bed joint) residual shear strength for modified triplet
$f_w$	Masonry uniaxial bond strength between the masonry unit and the mortar
$l_j$	Length of the mortar bed joint in a masonry specimens
$l_m$	Length of the mortar specimen
$l_s$	Length of the masonry specimen as built
$l_p$	Length of the loading plate for compression tests on mortar specimens
$l_u$	Length of the masonry unit as used in the construction of masonry
$h_m$	Height of the mortar specimen
$h_s$	Height of the masonry specimen as built
$h_u$	Height of the masonry unit as used in the construction
$t_s$	Thickness of the masonry specimen as built
$t_m$	Thickness of the mortar specimen
$t_u$	Thickness of the masonry unit as used in the construction of masonry
$A_s$	Cross sectional area of the specimen parallel to the bed joints (shear test)
$E_{sb}$	Elastic modulus of masonry unit calculated from compression tests on the stacked bricks
$E_1$	Secant elastic modulus of masonry subject to a compressive loading perpendicular to the bed

	joints, evaluated at 1/3 of the maximum stress
$E_2$	Secant elastic modulus of masonry subject to a compressive loading perpendicular to the bed joints, evaluated at 1/10 of the maximum stress
$E_3$	Chord elastic modulus of masonry subject to a compressive loading perpendicular to the bed joints, evaluated at between 1/10 and 1/3 of the maximum stress
$E_{c1}$	Cyclic stiffness evaluated in the cycle corresponding to a stress level equal to 0.07 of the expected maximum strength.
$E_{c2}$	Cyclic stiffness evaluated in the cycle corresponding to a stress level equal to 0.1 of the expected maximum strength.
$E_{c3}$	Cyclic stiffness evaluated in the cycle corresponding to a stress level equal to 0.25 of the expected maximum strength.
$F_1$	Applied vertical load (bond-wrench test)
$F_2$	Vertical load due to the weight of the top clamping system (bond-wrench test)
$F_3$	Vertical load due to the top masonry unit (bond-wrench test)
$F_{\max}$	Maximum vertical load
$G_{f-c}$	Fracture energy in compression for loading perpendicular to the bed joints
$G_{fII}$	Mode-II fracture energy in shear-compression test

## 2.2 Abbreviations

Avg.	Average
C.o.V.	Coefficient of variation
CS	Calcium silicate
LVDT	Linear variable differential transformer
St. dev.	Standard deviation
DT	Destructive test
NDT	Non-destructive test
SDT	Slightly destructive test

### 3 Construction of the samples

The masonry specimens were built in the Stevin II laboratory at the Delft University of Technology. The masonry was made of calcium silicate bricks and cement based mortar. The declarations of performance of the materials are reported in Appendix A.

Figure 1 shows the adopted masonry unit. Their dimensions are defined considering the orientation of the masonry unit as used in the construction of the masonry. This definition is consistently adopted in this report despite the position of the specimen in the test set-up. A similar consideration is applied to describe the dimensions of masonry specimens.

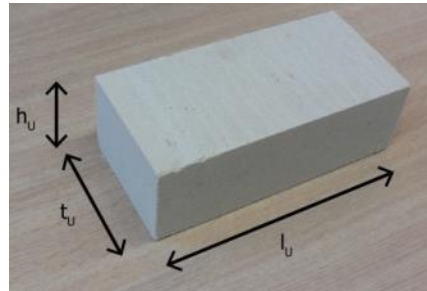


Figure 1 – Calcium silicate brick.

In order to ensure quality control, the construction followed the prescription as reported in the construction protocol [31]:

- The bags of mortar mix have been stored dry and separated from the soil;
- The mortar mix has been used within 18 months after production;
- The mortar has been mixed with clean water;
- The mortar has been prepared using a fixed water content;
- The flow of the mortar should be determined in agreement with EN 1015-3:1999 [4].
- At least three samples of mortar (size 160x40x40-mm<sup>3</sup>) should be made at every start of the day during construction of masonry for testing the properties. The samples will be tested under flexural and compressive loading in agreement with EN 1015-11:1999 [32];
- The mortar has been prepared and used between 5 and 25 degrees;
- The mortar has been used within 2 hours after preparation;
- No additives have been mixed after preparation of the mortar;
- Bricks have been covered against moisture;
- Bricks were clean before use;
- Bricks have not been wetted before use;

The mortar was prepared with fixed water content per bag of mix (25 kg): 2.8 l/bag for calcium silicate masonry.

## 4 Compression strength of masonry unit

The compressive strength of a masonry unit (brick) is determined in agreement with EN 772-1:2000 [33].

### 4.1 Testing procedure

A single CS masonry unit having a length  $l_u$ , a height  $h_u$  and thickness  $t_u$  was used for the compression test in agreement with EN 772-1:2000 [33]. This test allowed determining the compressive strength of masonry unit (brick) (Figure 2). Six masonry unit specimens were subjected to the compression tests.

In order to estimate the Young's modulus of the masonry unit, four LVDTs were attached to the loading plates of the testing machine.



Figure 2 – Compressive test on the single masonry unit.

The test is carried out through a displacement-controlled apparatus including a hydraulic jack with 350-ton capacity. The hydraulic jack lifts a steel plate, the active side, and there is a passive load plate at the top. A hinge between the load cell and the top steel plate reduces possible eccentricities during loading. A load cell that measures the applied force is attached to the top steel plate. The masonry unit specimens were tested with its bed joint plane perpendicular to the loading direction.

The rate of the jack displacement was set to 0.01 mm/s to reach the maximum load in 2 min.

### 4.2 Experimental results

Assuming a linear stress distribution over the loaded cross section of the masonry unit, the compressive strength of the masonry unit  $f_b^*$  can be determined from test on single masonry unit as:

$$f_b^* = \frac{F_{\max}}{l_u \cdot t_u} \quad (1)$$

where  $F_{\max}$  is the maximum load,  $l_u$  and  $t_u$  are the length and thickness of the masonry unit respectively.

Following the Annex A of standard EN 772-1 [33], the normalised compressive strength of the masonry unit  $f_b$  is determined as:

$$f_b = \delta \cdot f_b^* \quad (2)$$

where  $\delta$  is the shape factor determined in agreement with Table A.1 in Ref. [33].

Table 3 lists the compressive strength of the bricks as well as the normalised compressive strength obtained by tests on the single masonry unit. All the specimens failed in the compression tests by crushing.

In addition, the chord elastic modulus, evaluated between 1/10 and 1/3 of the maximum, are reported. The elastic modulus was calculated considering the LVDTs' reading. Comparing the average value of the elastic modulus with those results obtained in the last camping [1], through performing three-point bending tests on the single unit, it can be concluded that this method is not able to provide a proper estimation of the Young's modulus. As a result, tests on the stacked masonry unit adopted by Ad Vermeltfoort [7] will be conducted. The results of the tests will be included in the correlation report.

Table 3 – Compressive strength for the calcium silicate bricks.

Calcium silicate bricks				
Sample name	$f_b$	$\delta$	$f_b$	$E_b$
	MPa	-	MPa	MPa
TUD_MAT-B11a	20.5	0.707	14.5	4184
TUD_MAT-B11b	17.9	0.707	12.6	3881
TUD_MAT-B11c	15.1	0.707	10.7	2377
TUD_MAT-B11d	17.2	0.707	12.2	4239
TUD_MAT-B11e	20.8	0.707	14.7	2767
TUD_MAT-B11f	21.1	0.707	14.9	5247
<b>Average</b>	<b>18.76</b>	<b>-</b>	<b>13.26</b>	<b>3783</b>
<b>Standard deviation</b>	<b>2.42</b>	<b>-</b>	<b>1.71</b>	<b>1052</b>
<b>Coefficient of variation</b>	<b>0.13</b>	<b>-</b>	<b>0.13</b>	<b>0.28</b>

## 5 Flexural and compressive strength of mortar

During the masonry construction, mortar samples were collected and cast in moulds to be tested for the flexural and compressive strength in agreement with EN 1015-11:1999 [32]. The consistency of the mortar was determined in accordance with EN 1015-3:1999 [4].

### 5.1 Testing procedure

During each day of construction, at least three mortar specimens having a length of  $l_m = 160$  mm, a height of  $h_m = 40$  mm and thickness of  $t_m = 40$  mm were collected. The samples were stored in controlled conditions. The first two days they were placed in a fog room ( $T = 20 \pm 2$  °C,  $RH = 95 \pm 5\%$ ) with the moulds. After two days, they were un moulded and kept for other five days in the fog room. Eventually, they were placed in a conditioning room with a temperature of  $20 \pm 2$  °C and a relative humidity of  $50 \pm 5$  % until testing. The test was performed after at least 28 days from construction.

The flexural strength was determined by three-point bending test (Figure 3a). The test set-up is composed by two steel bearing rollers having a diameter of  $10 \pm 0.5$  mm and spaced  $d_l = 100 \pm 0.5$  mm. A third roller is centrally placed on top of the sample to apply the load.

The compression test was performed on the broken pieces obtained from the flexural test, which have at least a length of 40 mm. The specimen is placed between two steel plates with a length of  $l_p = 40$  mm. For the interpretation of the results the specimens considered to be 40x40x40-mm (Figure 3b).

For both test, the load was applied without shock at a uniform rate so that failure occurred within a period of 30 to 90 s. The maximum load was recorded.

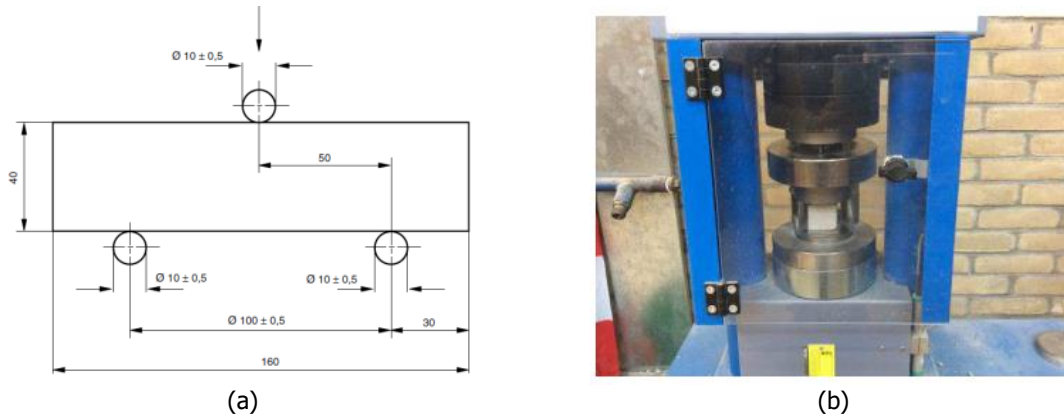


Figure 3 – Test on masonry mortar specimens: (a) three-point bending test; (b) compression test.

### 5.2 Experimental results

The flexural strength  $f_{mt}$  of the mortar was calculated as [32]:

$$f_{mt} = \frac{3 F_{\max} d_l}{2 t_m h_m^2} \quad (3)$$

where  $F_{\max}$  is the maximum load,  $d_l$  is the distance between the supports ( $100 \text{ mm} \pm 0.5 \text{ mm}$ ),  $h_m$  is the height of the mortar specimen (40 mm) and  $t_m$  is the thickness of the mortar specimen (40 mm).

The compressive strength  $f_m$  of the mortar was calculated as [32]:

$$f_m = \frac{F_{\max}}{t_m l_p} \quad (4)$$

where  $F_{\max}$  is the maximum load,  $t_m$  is the thickness of the mortar specimen (40 mm) and  $l_p$  is the length of the loading plate (40 mm).

During the masonry construction, the slump flow tests were performed when a new batch of mortar was prepared. The diameter of the cone was obtained by the flow test described in EN 1015-3:1999 [4]. The measured diameter varied between 147 to 163 mm (see Table 4). As to follow the previous construction procedure, the same amount of water (2.8 l/bag) was used; although the flow results were lower than those measured in the previous construction phases (see Table 6).

Aside from the large walls and the companion samples constructed with the aim of testing for the scope of WP1a, one large-scale CS brick wall (COMP20) also was prepared to be tested for the research purpose of WP3. It should be mentioned that the NDT5 wall was tested by SGM and the NDT4 wall was tested by NEBEST.

Table 4 – Consistency of calcium silicate masonry mortar measured during the third phase of construction in Aug. 2016.

Date	Cast	Flow (mm)
16-8-2016	1	153
	2	163
	4	163
17-8-2016	1	162
	2	157
	3	151
18-8-2016	1	156
	2	157
	3	158
	4	154
	5	155
	6	152
19-8-2016	1	149
	2	153
	3	149
	4	159
22-8-2016	1	147
	2	154
	3	155
	4	157
23-8-2016	1	147
	2	154
	3	157
	4	163
Average		<b>155</b>

The flexural and compression tests on the hardened mortar were performed at least after 28 days. Table 17 lists the results for the three-point bending tests and compression tests. Three-point bending tests were performed on 75 specimens and compressive tests were conducted on 150 specimens. The mortar has a compressive strength of 7.6 MPa and flexural strength of 3.2 MPa. In both cases, the coefficient of variation is limited to less than 10%.

Table 6 compares the results of tests on the fresh and hardened mortar constructed at the three phases of constructions at TU Delft. There is a slightly differences between the flexural strength values of the mortar produced during the three phases of construction. It should be mentioned that although the mortar used for the construction of the samples were taken from the same batch, the aging of the cement (around 13 to 15 month), environmental conditions and the mixing procedure can influence the mortar properties. Figure 4 shows the statistical distribution of flexural and compressive strength of mortar in three different construction phases.



Table 5 – Flexural and compressive strength of calcium silicate masonry mortar constructed in Aug. 2016.

Date	Companion samples	Cast	Flexural tests			Compression test		
			$f_{mt}$ (MPa)	St. Dev.	C.o.V.	$f_m$ (MPa)	St. Dev.	C.o.V.
16-8-2016	MAT-16A	1	3.3	0.19	0.06	7.9	0.46	0.06
	MAT-16B	2	2.5	0.18	0.07	5.3	0.27	0.05
	MAT-11	4	3.1	0.11	0.03	7.3	0.36	0.05
17-8-2016	MAT-11	1	3.0	0.11	0.04	6.6	0.41	0.06
	NDT5	2	3.5	0.10	0.03	7.1	1.92	0.27
	NDT5	3	3.0	0.10	0.03	6.8	0.42	0.06
18-8-2016	NDT5	1	3.1	0.13	0.04	7.9	0.29	0.04
	NDT5	2	3.4	0.06	0.02	7.8	0.64	0.08
	NDT5	3	3.1	0.05	0.02	7.0	0.95	0.14
	NDT4	4	3.0	0.32	0.11	7.7	0.28	0.04
	NDT4	5	3.2	0.29	0.09	8.7	0.44	0.05
	NDT4	6	3.1	0.17	0.06	7.0	0.14	0.02
19-8-2016	NDT4/COMP20	1	3.3	0.38	0.12	7.4	0.29	0.04
	NDT4	2	3.5	0.17	0.05	8.1	0.28	0.03
	NDT3/ COMP20	3	3.2	0.10	0.03	8.6	0.34	0.04
	NDT3/ COMP20	4	3.7	0.36	0.10	9.0	0.37	0.04
22-8-2016	NDT2	1	2.7	0.02	0.01	5.7	0.29	0.05
	NDT2	2	2.7	0.18	0.07	7.1	0.26	0.04
	NDT2	3	3.4	0.21	0.06	8.2	0.70	0.09
	NDT2	4	3.4	0.15	0.04	8.5	0.32	0.04
23-8-2016	NDT2/1	1	3.3	0.10	0.03	7.4	0.24	0.03
	NDT1	2	3.6	0.18	0.05	8.8	0.30	0.03
	NDT1	3	3.4	0.27	0.08	7.5	0.56	0.07
	NDT1	4	3.4	0.30	0.09	8.4	0.43	0.05
Average all casts			3.21			7.57		
Standard deviation			0.18			0.46		
Coefficient of variation			0.05			0.06		

Table 6 – Comparison between the results of tests on fresh and hardened mortar at three phases of construction.

Period of construction	Flow	Flexural strength	Compressive strength
	(mm)	MPa	MPa
First phase (Apr/May 2015)	174	2.79 [0.08]	6.59 [0.10]
Second phase (Sept. 2015)	162	3.56 [0.05]	7.24 [0.08]
Third phase (Aug. 2016)	155	3.21 [0.05]	7.57 [0.06]

The coefficient of variation is presented between brackets.

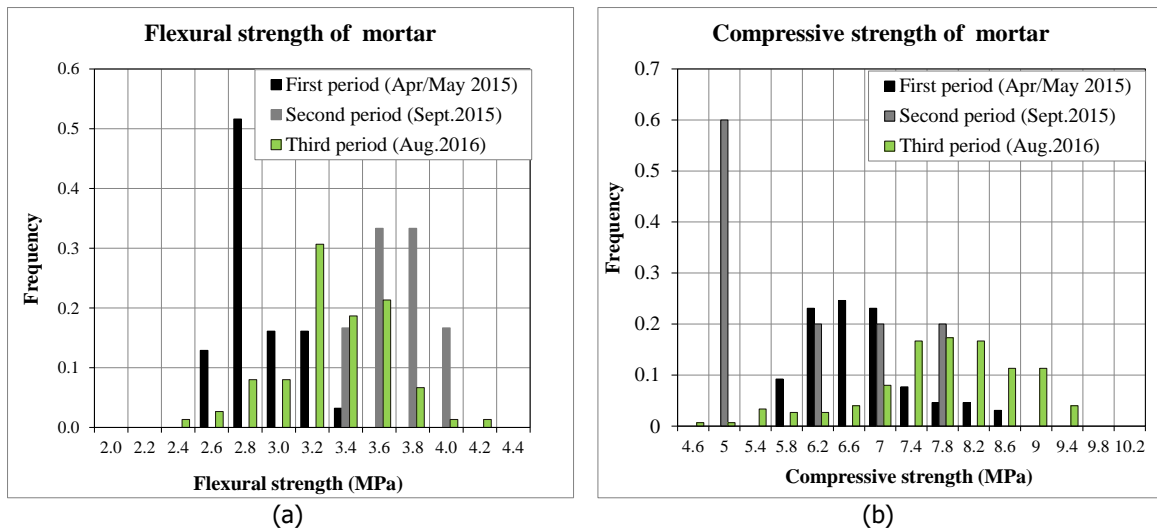


Figure 4 – Statistical distribution of mortar strength: (a) flexural strength; (b) compressive strength.

## 6 Compression strength of masonry

The compression strength and elastic modulus of the masonry were determined in agreement with EN 1052-1:1998 [9]. Additional test configuration was adopted to investigate the cyclic response of the material, to have the same testing procedure adopted in double flat jack tests [10].

### 6.1 Testing procedure

The size of the specimens was determined on the basis of the masonry units [9]. The calcium silicate masonry specimens have dimensions of 434x476x102-mm (2x6x1-brick). A 10 mm thick layer of gypsum was applied to faces in contact with the loading plates, to ensure that the loaded faces of the specimens are levelled and parallel to one another. This is done to prevent additional stresses in the specimens.

The compression strength and elastic modulus of the masonry were determined in a vertical configuration in which the loading was perpendicular to the bed joints. The test is prescribed by the standard EN 1052-1:1998 [9].

The testing apparatus was provided with a 3500 kN hydraulic jack, positioned at the bottom. The hydraulic jack lifts a steel plate, the active side, and there is a passive load plate at the top. A hinge between the load cell and the top steel plate reduces possible eccentricities during loading. The hydraulic jack is operated in deformation control, using the displacement of the jack as control variable. A load cell that measures the applied force is attached to the top steel plate (Figure 5a).

Four LVDTs (two for each side) are attached to the specimen to register vertical relative displacements over the height of the specimen (Figure 5b). They are installed as closely as possible to the surface of the specimen to reduce possible errors caused by rotation of the contact points to which they are attached. Their measuring range is 10 mm with an accuracy of 0.5%. Additionally, two LVDTs (one for each side) are attached to the specimen to register the horizontal relative displacement over the length of the specimen. Their measuring range is 10 mm with an accuracy of 0.5%.

Three specimens were tested by applying a *monotonic loading* as prescribed by the EN 1052-1:1998 [9] (Figure 6). Half of the expected maximum compression force is applied in three equal steps and was kept constant for  $2 \pm 1$  min. Afterwards, the maximum stress is reached monotonically. Subsequently, the test was continued to explore the post-peak behaviour. The load was applied with a rate of 0.002 mm/s to reach the peak stress in 15 to 30 min. The deformation and the force were registered, including the post-peak softening regime.

Four specimens were tested by applying a *cyclic loading* (Figure 6). This loading scheme gives additional information regarding the loading-unloading behaviour. Five cycles of three runs were applied at approximately 0.07, 0.1, 0.25, 0.5 and 0.75 of the expected maximum strength. The load was applied with a rate of 0.0075 mm/s to reach the peak stress in approximately 30 min. The deformation and the force were registered.

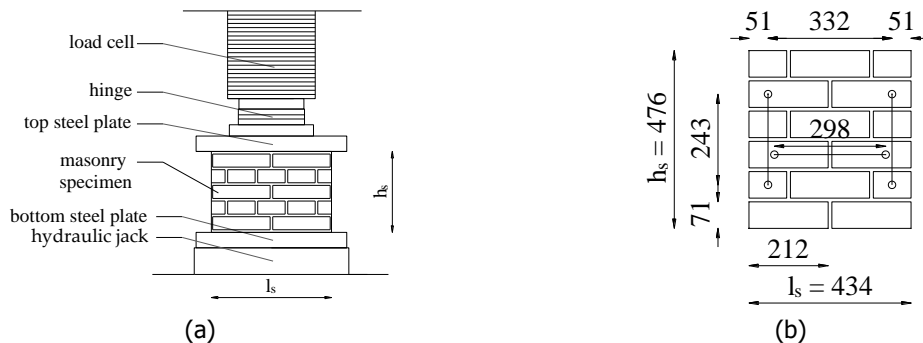


Figure 5 – Compression test on masonry: (a) test set-up; (b) position of the LVDTs.

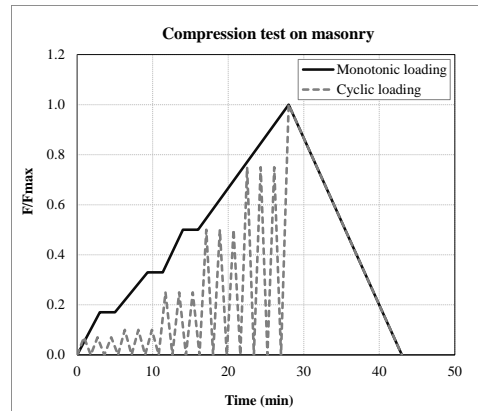


Figure 6 – Monotonic and cyclic loading scheme for compression test on masonry specimen.

## 6.2 Experimental results

Assuming that the stress is constant over the cross-section of the specimen, the compressive strength of masonry,  $f'_m$ , can be determined as follows:

$$f'_m = \frac{F_{\max}}{t_s l_s} \quad (5)$$

where  $F_{\max}$  is the maximum load,  $l_s$  and  $t_s$  are the dimensions of the masonry specimen as built (Figure 5).

During the test the displacements and the force were measured continuously allowing the determination of the stress-strain relationship along the loading direction, which was defined as normal direction. From this relation was possible to determine the elastic modulus of masonry. Three estimates of the elastic modulus were adopted (Figure 7a):

- $E_1$  is the secant elastic modulus evaluated at 1/3 of the maximum stress;
- $E_2$  is the secant elastic modulus evaluated at 1/10 of the maximum stress;
- $E_3$  is the chord elastic modulus evaluated between 1/10 and 1/3 of the maximum stress.

The first estimate was consistent with the prescription of EN 1052-1:1998. The third estimate aimed to exclude the initial start-up of the stress-strain diagram, which would unrealistically affects the other two secant estimates with the initial lower slope.

In the case of cyclic compression tests, aside from the elastic modulus, the stiffness was evaluated for the cycles that were performed in the elastic phase (i.e. 0.07, 0.1, and 0.25 of the expected maximum strength). The cyclic stiffness for each cycle was evaluated as follows: (a) identifying the maximum and minimum stress and strain for each run; (b) taking an average for the specified maximum and minimum points of the three runs; (c) calculating the slope of the line passing through those average points (Figure 7b).

Three estimations of the cyclic stiffness are defined as follows:

- $E_{c1}$  is the cyclic stiffness evaluated in the cycle corresponding to a stress level equal to 0.07 of the expected maximum strength.
- $E_{c2}$  is the cyclic stiffness evaluated in the cycle corresponding to a stress level equal to 0.1 of the expected maximum strength.
- $E_{c3}$  is the cyclic stiffness evaluated in the cycle corresponding to a stress level equal to 0.25 of the expected maximum strength.

The Poisson ratio  $\nu$  is determined in the elastic phase as the ratio between the lateral strains, which are evaluated in the direction perpendicular to the loading one, and the normal strains (Figure 7c).

The displacement control procedure of the test allowed determining the post-peak behaviour of the material. The fracture energy in compression  $G_{fc}$  was determined as the area underneath the normal stress versus normal strain diagram, taking the height of the specimen into account. This concept was introduced by van Mier [35] for concrete material and subsequently applied to masonry by Lourenco [36]. In the case of cyclic loading, the envelope curve was considered for the calculation of the fracture energy.

Due to the instinct stiffness of the testing machine, there is a difference between the LVDTs' reading and jack's measurement. Therefore, the LVDTs' readings were used as a basis for evaluating the elastic modulus and the Poisson ratio. Because of extensive cracking in the post-peak phase, LVDTs might be detached from the specimen and there is no measuring data at this phase (Figure 8a). In the previous testing campaign, the fracture energy was calculated considering the jack's measurement.

The fracture energy is evaluated as the area underneath the complete stress-strain relationship along the loading direction. The LVDTs' readings provide the most accurate measurement of the stain; however due to the extensive cracking they may be detached from the specimen during the post-peak phase. Consequently, the jack's measurement should be used to obtain a complete stress-strain relationship. During the measurements, a linear relationship between the LVDTs' reading and jack's readings has been observed in the post-peak phase (Figure 7d). For this reason the complete stress-strain relationship is defined by using both the LVDTs' and jack's readings. Consequently, the complete stress strain relationship is defined as: in the pre-peak phase the LVDTs' readings are adopted, in the post-peak phase the jack's readings are used and modified by imposing that the peak strain defined by the jack's measurement is the

same of the one determined by the LVDTs' measurements. The peak strain is defined as the strain corresponding to the maximum stress (Figure 7e).

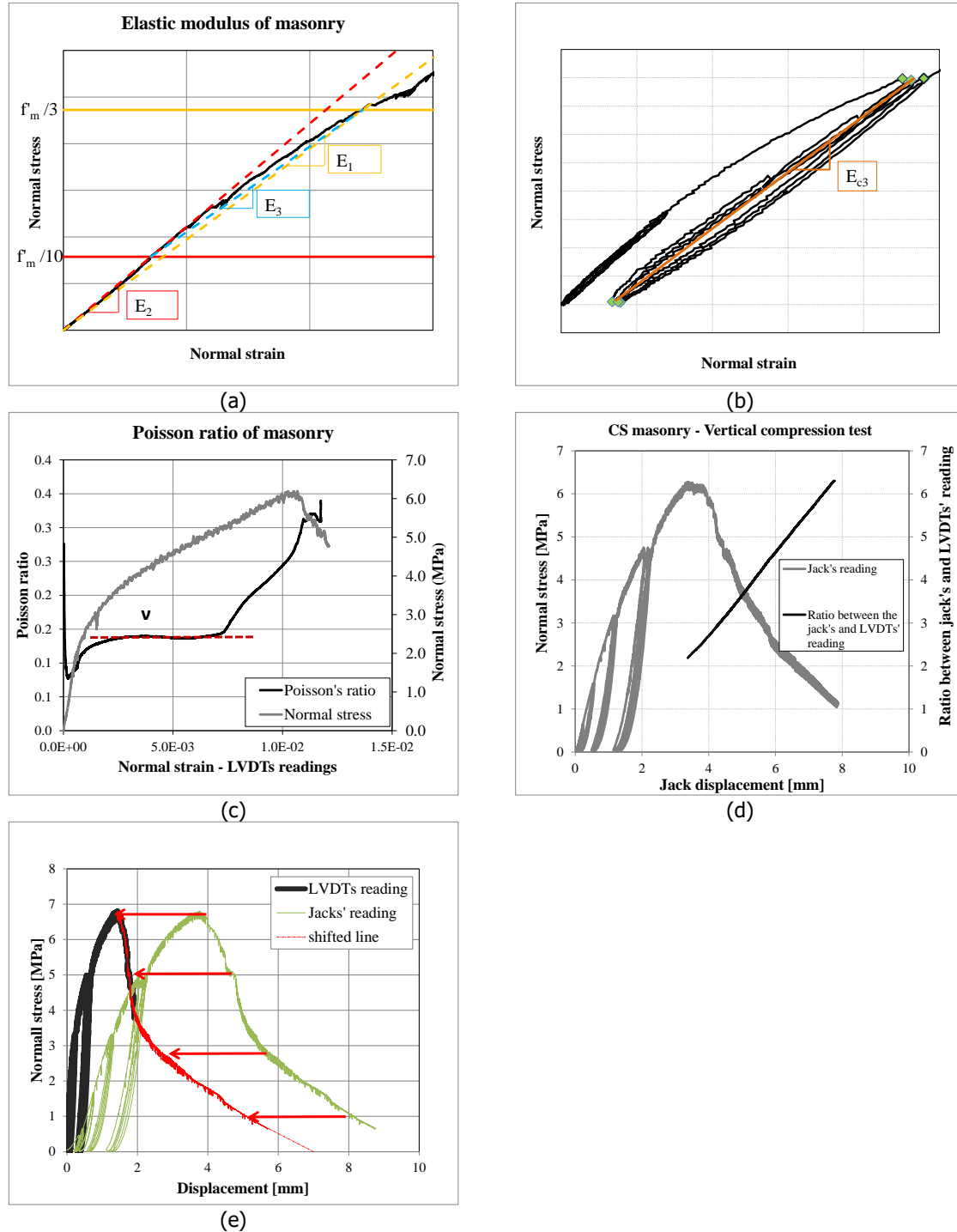


Figure 7 – Compression test on masonry: (a) three estimates of the elastic modulus; (b) estimate of the cyclic stiffness; (c) evaluation of Poisson ratio; (d) comparison between jack's reading and LVDTs' reading in the post-peak phase; (e) adopted method to evaluate the fracture energy.

Figure 8a show the stress-strain diagram for the calcium silicate masonry under vertical compression tests. The graphs refer to the normal direction that is defined as the one parallel to the loading direction.

The pre-peak stage was characterised by linear-elastic followed by a hardening behaviour until the peak. In this stage, the nonlinearity occurred at a stress level approximatively of 1/10 of the maximum stress. After the maximum stress was reached, a softening behaviour was observed. The softening branch was approximatively linear. In the case of cyclic loading, the masonry showed an elastic unloading.

Figure 9 analyses the development of cracks in one specimen tested under vertical compression test. The cracks started at the mortar-brick interface for the joints orthogonal to the loading direction (Figure 9a). When the maximum stress was reached, vertical cracks develop in the bricks. The cracks mainly occurred in the central part of the specimens (Figure 9b). In the post-peak phase, the vertical cracks mainly occurred in the bricks and develops uniformly through the length of the specimen, by splitting it in two parts (Figure 9c, Figure 9d). The cracking was observed to occur in a distributed manner over the height of the specimen; no localisation of the cracking at the boundary was observed.

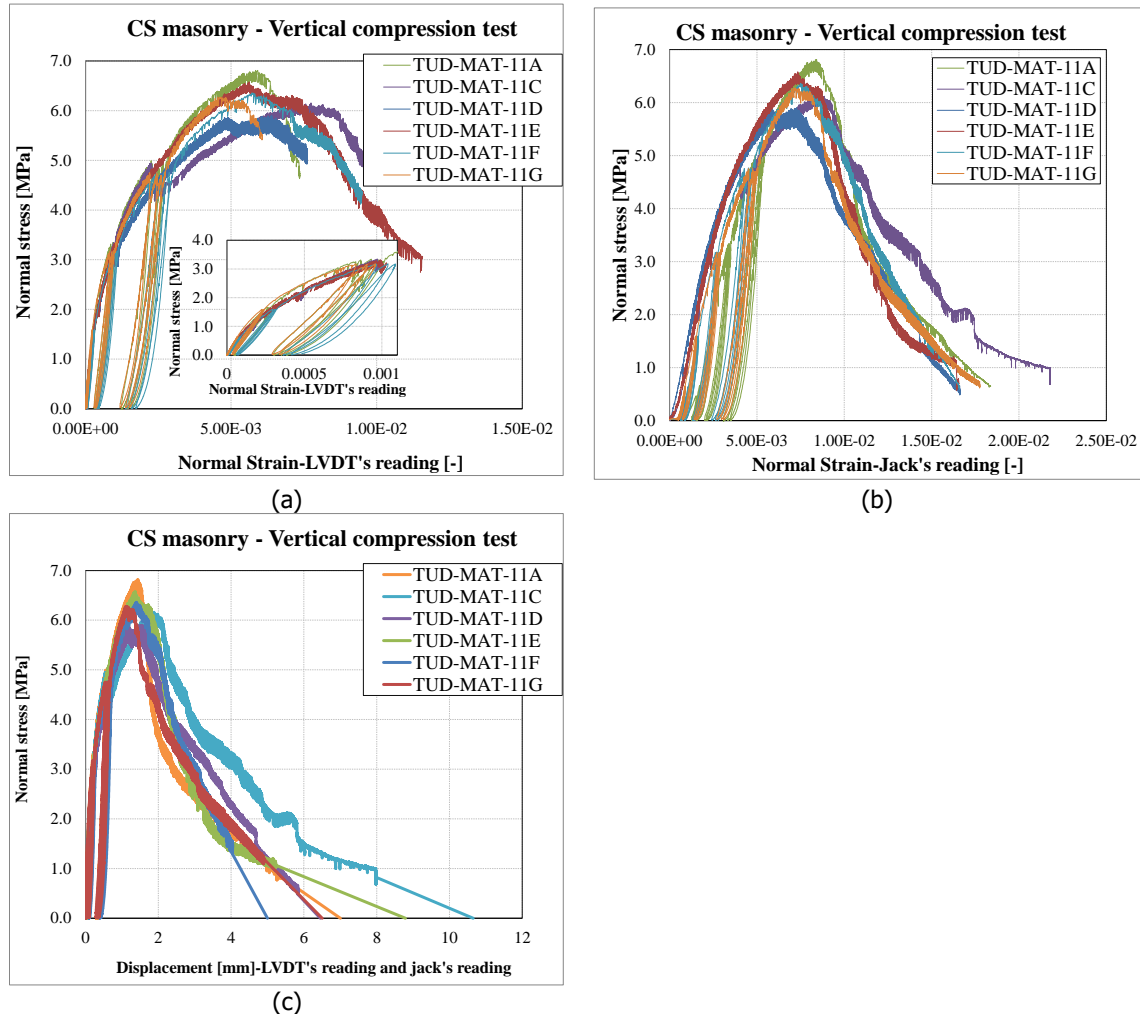


Figure 8 – Vertical compression tests on calcium silicate masonry specimens: (a) normal strain obtained by LVDTs reading; (b) normal strain obtained by jack's reading; (c) stress- strain curve where the displacement obtained from the LVDTs' reading in the pre-peak phase and jack's reading in the post-peak phase to evaluate the fracture energy.

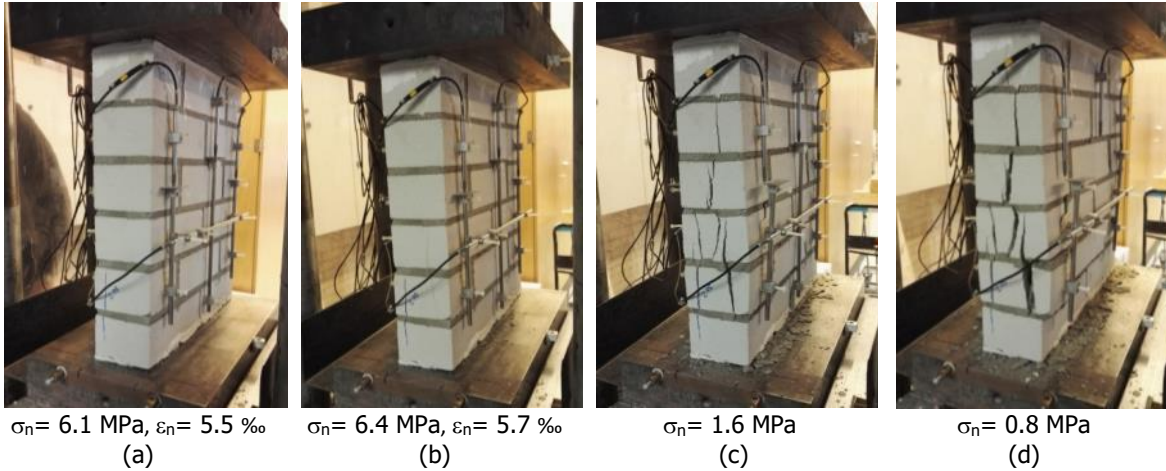


Figure 9 – Crack pattern of specimen TUD\_MAT-11F tested under cyclic vertical compression test: (a) first crack; (b) maximum stress; (c)-(d) post-peak phase.

Table 21 lists the main experimental results for the calcium silicate masonry specimens. Figure 10 shows the results with the histogram representation.

The secant elastic modulus  $E_1$  evaluated at 1/3 of the maximum stress and the chord modulus  $E_3$  provided a similar estimation, while the elastic modulus  $E_2$  at 1/10 of the maximum stress provided higher values. This confirms the start of the non-linearity for lower values of normal stress.

The stiffness evaluated at the first,  $E_{c1}$ , and the second,  $E_{c2}$ , cycle provided a similar estimation, while the stiffness evaluated at the third cycle  $E_{c3}$  resulted lower value.

The average Poisson ratio  $\nu$  was estimated equal to 0.16.

Table 7 – Vertical compression test results on calcium silicate masonry specimens (Aug. 2016).

Specimen name*	Test type	$f'_m$	$E_1$	$E_2$	$E_3$	$G_{f-c}^*$	$E_{c1}$	$E_{c2}$	$E_{c3}$	$\nu$
		MPa	MPa	MPa	MPa	N/mm	MPa	MPa	MPa	
TUD_MAT-11A	cyclic	6.81	5274	8391	4550	18.1	9072	8566	6952	0.17
TUD_MAT-11C	monotonic	6.16	4652	6833	4092	26.8	-	-	-	0.11
TUD_MAT-11D	monotonic	5.90	5111	7548	4490	19.4	-	-	-	0.17
TUD_MAT-11E	monotonic	6.58	4485	8778	3708	19.9	-	-	-	-
TUD_MAT-11F	cyclic	6.36	4415	7953	3708	18.0	8522	8313	6159	0.17
TUD_MAT-11G	cyclic	6.27	5895	9736	5043	18.0	10250	9684	7609	-
Average	All	<b>6.35</b>	<b>4972</b>	<b>8206</b>	<b>4265</b>	<b>20.0</b>	<b>9281</b>	<b>8854</b>	<b>6907</b>	<b>0.16</b>
Standard deviation		<b>0.32</b>	<b>568</b>	<b>1008</b>	<b>527</b>	<b>3.43</b>	<b>883</b>	<b>730</b>	<b>726</b>	<b>0.03</b>
Coefficient of variation		<b>0.05</b>	<b>0.11</b>	<b>0.12</b>	<b>0.12</b>	<b>0.17</b>	<b>0.10</b>	<b>0.08</b>	<b>0.11</b>	<b>0.19</b>

\* TUD\_MAT-11B was subjected to the cyclic load. The results were excluded from the average, since the sample was not straight.



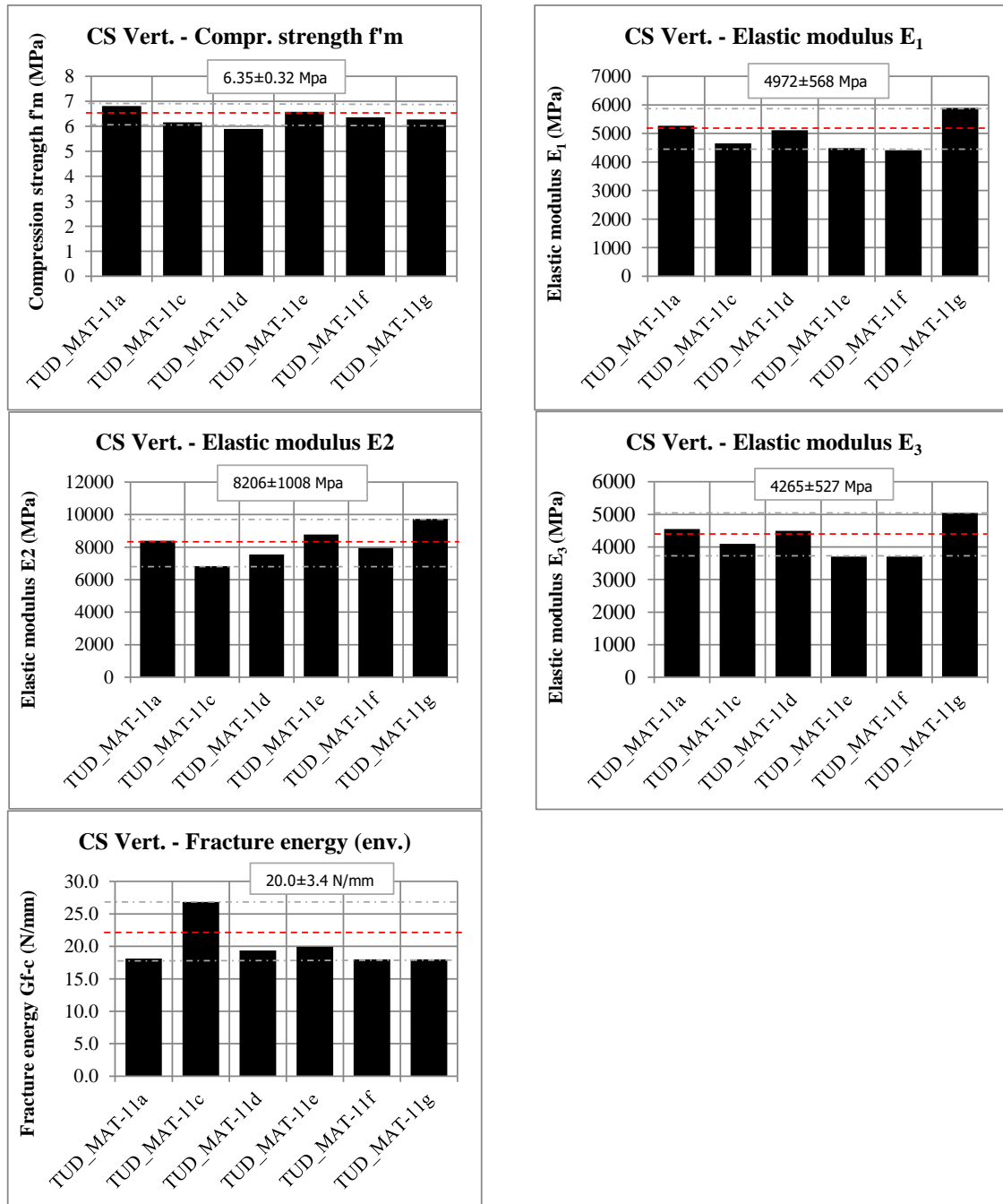


Figure 10 – Vertical compression tests on calcium silicate masonry specimens (third period): histogram

Table 8 shows a comparison between the results of tests on the calcium silicate brick masonry wallets build during the three construction phases. The results of tests on the third phase of construction show slightly higher values for the compressive strength  $f'_m$ , while the secant elastic moduli  $E_1$ ,  $E_2$  and the elastic modulus  $E_3$  show higher values.

Table 8 – Calcium silicate masonry subject to vertical compression test: comparison between different construction phases.

Series	Statistical parameter	$f'_m$	$E_1$	$E_2$	$E_3$	$\nu$
		MPa	MPa	MPa	MPa	
First period (Apr/May 2015)	Average	<b>5.93</b>	<b>3174</b>	<b>5091</b>	<b>2746</b>	<b>0.14</b>
	Standard deviation	0.52	467	1774	282	0.01
	Coefficient of variation	0.09	0.15	0.35	0.10	0.07
Second period (Sept. 2015)	Average	<b>5.76</b>	<b>3340</b>	<b>4537</b>	<b>3005</b>	<b>0.18</b>
	Standard deviation	0.59	800	1888	568	0.07
	Coefficient of variation	0.10	0.24	0.42	0.19	0.41
Third period (Aug. 2016)	Average	<b>6.35</b>	<b>4972</b>	<b>8206</b>	<b>4265</b>	<b>0.16</b>
	Standard deviation	0.32	568	1008	527	0.03
	Coefficient of variation	0.05	0.11	0.12	0.12	0.19
$(P_{\text{Third}} - P_{\text{first}}) / P_{\text{Third}}$		<b>0.07</b>	<b>0.36</b>	<b>0.38</b>	<b>0.36</b>	<b>0.11</b>
$(P_{\text{Third}} - P_{\text{second}}) / P_{\text{Third}}$		<b>0.09</b>	<b>0.33</b>	<b>0.45</b>	<b>0.30</b>	<b>-0.15</b>

Figure 11 shows the envelope curve from the LVDTs' reading for the results of the vertical compression tests on the masonry wallets constructed at three different phases.

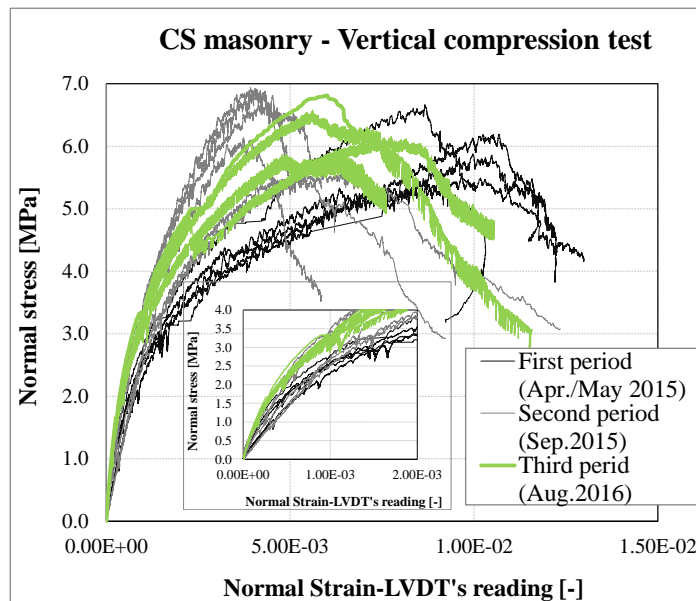


Figure 11 – Vertical compression tests on the calcium silicate masonry specimens constructed at three construction periods.

## 7 Bond strength of masonry

The bond strength between masonry unit and mortar was determined in agreement with the bond wrench test proposed by EN 1052-5:2002 [13].

### 7.1 Testing procedure

The test set-up used in the previous experimental campaign in 2015 is shown in Figure 12a. In this set-up a lever was used to apply a bending moment to the brick-mortar interface. The applied moment was registered on an analogue scale. The apparatus was officially calibrated in the range 20–215 Nm, with a tolerance of 4%.

Due to the difficulties of dealing with the retaining frame, the bond wrench set-up used in the previous campaigns was improved. The improved set-up used in the current campaign is shown in Figure 12b. The specimen is rigidly held by a support frame that holds the specimen in accordance with EN 1052-5:2005 [13]. A clamp, with a lever attached, was applied to the masonry unit above the tested. The lever was used to apply a bending moment to the brick-mortar interface. The load was applied by a jack operated manually and a load cell attached to the jack measures the applied force. Therefore, the improved set-up provides the possibility for registering the load as well as applying higher range of load, in particular for the samples with the higher value of bond strength (e.g. calcium silicate element).

A couplet specimen was adopted for the bond wrench tests (Figure 12c).

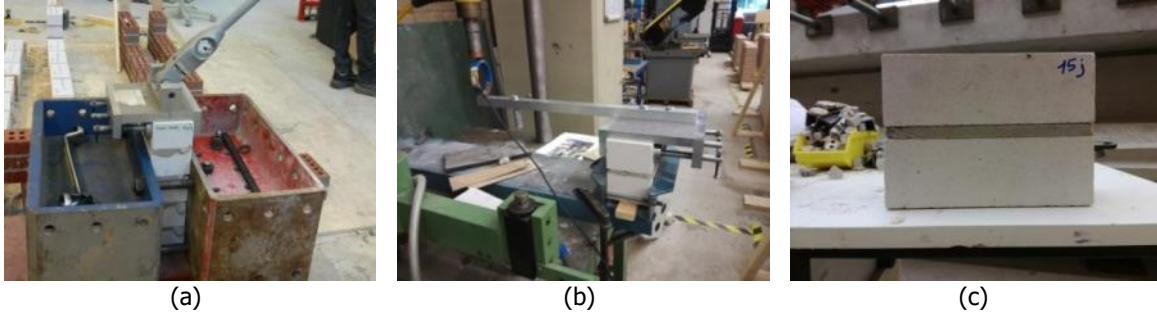


Figure 12 – Bond wrench tests: (a) bond wrench set-up used in the previous campaigns; (b) improved bond wrench set-up used in this campaign; (c) couplet specimen.

### 7.2 Experimental results

The bond wrench strength  $f_w$  is calculated on the assumption that the stress distribution is linear over the width of the top masonry unit [13]:

$$f_w = \frac{F_1 e_1 + F_2 e_2 - \frac{2}{3} t_u \left( F_1 + F_2 + \frac{F_3}{4} \right)}{l_j w_j^2 / 6} \quad (6)$$

where  $F_1$  is the failure load, measured and applied by the jack.  $F_2$  is the normal force as a result of the weight of the bond wrench apparatus ( $F_2 = 50.9$  N).  $F_3$  is the weight of the masonry unit pulled off the specimen, including the weight of adherent mortar. Furthermore,  $e_1$  is the distance from the applied load to the tension face of the specimen,  $e_2$  is the distance from the centre of gravity of the clamp to the tension face of the specimen,  $l_j$  is the mean length of the bed joint, and  $w_j$  is the mean width of the bed joint. Figure 13 show the set-up and the definition of the various quantities.

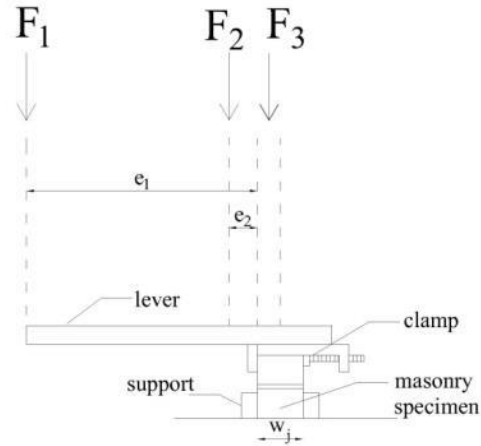


Figure 13 – Test set-up for the bond wrench test.

Figure 14 reports the classification of the type of failures [13], while Figure 15 shows the observed failure mechanisms.

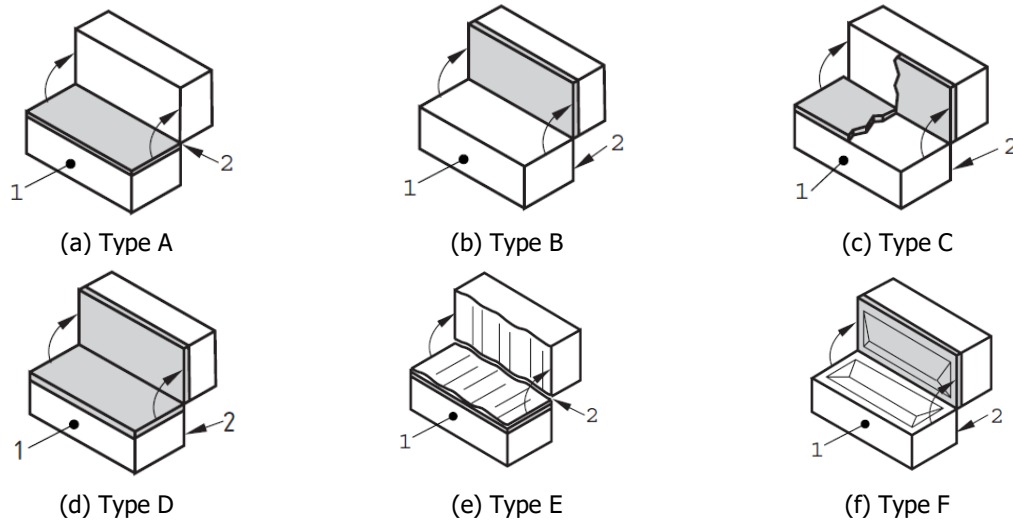


Figure 14 – Classification of failure modes in agreement with EN-1052-5:2005 (1 tension face, 2 compression face).



Figure 15 – Observed failure mechanisms: (a) type A; (b) type B.

Figure 16 shows the applied load ( $F_1$ ) versus time. From the graph the brittle behaviour of the samples are clear.

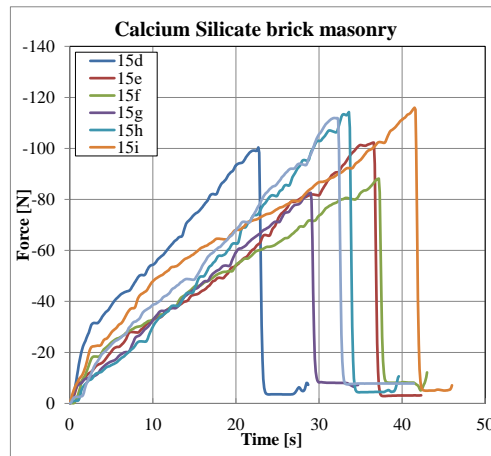


Figure 16 – Time versus force ( $F_1$ ) applied by manually controlled jack.

Table 9 lists the results of the calcium silicate masonry. Three samples 15a-15b-15c showed detachment of the two brick during the installation of the specimen in the set-up; consequently they are not considered in the statistical analysis.

Table 9 – Bond strength of calcium silicate masonry samples (Aug.2016).

Specimen Name*	Maturation	$l_j$	$w_j$	$F_3$	$F_1$	$f_w$	Failure mode
	days	mm	mm	N	N	MPa	
15d	81	210	101	21.2	100.51	0.12	A
15e	81	209	101	22.4	102.41	0.12	A
15f	81	210	100	36.2	88.24	0.11	B
15g	81	210	101	37.0	82.61	0.10	B
15h	81	210	101	38.7	114.43	0.13	B
15i	81	209	102	38.9	116.13	0.13	B
15j	81	209	102	21.7	104.80	0.12	A
average						0.12	
st. dev.						0.01	
c.o.v.						0.12	

\* Complete specimen name starting with TUD\_MAT-.

Table 10 lists an overview of the bond wrench test results for the calcium silicate masonry samples tested at different phases of construction. It can be observed that the results correlated to the third construction phase show a significant lower coefficient of variation. This improvement can be addressed to the change in set-up from manual to automatic control.

Figure 17 shows the results in terms of probability distribution function.

Table 10 – Comparison between the bond wrench test results obtained in the three construction phases.

Period	No. Specimens	$f_w$		
		Average (MPa)	St. dev.	C.o.V.
First phase (Apr/May 2015)	35	<b>0.27</b>	0.12	0.43
Second phase (Sept. 2015)	36	<b>0.28</b>	0.08	0.29
Third phase (Aug. 2016)	7	<b>0.12</b>	0.01	0.12

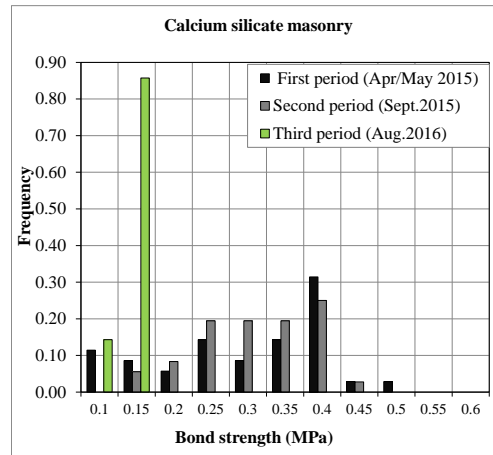


Figure 17 – Probability distribution functions of bond strength for calcium silicate masonry sample for three phases of construction.

## 8 Shear strength of masonry

The initial shear properties of masonry were determined in agreement with EN 1052-3:2002 [14]. However, a displacement control procedure was used, instead of the prescribed force control procedure, to evaluate the residual strength properties and the mode-II fracture energy.

### 8.1 Testing procedure

Two types of specimens, standard triplet and modified triplet, were adopted. Fourteen specimens for each type of triplet were prepared. The standard triplet is a three stacked bonded brick specimen (Figure 19a), while the modified triplet is formed by bricks bonded in different patterns (Figure 19b). Prior to testing, a layer of gypsum was applied to the external faces of the specimens.

Figure 18 shows the used test set-up. During the test, the specimen was rotated of 90 degrees with respect to the casting position. The specimen was kept under constant lateral pre-compression, while a shear load was applied at the mid masonry unit. Three different levels of pre-compression were investigated. Being the compressive strength of the masonry unit greater than 10 N/mm<sup>2</sup> [14], the pre-compression stresses applied were 0.2, 0.6 and 1.0 N/mm<sup>2</sup>. For each pre-compression level, three specimens were tested.

Two independently operated jacks were required to apply the shear and pre-compressive load. The shear load acts in a vertical direction using a displacement controlled apparatus. The apparatus has a 100 kN jack and a spherical joint. The displacement increased with a rate of 0.005 mm/s. During unloading, the displacement was decreased with a rate of 0.05 mm/s. The pre-compressive load was applied perpendicular to the bed joint plane by a manually operated hydraulic jack. The horizontal hydraulic jack was load controlled and applied different levels of transverse compressive load to the specimen. The jack was kept in position by means of four steel rods positioned on opposite sides of the specimen, which were in turn kept in position by steel plates (Figure 18). In order to keep the transverse compressive load constant ( $\pm 2\%$ ), a spring system is used between the hydraulic jack and the load cell. The stiffness of the springs is defined on the basis of the required pre-compression level. Two types of the spring having the stiffness of 123 N/mm and 3300 N/mm were used. A load cell is placed between the spring and the steel plate to measure the applied load.

Both on the front and the back side of the specimens, LVDTs are attached. Vertical LVDTs measure the relative vertical displacement of the middle brick with respect to the later ones. Horizontal LVDTs measures the horizontal displacement between the two external bricks. Their measuring range is 10 mm with an accuracy of 0.5% (Figure 19).

In order to follow the same testing procedure for the shove test, the pre-compression load was increased and kept constant at different levels in the residual phases.

In order to get more insight into the initial shear strength, one sample for each type of triplets was tested at a very low pre-compressive stress of 0.05 MPa.



Figure 18 – Test set-up for the shear-compression test on masonry specimen.

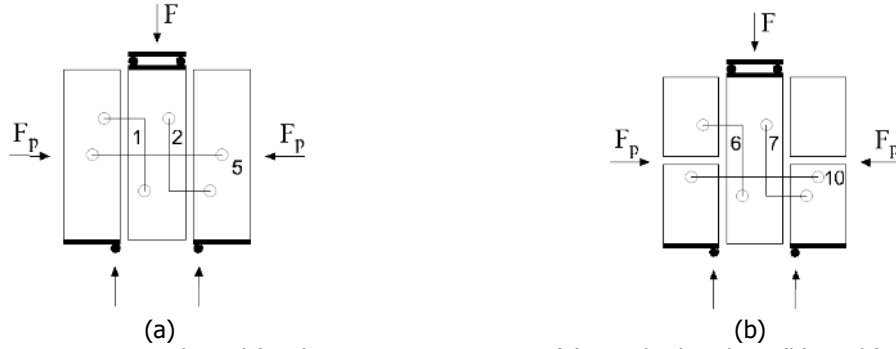


Figure 19 – Specimens adopted for shear-compression test: (a) standard triplets; (b) modified triplets.

## 8.2 Experimental results

The shear strength  $f_v$  was calculated for each specimen as follows [14]:

$$f_v = \frac{F_{\max}}{2A_s} \quad (7)$$

where  $F_{\max}$  is the maximum load,  $A_s$  is the cross sectional area of the specimen parallel to the bed joints. The pre-compression stress  $f_p$  can be calculated for each specimen as follows [14]:

$$f_p = \frac{F_p}{A_s} \quad (8)$$

where  $F_p$  is the pre-compression force.

The test was carried out in displacement control allowing for the determination of the post-peak behaviour. As a consequence, the residual shear strength  $f_{v,res}$  was also determined. The residual strength occurred at an almost constant load where a plateau of large sliding displacement was observed. The resistance in the post-peak phase can be associated to friction only, since large relative displacement occurs.

The results of all the tests were plotted in a pre-compressive stress versus shear strength diagram. Considering a linear regression of the data, the initial shear strength  $f_{v0}$  and the coefficient of friction  $\mu$  can be found such as the intercept with the vertical axis and the gradient of the line, respectively. The angle of internal friction  $\alpha$  was determined as the angle between the regression line and the horizontal axis. Similar consideration can be applied to determine the residual shear strength  $f_{v0,res}$  and the residual coefficient of friction  $\mu_{res}$ . In the Coulomb friction formulation, the result is:

$$f_v = f_{v0} + \mu f_p \quad (9)$$

$$f_{v,res} = f_{v0,res} + \mu_{res} f_p \quad (10)$$

Table 11 and Figure 20 show the results for *standard triplets*. The calcium silicate masonry showed an initial shear strength equal to 0.11 MPa and a coefficient of friction equal to 0.52. In the residual phase, the coefficient of friction increased to 0.55. All the specimens presented a shear failure in the unit/mortar bond area. Figure 22 shows a typical crack pattern.

Table 12 and Figure 21 show the results for *modified triplets*. The calcium silicate masonry showed an initial shear strength equal to 0.18 MPa and a coefficient of friction equal to 0.46. In the residual phase, the coefficient of friction increased to 0.47. All the specimens presented a shear failure in the unit/mortar bond area. Figure 23 shows a typical crack pattern.



Table 11 - Maximum and residual shear strength and mode-II fracture energy of standard triplets.

$f_p = 0.2 \text{ MPa}$				$f_p = 0.6 \text{ MPa}$				$f_p = 1.2 \text{ MPa}$			
Specimen name <sup>(*)</sup>	$f_v$	$f_{v,res}$	$G_{f-II}$	Specimen name <sup>(*)</sup>	$f_v$	$f_{v,res}$	$G_{f-II}$	Specimen name <sup>(*)</sup>	$f_v$	$f_{v,res}$	$G_{f-II}$
	MPa	MPa	N/mm		MPa	MPa	N/mm		MPa	MPa	N/mm
16AF	0.21	0.11	0.022	16AD	0.47	0.35	0.085	16AB	0.69	0.67	0.014
16AI	0.18	0.13	0.012	16AG	0.44	0.33	0.054	16AE	0.74	0.67	0.111
16AO	0.19	0.11	0.024	16AM	0.45	0.33	0.067	16AL	0.70	0.62	0.341
Average	<b>0.19</b>	<b>0.12</b>	<b>0.02</b>	Average	<b>0.45</b>	<b>0.34</b>	<b>0.07</b>	Average	<b>0.71</b>	<b>0.65</b>	<b>0.16</b>
St. dev.	<b>0.02</b>	<b>0.01</b>	<b>0.01</b>	St. dev.	<b>0.02</b>	<b>0.01</b>	<b>0.02</b>	St. dev.	<b>0.03</b>	<b>0.03</b>	<b>0.17</b>
C.o.V.	<b>0.08</b>	<b>0.11</b>	<b>0.33</b>	C.o.V.	<b>0.03</b>	<b>0.03</b>	<b>0.23</b>	C.o.V.	<b>0.04</b>	<b>0.04</b>	<b>1.08</b>

<sup>(\*)</sup> Complete specimen name starting with TUD\_MAT-.

Table 12 - Maximum and residual shear strength and mode-II fracture energy of modified triplets.

$f_p = 0.2 \text{ MPa}$				$f_p = 0.6 \text{ MPa}$				$f_p = 1.2 \text{ MPa}$			
Specimen name <sup>(*)</sup>	$f_v$	$f_{v,res}$	$G_{f-II}$	Specimen name <sup>(*)</sup>	$f_v$	$f_{v,res}$	$G_{f-II}$	Specimen name <sup>(*)</sup>	$f_v$	$f_{v,res}$	$G_{f-II}$
	MPa	MPa	N/mm		MPa	MPa	N/mm		MPa	MPa	N/mm
16BF	0.22	0.12	0.034	16BD	0.47	0.34	0.094	16BC	0.69	0.52	1.036
16BH	0.25	0.12	0.046	16BE	0.48	0.33	0.096	16BG	0.73	0.60	0.368
16BI	0.33	0.11	0.076	16BN	0.42	0.32	0.221	16BA	0.72	0.62	0.011
Average	<b>0.27</b>	<b>0.12</b>	<b>0.05</b>	Average	<b>0.46</b>	<b>0.33</b>	<b>0.14</b>	Average	<b>0.71</b>	<b>0.58</b>	<b>0.47</b>
St. dev.	<b>0.06</b>	<b>0.01</b>	<b>0.02</b>	St. dev.	<b>0.03</b>	<b>0.01</b>	<b>0.07</b>	St. dev.	<b>0.02</b>	<b>0.05</b>	<b>0.52</b>
C.o.V.	<b>0.22</b>	<b>0.05</b>	<b>0.42</b>	C.o.V.	<b>0.08</b>	<b>0.03</b>	<b>0.53</b>	C.o.V.	<b>0.03</b>	<b>0.09</b>	-

<sup>(\*)</sup> Complete specimen name starting with TUD\_MAT-.

Table 13 lists the shear properties for both the standard and modified triplet tests. It should be mentioned that instead of applying 1.0 MPa pre-compression stress (suggested by the standards), the pre-compression stress of 1.2 MPa was applied for both tests on the standard and modified triplets. In the case of testing on the modified triplet specimens, one sample was tested at pre-compressive stress of 1.0 MPa; the results are in line with the test performed for pre-compression level of 1.2 MPa.

The initial shear strength obtained from the tests on the standard triplets shows lower values than the initial shear strength obtained from the tests on the modified triplets. The coefficient of friction for the standard triplets shows higher value than those of modified triplets. Although, there is a difference between the obtained results from tests on the two types of the adopted samples, the results of modified triplets are almost in line with those of standard triplets.

Table 13 - Shear properties of standard triplets and modified triplets.

Property	Symbol	Unit	Standard triplets	Modified triplets
Initial shear strength	$f_{v0}$	MPa	0.11	0.18
Coefficient of friction	$\mu$		0.52	0.46
Angle of internal friction	$\alpha$		27.5°	24.7°
Residual shear strength	$f_{res,v}$	MPa	0.01	0.03
Residual coefficient of friction	$\mu_{res}$		0.55	0.48
Residual angle of internal friction	$\alpha_{res}$		28.8°	25.6°

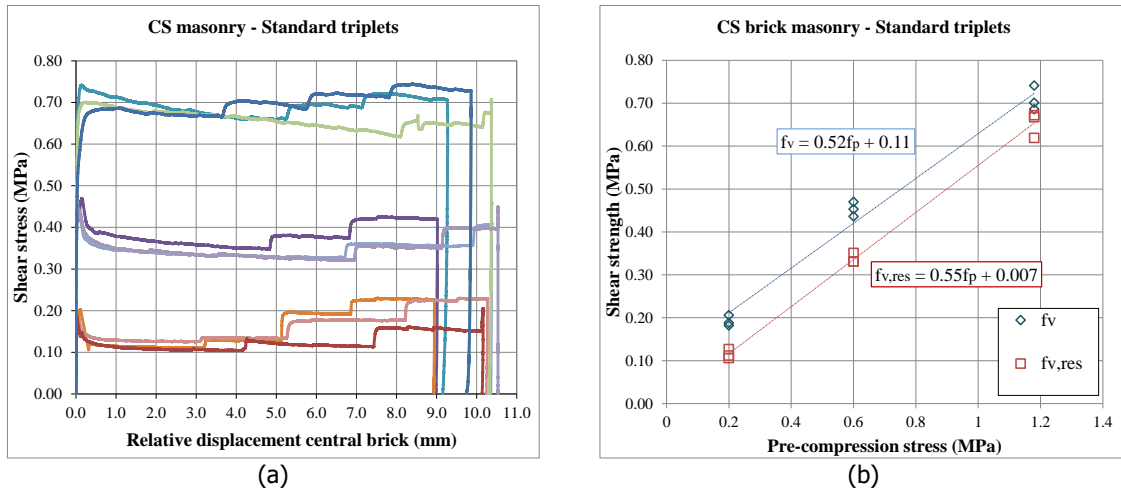


Figure 20 – Shear test results for standard triplets: (a) shear stress versus relative displacement of the central brick (LVDTs readings); (b) shear strength versus pre-compression stress.

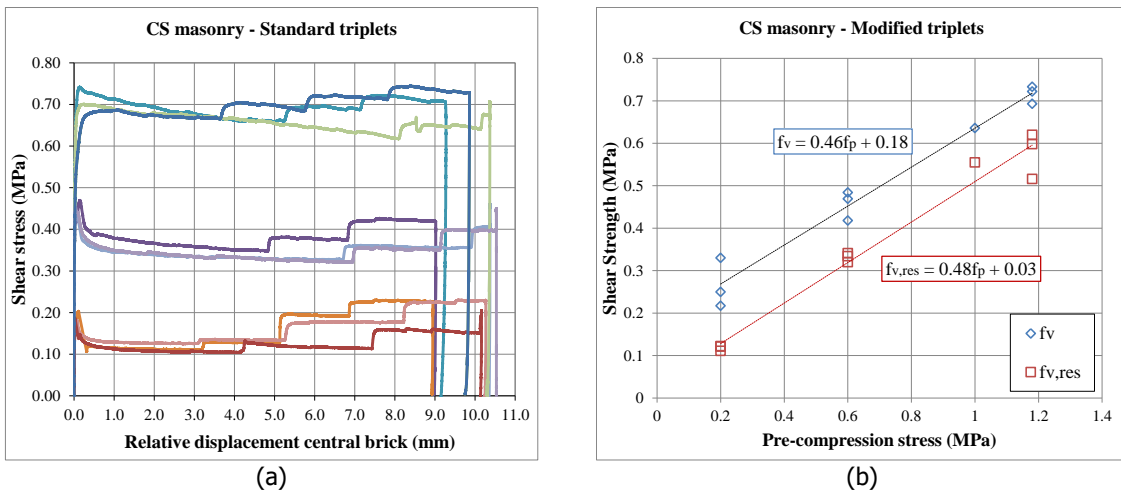


Figure 21 – Shear test results for modified triplets: (a) shear stress versus relative displacement of the central brick (LVDTs readings); (b) shear strength versus pre-compression stress.

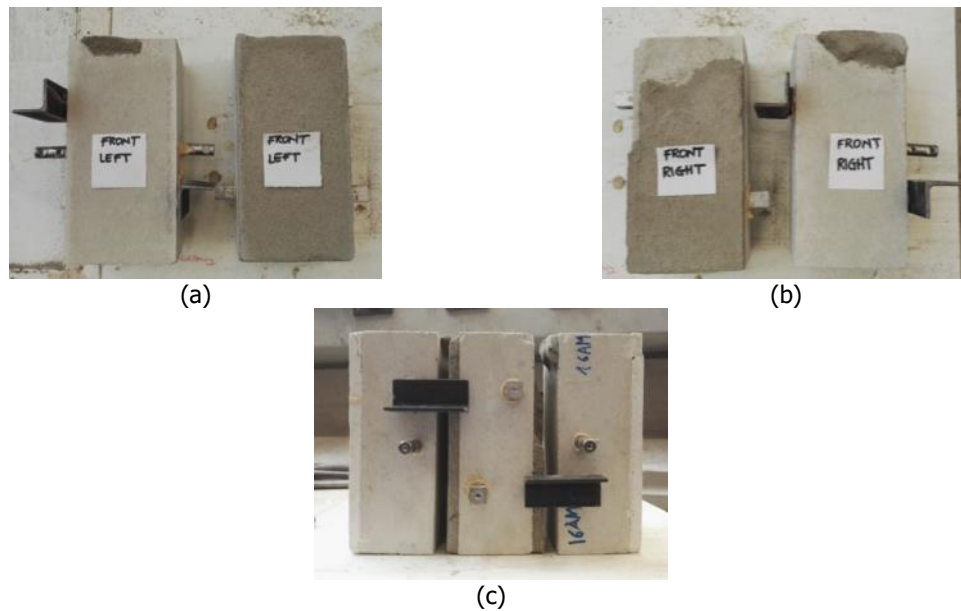


Figure 22 – Crack pattern of standard triplets under shear test: (a) front-left joint; (b) front-right joint; (c) front view.

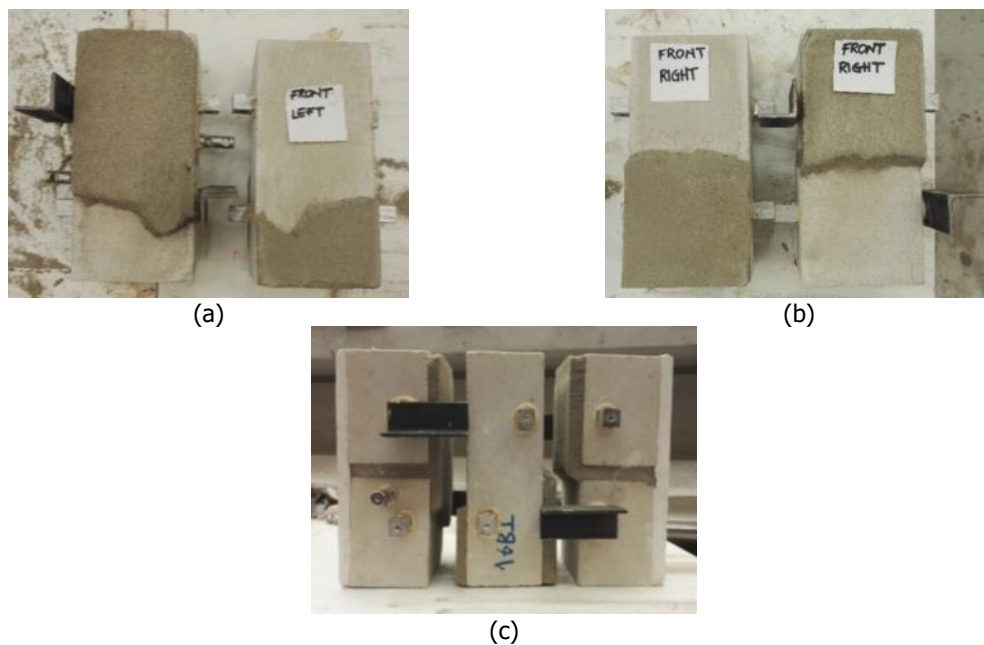


Figure 23 – Crack pattern of modified triplets under shear test: (a) front-left joint; (b) front-right joint; (c) front view.

The tests on triplets were aimed to have a sufficiently reliable measure of the bed joint shear strengths under controlled normal stress. These results will be used as a benchmark for the interpretation of the shove tests. In order to get better insight into the initial shear strength, one sample for each type of triplet was tested at a very low pre-compressive stress of 0.05 MPa. The measured data are shown in Figure 24 with dark blue dots. To get more precise envelope at residual state, the pre-compression load was increased and kept constant at different levels in the residual phases. The measured data are shown in Figure 24 with red filled dots.

Figure 24 shows the shear properties for the standard and modified triplet tests, compiling the data measured according to the testing protocols and all the data including the additional ones measured for the correlation purposes.

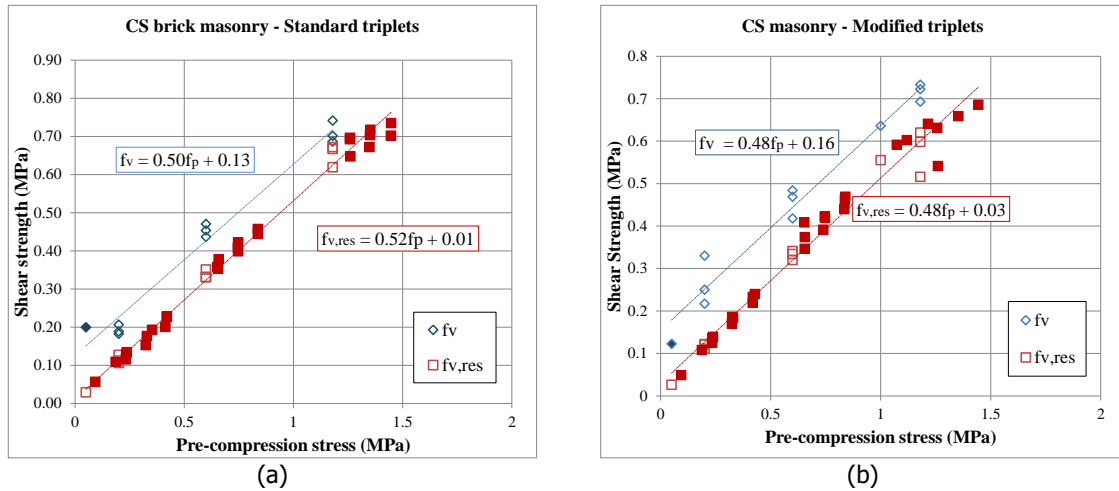


Figure 24 – Shear strength versus pre-compression stress for all the measured data: (a) standard triplet; (b) modified triplet.

Table 14 shows the comparison between the shear properties of the standard triplet specimens build in the first construction phase and the standard triplet build in the third construction phase. The shear properties for the third construction phase are reported considering all the measured data, as shown in Figure 24. Similar initial shear strength is obtained in the two periods, while an increase of the coefficient of friction is observed for the specimens build in the third construction phase. Additionally, for the specimens build in the third construction phase the coefficient of friction is constant both for the initial and residual stresses, while for the specimens build in the first construction phase a friction-hardening behaviour was observed.

Table 14 - Comparison between the results of tests on standard triplets at two phases of construction.

Property	Symbol	Unit	First phase (Apr/May2015)	Third phase (Aug. 2016)
Initial shear strength	$\bar{f}_{v0}$	MPa	0.14	0.13
Coefficient of friction	$\mu^*$		0.43	0.50
Angle of internal friction	$\alpha^*$		23°	26.6°
Residual initial shear strength	$\bar{f}_{res,v0}$	MPa	0.03	0.01
Residual coefficient of friction	$\mu^*_{res}$		0.54	0.52
Residual angle of internal friction	$\alpha^*_{res}$		28°	27.5°

## 9 Summary and properties overview

The main goal of the WP1a is to qualify the firms with respect to the in-situ activities, while the sub-goal is to study the correlation between destructive tests (DT) and non/slightly destructive tests (NDT/SDT). As a result, NDT/SDT were performed in a controlled laboratory environment on the replicated calcium silicate brick masonry walls. In addition, DT were performed on the companion samples by TUDelft. This document reports the material properties of CS brick masonry by performing DTs on the replicated specimens. These material properties reported in this document can be used to further study the correlation between NDT and SDT, as well as to be used as a benchmark to interpret the obtained results of SDT (e.g. shove test).

Characterising the material properties of CS brick masonry have been planned in the large-scale testing campaign of 2015, at TU Delft. The material characterisation of masonry was performed by investigating its behaviour under compressive, bending and shear loading. For every type of test, both the maximum capacity of the masonry and the stress-strain relationship were investigated. To characterise the orthotropic behaviour of masonry, both compressive and out-of-plane bending tests were performed along two loading directions: one generating cracking parallel to the bed joints and one generating cracking perpendicular to the bed joints. The tests were performed in two periods: in the first construction period (March-April 2015) specimens for the material (MAT) and component tests (COMP) were built, while in the second period (September 2015) the construction of the assemblage took place, and a limited number of material tests was repeated. The results of the second testing period are in line with the one obtained in the first period, as shown in Table 15. As a result, the complete overview of the behaviour of CS brick masonry has been established in the large-scale testing campaign of 2015.

In the pre-qualification project, the companion samples were constructed, aside from the large-scale walls adopted for the NDT/SDT testing activities by firms. The companion samples were adopted with the aim to be subjected to DT. The results of the last testing period are listed in Table 15. The compressive strength of mortar, the compressive strength of masonry and the shear properties obtained in the last construction period are in line with those obtained in the first and second periods. On the contrary, the obtained values of the Young's modulus are higher than those measured in the previous periods. This difference can be inputted to the different environmental conditions, the mixing technique adopted for the mortar and the aging of the pre-mix mortar. The average of the obtained results at different construction periods are reported in Table 15 and can be used as a benchmark to reflect on the behaviour of the CS brick masonry studied in the WP1a.

Table 15 – Overview of mechanical properties for calcium silicate masonry.

Property	Symbol	Unit	Calcium silicate masonry											
			First period (Mar/Apr 2015)			Second period (Sept 2015)			Third period (Aug 2016)			All results		
			Average	St. dev.	C.o.V.	Average	St. dev.	C.o.V.	Average	St. dev.	C.o.V.	Average	St. dev.	C.o.V.
Compressive strength of mortar	$f_m$	MPa	<b>6.59</b>	0.66	0.10	<b>7.24</b>	0.60	0.08	<b>7.57</b>	0.46	0.06	<b>7.27</b>	1.02	0.14
Flexural strength of mortar	$f_{mt}$	MPa	<b>2.79</b>	0.22	0.08	<b>3.56</b>	0.18	0.05	<b>3.21</b>	0.18	0.05	<b>3.11</b>	0.36	0.12
Normalised compressive strength of masonry unit	$f_b$	MPa	-	-	-	-	-	-	<b>13.26</b>	1.71	0.13	<b>13.26</b>	1.71	0.13
Compressive strength of masonry in the direction perpendicular to bed joints	$f'_m$	MPa	<b>5.93</b>	0.52	0.09	<b>5.76</b>	0.59	0.10	<b>6.35</b>	0.32	0.05	<b>6.01</b>	0.53	0.09
Elastic modulus of masonry in the direction perpendicular to bed joints	$E_1$	MPa	<b>3174</b>	467	0.15	<b>3340</b>	800	0.24	<b>4972</b>	568	0.11	<b>3828</b>	1033	0.27
	$E_2$	MPa	<b>5091</b>	1774	0.35	<b>4536</b>	1888	0.42	<b>8206</b>	1008	0.12	<b>5945</b>	2260	0.38
	$E_3$	MPa	<b>2746</b>	282	0.10	<b>3005</b>	568	0.19	<b>4265</b>	527	0.12	<b>3339</b>	824	0.25
Cyclic modulus of masonry in the direction perpendicular to bed joints	$E_{c1}$	MPa	-	-	-	-	-	-	<b>9281</b>	883	0.10	<b>9281</b>	883	0.10
	$E_{c2}$	MPa	-	-	-	-	-	-	<b>8854</b>	730	0.08	<b>8854</b>	730	0.08
	$E_{c3}$	MPa	-	-	-	-	-	-	<b>6907</b>	726	0.11	<b>6907</b>	726	0.11
Poisson ratio of masonry in the direction perpendicular to bed joints	$\nu$		<b>0.14</b>	0.01	0.07	<b>0.18</b>	0.07	0.41	<b>0.16</b>	0.03	0.19	<b>0.16</b>	0.05	0.32
Fracture energy in compression for loading perpendicular to bed joints*	$G_{f-c}$	N/mm	<b>31.5</b>	5.1	0.16	<b>21.8</b>	3.6	0.17	<b>20.0</b>	3.43	0.17	<b>20.0</b>	3.43	0.17
Flexural bond strength	$f_w$	MPa	<b>0.27</b>	0.12	0.43	<b>0.28</b>	0.08	0.29	<b>0.12</b>	0.01	0.12	<b>0.26</b>	0.11	0.40
Masonry (bed joint) initial shear strength	standard triplets $f_{v0}$	MPa	<b>0.14</b>	-	-	-	-	-	<b>0.13</b>	-	-	<b>0.14</b>	0.007	0.05
	modified triplets $f'_{v0}$		-	-	-	-	-	-	<b>0.16</b>	-	-	<b>0.16</b>	-	-
Masonry (bed joint) shear friction coefficient	standard triplets $\mu$		<b>0.43</b>	-	-	-	-	-	<b>0.50</b>	-	-	<b>0.47</b>	0.05	0.11
	modified triplets $\mu^*$		-	-	-	-	-	-	<b>0.48</b>	-	-	<b>0.48</b>	-	-
Residual masonry (bed joint) shear strength	standard triplets $f_{v0,res}$	MPa	<b>0.03</b>	-	-	-	-	-	<b>0.01</b>	-	-	<b>0.02</b>	0.01	0.71
	modified triplets $f'_{v0,res}$		-	-	-	-	-	-	<b>0.03</b>	-	-	<b>0.03</b>	-	-
Residual masonry (bed joint) shear friction coefficient	standard triplets $\mu_{res}$		<b>0.54</b>	-	-	-	-	-	<b>0.52</b>	-	-	<b>0.53</b>	0.01	0.03
	modified triplets $\mu^*_{res}$		-	-	-	-	-	-	<b>0.48</b>	-	-	<b>0.48</b>	-	-

\* Different methods were adopted to evaluate the fracture energy in the last campaigns and current campaign. Therefore, only the results of the current campaign are reported in the average of all results.

## References

- [1] Esposito R., Messali F., Crielaard R., Rots J.G. "Tests for the characterization of replicated masonry, Delft University of Technology, Dept. Structural Engineering, April 2016.
- [2] EN 1996-1-1+A1 (2013). Eurocode 6 – Design of masonry structures – Part 1-1: General rules for reinforced and unreinforced masonry structures. Nederlands Normalisatie-instituut (NEN).
- [3] Protocol for the construction of masonry, ver. 18-03-2015.
- [4] EN 1015-3 (1999). Method of test for mortar for masonry – Part 3: Determination of consistence of fresh mortar (by flow table). Nederlands Normalisatie-instituut (NEN).
- [5] EN 1015-11 (1999). Method of test for mortar for masonry – Part 11: Determination of flexural strength of hardened mortar. Nederlands Normalisatie-instituut (NEN).
- [6] EN 772-1 (2000). Methods of test for masonry units - Part 1: Determination of compressive strength. Nederlands Normalisatie-instituut (NEN).
- [7] Ad Vermeltfoort. (2005) Brick-mortar interaction in masonry under compression, PhD thesis, Eindhoven University of Technology.
- [8] Jafari, S., Panoutsopoulou, L. and Rots, J.G. Tests for the characterisation of original Groningen masonry. Delft University of Technology. Final report 18 December 2015.
- [9] EN 1052-1 (1998). Method of test masonry – Part 1: Determination of compressive strength. Nederlands Normalisatie-instituut (NEN).
- [10] Procedures of in-situ test. Protocol for the in-situ testing of masonry. 2015; EUCentre Foundation and Risk Centre Pavia.
- [11] Van Mier, J.G.M. (1984) Strain Softening of concrete under multiaxial loading conditions, PhD thesis, Eindhoven University of Technology.
- [12] Lourenco, P.B., De Borst, R. and Rots, J.G. (1997). A plane stress softening plasticity model for orthotropic materials. International Journal for Numerical Methods in Engineering 40(21), 4033-4057.
- [13] EN 1052-5 (2005). Method of test masonry – Part 5: Determination of bond strength by bond wrench method. Nederlands Normalisatie-instituut (NEN).
- [14] EN 1052-3 (2002). Method of test masonry – Part 3: Determination of initial shear strength. Nederlands Normalisatie-instituut (NEN).

## Appendix A

This appendix reports the declaration of performance for the construction materials used during the experimental campaign.

Table A.1 refers to the calcium silicate bricks.

Table A.2 lists the characteristic of mortars for calcium silicate masonry.

Table A.1 – Declaration of performance of calcium silicate bricks ([www.calduran.nl/producten/stenen/](http://www.calduran.nl/producten/stenen/)).

Wanddikte in mm	Type steen	Afmetingen (BxHxL) mm	Gewicht per stuk in kg	Druksterkte N/mm <sup>2</sup>	Aantal per m <sup>2</sup> (incl. voeg)	Kg Metselfix per m <sup>2</sup> excl. morsverlies
55 (klamp)	Waalformaat	102x55x214	2	16	39,9	12,3
72 (klamp)	Amstelformaat	102x72x214	3	16	39,9	16,1
82 (klamp)	Maasformaat	102x82x214	3	16	39,9	18,4
102	Waalformaat	102x55x214	2	16	68,7	33,7
102	Amstelformaat	102x72x214	3	16	54,4	28,3
102	Maasformaat	102x82x214	3	16	48,5	26,1
150	Dubbel amstelformaat	150x72x214	4	16	54,4	42,5
150	Dubbel maasformaat	150x82x214	5	16	48,5	39,2




Table A.2 – Declaration of performance for calcium silicate masonry mortar (www.remix.nl)

1. Unieke identificatie	Sakrete Brickfix	Nr. RV001 – 2013-11-05
2. Aanduiding	<b>M5 type G (voor algemene toepassing) conform NEN-EN 998-2: 2010</b>	
3. Toepassing	<b>Metselmortel voor binnen- en buitentoepassing</b>	
4. Naam en contactadres fabrikant	<b>Remix Droge Mortel BV Hoofdstraat 41 NL-9531 AB Borger Postbus 3 NL-9530 AA Borger</b>	
5. Naam en contactadres gemachtigde	geen	
6. Systeem voor de beoordeling en verificatie van de prestatiebestendigheid	systeem 2+	
7. Activiteit van de aangemelde certificatie instantie zoals vereist in de geharmoniseerde norm	De aangemelde certificatie instantie Kiwa BMC B.V. (identificatienummer 0620) heeft onder systeem 2+ de initiële inspectie van de productie-installatie en van de productiecontrole in de fabriek uitgevoerd en zal tevens de permanente bewaking, beoordeling en evaluatie van de productiecontrole op zich nemen. Op basis daarvan is het conformiteitscertificaat voor de productiecontrole in de fabriek verstrekt.	
8. Europese Technische beoordeling	niet van toepassing	
9. Aangegeven prestaties		
<b>Essentiële kenmerken (NEN-EN 998-2)</b>	<b>Prestaties</b>	<b>Europees beoordelingsdocument</b>
5.4.1 druksterkte	M5	NEN-EN 998-2:2010
5.4.2 Hechtsterkte (kruisproef)	$\geq 0,3 \text{ N/mm}^2$ (tabelwaarde)	
5.2.2 chloridegehalte	$< 0,1 \text{ M.-%}$	
5.6 brandklasse	A1	
5.3.3 waterabsorptie	$\leq 0,40 \text{ kg/(m}^2 \cdot \text{min}^{0,5})$	
5.4.4 waterdampdoorlaatbaarheid	15/35 (tabelwaarde)	
5.4.6 warmtegeleidbaarheid	$\leq 0,82 \text{ W/(m}^2 \cdot \text{K)}$ P = 50% $\leq 0,89 \text{ W/(m}^2 \cdot \text{K)}$ P = 90% (tabelwaarden)	
5.4.7 duurzaamheid	NPD	
vrijkomende gevaarlijke bestanddelen	NPD	
10. De prestaties van het in de punten 1 en 2 omschreven product zijn conform de in punt 9 aangegeven prestaties. Deze prestatieverklaring wordt verstrekt onder de exclusieve verantwoordelijkheid van de in punt 4 vermelde fabrikant.		
Borger, 5 November 2013		Getekend: AGAR Holding BV
 Remix Droge Mortel BV is een werkmaatschappij van Agar Holding BV.		 Mr. R.M.P.P. Reef Algemeen directeur

# **SLIGHTLY-DESTRUCTIVE TESTS ON CORES: METHOD VALIDATION AND CORRELATIONS**

*TU Delft large-scale testing campaign 2016 – WP1b*

Authors	Samira Jafari s.jafari@tudelft.nl Lucia Licciardello l.licciardello@tudelft.nl Rita Esposito r.esposito@tudelft.nl
Lab collaborators	Elena Casprini
Address	Delft University of Technology Faculty of Civil Engineering and Geosciences Stevinweg 1, 2628 CN, Delft

 <p> Faculty of Civil Engineering and Geosciences  Stevinweg 1  2628 CN Delft  PO 5048  2600 GA Delft  <a href="http://www.citg.tudelft.nl">www.citg.tudelft.nl</a> </p>		<b>REPORT</b>	
		<i>Title:</i> Slightly-destructive tests on cores: method validation and correlations	
		<i>Author(s):</i> Samira Jafari Lucia Licciardello Rita Esposito	
		<i>Date:</i> 25 December 2017	
<i>Client(s):</i> Nederlandse Aardolie Maatschappij B.V.		<i>Version:</i> 01	<i>Status:</i> Final
<i>Project number:</i> C31B67	<i>Project name:</i> Testing program NAM 2016	<i>File reference:</i> C31B67WP1-13	
<i>Cite as:</i> Jafari, S. Licciardello, L. Esposito, R. (2017). Slightly-destructive tests on cores: method validation and correlations . Delft University of Technology. Report number C31B67WP1-13, version 01, 25 December 2017.			

TU Delft Document checking				
	Prepared by		Checked by	
Name	Samira Jafari		Rita Esposito	
Signature	SJ		RE	
Revision History				
Document		Revision		
Version	Date	Date	Author	Description

***Copyright statement***

All rights reserved. No part of this publication may be reproduced, stored in a retrieval system of any nature, or transmitted, in any form or by any means, electronic, mechanical, photocopying, recording or otherwise, without the prior written permission of TU Delft.

***Liability statement***

TU Delft and those who have contributed to this publication did exercise the greatest care in putting together this publication. However, the possibility should not be excluded that it contains errors and imperfections. Any use of this publication and data from it is entirely on the own responsibility of the user. For everybody who has contributed to this publication, TU Delft disclaims any liability for damage that could result from the use of this publication and data from it, unless the damage results from malice or gross negligence on the part of TU Delft and/or those who have contributed to this publication.

## Table of Contents

1	Introduction.....	41
2	Nomenclature .....	42
2.1	Symbols.....	42
2.2	Abbreviations.....	43
3	Literature review .....	44
3.1	Compression tests on cores .....	44
3.2	Splitting tests on cores for the determination of shear properties .....	46
4	Characterisation of material components used in the TU Delft testing campaign.....	47
4.1	Properties of mortar .....	48
4.2	Properties of brick.....	49
5	Compression properties of masonry .....	50
5.1	Testing procedure.....	50
5.2	Experimental results.....	51
5.2.1	Single wythe clay brick masonry.....	52
5.2.2	Double wythe clay brick masonry .....	58
5.2.3	Calcium silicate brick masonry .....	66
5.2.4	Summary of the compression properties .....	74
6	Evaluation of shear properties .....	76
6.1	Testing procedure.....	76
6.2	Experimental results.....	76
6.2.1	Single wythe clay brick masonry.....	77
6.2.2	Double wythe clay brick masonry .....	82
6.2.3	Calcium silicate brick masonry .....	88
6.2.4	Summary of the shear properties.....	95
7	Spatial variability of the properties across the height of wall.....	96
8	Meta-analysis .....	98
9	Conclusions.....	100
	References .....	102
	Appendix A.....	103
	Appendix B.....	107

## 10 Introduction

Material characterisation of masonry can be pursued either by performing destructive tests (DT) in laboratory on the samples extracted from existing masonry buildings or by slightly-destructive tests (SDT) in-situ. Although the laboratory tests have the advantage of directly providing properties; such as strength, stiffness and stress-strain relationship, technical challenges as well as devastating sampling method put severe constraints on this technique. On the contrary, in-situ testing techniques have the advantage of being slightly-destructive and requiring less time; however, the accuracy of the obtained results is a matter of uncertainty.

As it was puzzled in the experimental campaign of 2015, a clear correlation has not been established between the result of standardised SDT results (double flat jack test [15] and shove test [16]) and standardised DT (compression tests [17] and shear-compression on wallets [18]). Therefore, an experimental study was conducted, within the “NAM Structural Upgrading Project” developed at TU Delft in 2016, aiming at investigating the tests on cores as a new slightly-destructive technique for a quick identification of masonry material properties.

Tests on cylindrical cores have been recently introduced as a novel in-situ testing method to identify the properties of existing clay brick masonry. Currently, some researchers reported promising results showing that the adopted methodology causes minor damage to the structures and it allows a direct estimation of the mechanical properties. To evaluate the mechanical properties of masonry, cores extracted perpendicular to the surface of a wall are subjected to splitting tests to estimate the compressive and shear properties of the masonry. The expected correlation between the properties obtained from splitting tests on core samples and those properties obtained from standard destructive tests on the wallets is shown in Table 16.

In this report, the validation of the core testing as a suitable technique for the characterisation of masonry material properties is presented including the correlation with the properties obtained by destructive tests. A brief overview of available literature information regarding the core testing is given in Section 12; an extensive overview can be found in Ref. [19]. The correlation established in the literature between the mechanical properties obtained from tests on masonry cores and those standard tests on the companion samples are outlined in this section. Eventually, based on the literature findings and the conclusions drawn, a research project has been set-up. The applicability of the core testing method is investigated for the replicated brick masonry; both solid clay and calcium silicate brick masonry. The masonry constituents are characterised in Section 13. Section 14 and Section 15 deal with the results of the core subjected to compressive load and splitting load. The compression properties and the shear properties of masonry are compared with the results of the destructive companion samples.

To investigate the possible spatial variability of the masonry properties across the wall a sampling strategy was defined aiming to extract the cores at different locations, which is briefly discussed in Section 16. The obtained data from the current research and information from the literature are incorporated and discussed in Section 8. Concluding remarks are presented in Section 9.

Table 16 – Correlation between SDT on core samples and DT on masonry wallets.

Type of test		Standardised test DT	
		EN1052-1:1998	EN1052-3:2005
		Compression test	Shear tests
Non-standardised SDT	Cores subjected to the compressive load		
	Cores subjected to the splitting load		

## 11 Nomenclature

### 11.1 Symbols

This report adopts mainly the nomenclature used in Eurocode 6 [20]. In addition, symbols used in the codes for testing are adopted.

$\alpha$	Masonry (bed joint) angle of internal friction
$\nu$	Poisson ratio of masonry
$\mu$	Masonry (bed joint) friction coefficient
$\mu_{res}$	Masonry (bed joint) residual shear strength coefficient
$d_1$	Distance between bearing supports
$f_m$	Compressive strength of masonry mortar
$f_{mt}$	Flexural strength of masonry mortar
$f'_m$	Compressive strength of masonry in the direction perpendicular to the bed joints
$f_p$	Compression stress
$f_v$	Shear strength
$f_{v0}$	Masonry (bed joint) initial shear strength
$f_b$	Normalised compressive strength of masonry unit
$f_{bt}$	Flexural strength of masonry unit
$l_s$	Length of the masonry specimen as built
$l_p$	Length of the loading plate for compression tests on mortar specimens
$l_u$	Length of the masonry unit as used in the construction of masonry
$h_s$	Height of the masonry specimen as built
$h_u$	Height of the masonry unit as used in the construction
$t_s$	Thickness of the masonry specimen as built
$t_u$	Thickness of the masonry unit as used in the construction of masonry
$A_s$	Cross sectional area of the specimen parallel to the bed joints (shear test)
$E_1$	Secant elastic modulus of masonry subject to a compressive loading perpendicular to the bed joints, evaluated at 1/3 of the maximum stress
$E_2$	Secant elastic modulus of masonry subject to a compressive loading perpendicular to the bed joints, evaluated at 1/10 of the maximum stress
$E_3$	Chord elastic modulus of masonry subject to a compressive loading perpendicular to the bed joints, evaluated at between 1/10 and 1/3 of the maximum stress
$F_{max}$	Maximum vertical load
$G_{f-c}$	Fracture energy in compression for loading perpendicular to the bed joints
$D$	Diameter of core
$L$	Length of core
$\Phi$	Width of cap

## 11.2 Abbreviations

Avg.	Average
St. dev.	Standard deviation
C.o.V.	Coefficient of variation
CS	Calcium silicate
LVDT	Linear variable differential transformer
NDT	Non-destructive test
SDT	Slightly-destructive test
DT	Destructive test



## 12 Literature review<sup>1</sup>

In this section, an overview of the literature information is presented. Based on this information the testing protocol has been derived [19].

### 12.1 Compression tests on cores

The great potential of using small diameter cores for assessing the compression properties of clay brick masonry has recently been shown by some researchers [8-12]. These researchers adopted companion compression tests on the masonry wallets or stacked-bonded prism to validate the testing method. The correlation between the results of tests on cores and companion samples for the compressive strength and the Young's modulus were investigated.

The International Union of Railway (UIC) [27] proposed a method to perform compression tests on cores with 150 mm in diameter, including two mortar bed joints and a head joint in the centre of the section. The UIC standard suggests conducting a minimum number of three compression tests on each kind of masonry, and preferably six tests if possible. The applicability of using 150 mm and 100 mm diameter cores were investigated for the clay brick masonry in the previous studies [8-12], even though further investigations are still essential in this field.

Brencich et al. [22], Ispir et al. [23] and Pelà et al. [24] adopted the same core geometry as proposed by the UIC. Moreover, Pelà et al. [24] introduced another type of 150 mm in diameter core consisting of only two bed joints. Sassoni et al. [11-12] studied the suitability of using 100 mm diameter cores, which were easier to extract from walls than the ones with 150 mm in diameter. They adopted two types of cores in their studies. The first type included a central bed joint, and the second type included one central bed joint and one head joint.

Figure 25 shows the ratio between the compressive strength obtained from performing tests on the masonry cores and those of companion destructive tests reported in the literature [8-12]. This ratio varies between 0.6 and 1.8 in different studies.

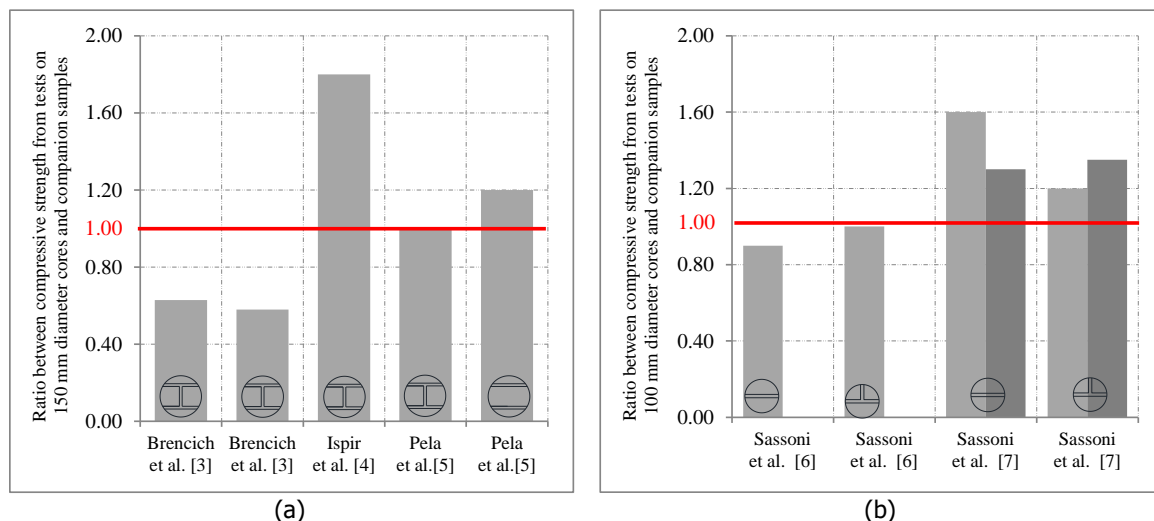


Figure 25 - Ratio between the compressive strength of cores and those of companion samples: (a) tests on cores with 150 mm in diameter; (b) tests on cores with 100 mm in diameter.

A ratio between results of tests on masonry cores and those of the companion samples was reported less than 1 by Brencich et al. [22]. This ratio deviates from the values reported in other studies. One reason for this outlier ratio might be explained by the stress concentration produced by imperfect contact between the steel cradles, used to distribute the compressive load, and the specimen. Instead of using steel cradles, Pelà et al. [24] and Sassoni et al. [11-12] suggested the use of high-strength mortar layers to cap the top and bottom part of the core in contact with the loading plates. An acceptable correspondence between the results of cores and companion samples were reported. The masonry cores completed with high-strength

<sup>1</sup> Parts of this section has been adapted from [21].

mortar to resemble the situation in a real wall, where the confinement effect is experienced. In addition, an optimum bond between the specimen and the high-strength mortar can be expected. Consequently, performing test on the masonry cores with casted high-strength mortar on their top and bottom is suggested.

A very high ratio of 1.8 was reported by Ispir et al. [23] between the compressive strength of core samples and those of companion samples. Since limited information was provided by them, no conclusions can be drawn.

Core geometries, both with head joint and without head joint, were investigated by Pelà et al. [24] and Sassoni et al. [11-12] to study influence of the vertical joint on the test results. From their studies, it was concluded that the collapse mechanisms in the masonry cores without head joint deviates from those of masonry companion samples subjected to compressive tests. However, it might be expected that in the absence of head joint, the compressive strength of masonry can be overestimated, particularly, in the case of masonry with weak mortar and strong brick. To gain deeper insight into the behaviour of masonry, cores with head joint are preferable to cores without head joint.

It is worth noting that a stack-bonded prism without head joint was adopted as companion sample by Pelà et al. [24]. Thus, it might be expected that the obtained results from companion samples are more comparable with those of cores without head joint. Consequently, it is suggested to adopt masonry wallets as a companion sample.

Comparing the results obtained by Pelà et al. [24] and Sassoni et al. [11-12] from tests on cores with different diameters, it can be concluded that both 100 mm and 150 mm diameter cores are able to adequately represent the compressive strength of masonry.

The ratio between the Young's modulus obtained from performing tests on the masonry cores and those of companion destructive tests reported in the literature is shown in Figure 2. The applicability of tests on core samples to evaluate the Young's modulus was investigated in the literature only for cores with 150 mm in diameter. This ratio varies between 0.3 and 1.3 in different studies. As shown in Figure 2, an acceptable correspondence was reported by Pelà et al. [24] for both types of cores (with and without head joint).

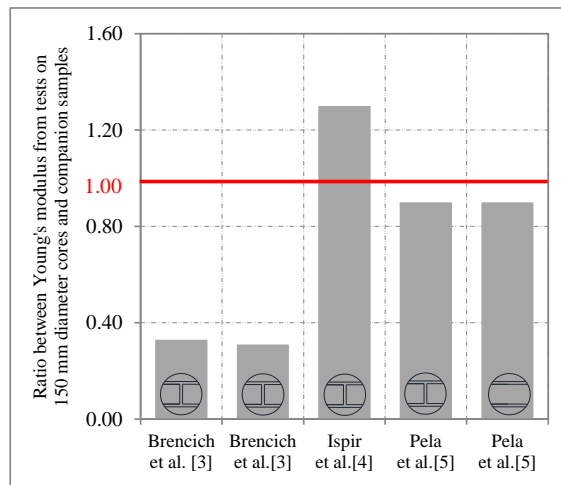


Figure 26 - Ratios between the Yong's modulus of cores and those of companion samples for cores with 150 mm in diameter.

## 12.2 Splitting tests on cores for the determination of shear properties

Performing splitting tests on masonry cores was firstly introduced by Benedetti et al. [28], to investigate the properties of mortar. Subsequently, this type of test was improved as a technique to study the shear properties of mortar-brick interface. However, very limited information was reported in the literature about the evaluation of shear properties of masonry by using this technique [15-16].

To determine the shear properties of the brick-mortar interface, Mazzotti et al. [29] and Pelà et al. [30] adopted cores with only a single bed joint subjected to splitting tests while they were inclined with respect to horizontal reference. A mixed compression-shear stress state was induced at the centre of the mortar joint. The shear stress and compression stress states could be derived, respectively, by projecting the failure stress in the parallel and orthogonal directions with respect to the rotated mortar layer. By employing Coulomb friction criterion, the initial shear strength and coefficient of friction were determined. The obtained results were compared with shear-compression tests on the companion samples. As shown in Figure 27, an acceptable correspondence between the results obtained from splitting tests on cores and from standard shear tests on the companion samples was observed. The applicability of cores with 100 mm and 90 mm in diameter was investigated in their research.

Different modes of failure were reported in the previous studies. The inclination angle of the mortar layer was found as a decisive factor in formation of the mode of failure. The observed different modes of failure at different mortar layer inclinations were reported as follows: (a) splitting of the cores, (b) mix of splitting and sliding along the mortar-brick interface and (c) sliding along the mortar-brick interface. For the masonry cores tested according to an inclination of 40°, 45° and 50°, the predominant observed failure mode was sliding along the brick-mortar interface. While the masonry cores that were tested at mortar layer inclinations of less than 40° and higher than 60° showed splitting and brick wedge detachment, respectively. The results obtained from performing tests on masonry cores at mortar layer inclination between 40° and 50° were used to determine the shear properties, since sliding along the brick-mortar interface was dominant failure mode.

To obtain the governing parameters of the Mohr-Coulomb failure criterion, the best-fit procedure was obtained by Mazzotti et al. [29] by taking into account the mean values for every considered angle. While the best-fit procedure was found by Pelà et al. [30] considering all the results for each inclination.

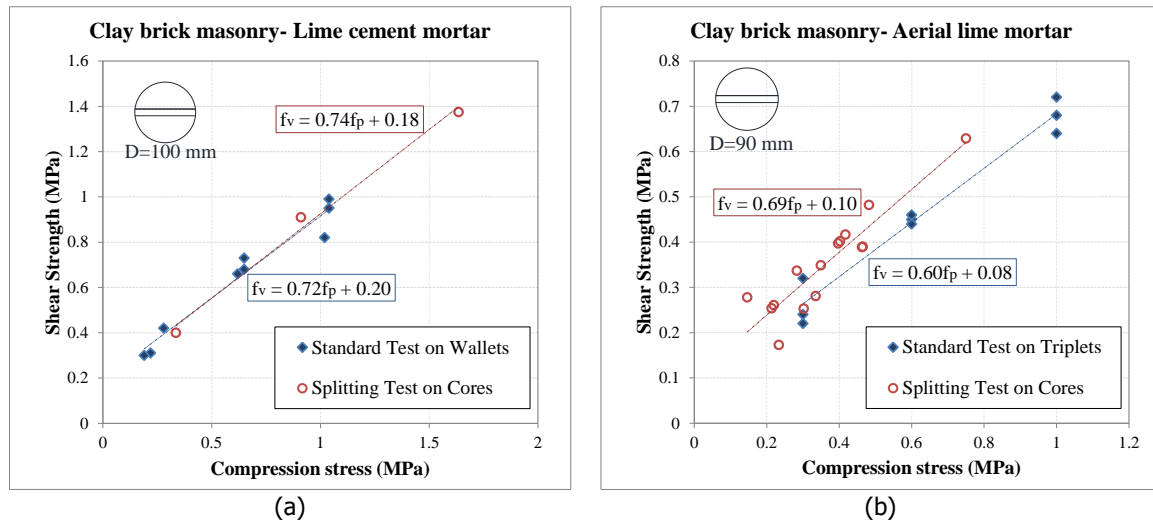


Figure 27 - Comparison between the results obtained from standard shear tests on the companion samples and splitting tests on the masonry cores with: (a) 100 mm in diameter [29]; (b) 90 mm in diameter [30].

### 13 Characterisation of material components used in the TU Delft testing campaign

The masonry walls to be used for the core drilling as well as the companion samples to be subjected to standardised destructive tests were constructed in the same period by employing the same materials. The specimens were built in the Stevin II laboratory at Delft University of Technology [31]. Two types of masonry were used: calcium silicate and solid clay brick masonry. The former was made of calcium silicate bricks and cement based mortar, while the latter was made of solid clay bricks and cement based mortar. The declarations of performance of the materials are reported in Appendix A.

Figure 28 shows the adopted masonry units. Their dimensions are defined considering the orientation of the masonry unit as used in the construction of the samples. This definition is consistently adopted in this report despite the position of the specimen in the test set-up. A similar consideration is applied to describe the dimensions of masonry specimens.



Figure 28 - Mean dimensions of: (a) solid clay brick; (b) calcium silicate brick.

Dedicated walls made of replicated calcium silicate brick masonry and double wythe clay brick masonry were built for extraction of the cores. The masonry cores were extracted, perpendicular to the surface of walls. A dry extraction process was preferred; however in the case of double wythe clay brick masonry a dry extraction procedure lead to loss of integrity of the core (Figure 29) and consequently a wet procedure was adopted. The layout of the sampling for both calcium silicate and double wythe clay brick masonry walls are specified in Figure 30 and Figure 29, respectively. To preserve the integrity of the replicated wallets during the core drilling, masonry walls were pre-compressed via pre-stressed rods connecting the bottom and top steel profiles placed on the walls. The applied pre-compression load was measured by using load cells. A sampling strategy to extract the core samples was specifically defined aiming to investigate the possible spatial variability of the masonry properties across the wall.

Additionally to the walls constructed for this purpose, limited number of cores was extracted from a single wythe clay brick masonry wall (TUD-COMP-22) previously subjected to in-plane shear-compression test. A wet extraction procedure was employed to drill cores.

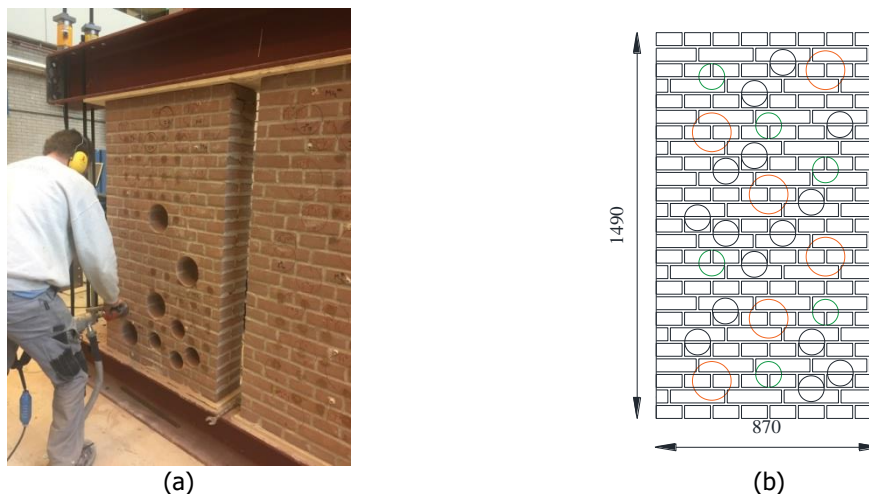


Figure 29 – Extraction of masonry cores from the double wythe clay brick masonry wall, dimensions are in mm.

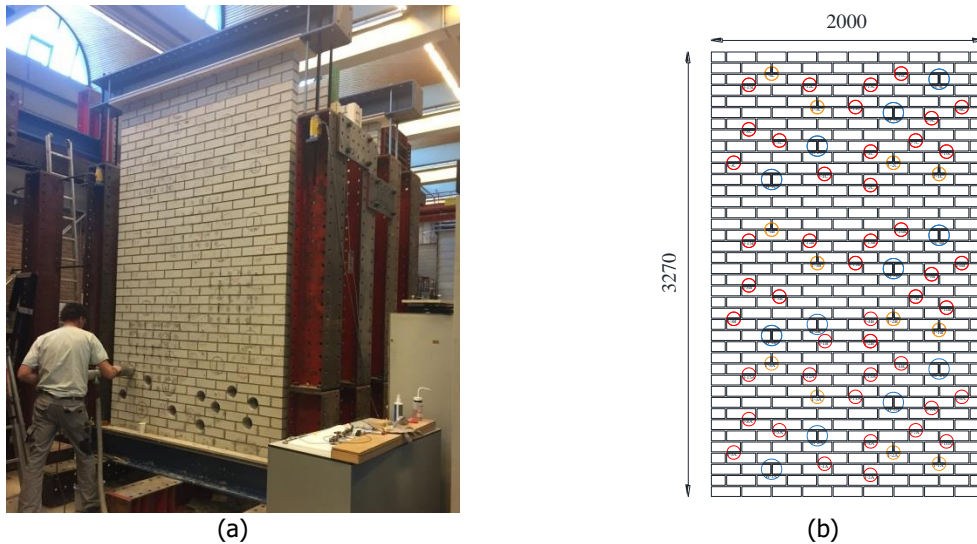


Figure 30 – Extraction of masonry cores from the calcium silicate masonry wall, dimensions are in mm.

### 13.1 Properties of mortar

During the masonry construction, mortar samples were collected and cast in moulds to be tested for the flexural and compressive strength in agreement with EN 1015-11:1999 [32]. At least three mortar specimens having a length of  $l_m = 160$  mm, a height of  $h_m = 40$  mm and thickness of  $t_m = 40$  mm were collected. The samples were stored in controlled conditions. The first two days they were placed in a fog room ( $T = 20 \pm 2$  °C,  $RH = 95 \pm 5\%$ ) with the moulds. After two days, they were unmoled and kept for other five days in the fog room. Eventually, they were placed in a conditioning room with a temperature of  $20 \pm 2$  °C and a relative humidity of  $50 \pm 5$  % until testing. The test was performed after at least 28 days from construction.

The flexural strength was determined by three-point bending test. The test set-up is composed by two steel bearing rollers having a diameter of  $10 \pm 0.5$  mm and spaced  $d_t = 100 \pm 0.5$  mm. A third roller is centrally placed on top of the sample to apply the load.

The compression test was performed on the broken pieces obtained from the flexural test, which have at least a length of 40 mm. The specimen is placed between two steel plates with a length of  $l_p = 40$  mm. For the interpretation of the results the specimens considered to be 40x40x40-mm.

For both tests, the load was applied without shock at a uniform rate so that failure occurred within a period of 30 to 90 s. The maximum load was recorded.

The flexural strength and compressive strength of the mortar used for the construction of the clay brick masonry and calcium silicate masonry are listed in Table 17.

Table 17 – Flexural and compressive strength of mortar.

Masonry type	Flexural tests				Compression test			
	No. test	$f_{mt}$	St. dev.	C.o.V.	No. test	$f_m$	St. dev.	C.o.V.
		MPa	MPa			MPa	MPa	
Clay brick masonry	54	1.40	0.17	0.12	108	3.81	0.34	0.09
CS brick masonry	75	3.21	0.18	0.05	150	7.57	0.46	0.06

### 13.2 Properties of brick

The normalised compressive strength of a masonry unit (brick) is determined in agreement with EN 772-1:2000 [33]. To estimate the compressive strength of masonry unit a single masonry unit having a length  $l_u$ , a height  $h_u$  and thickness  $t_u$  was subjected to compression load.

The flexure strength of the masonry unit was determined with the three-point bending test following NEN 6790:2005 [34]. The masonry units were tested by having the bed joint plane parallel to the loading direction. The specimen was supported by two roller bearings, which were placed 10 mm away from the end of the specimen. A third roller was used to apply load to the specimen at mid-span.

A summary of the compression and of the bending properties of calcium silicate and clay masonry unit are listed in Table 18.

Table 18 – Flexural strength and normalised compressive strength of masonry unit.

Masonry type	Flexural tests				Compression test			
	No. test	$f_{bt}$	St. dev.	C.o.V.	No. test	$f_b$	St. dev.	C.o.V.
		MPa	MPa			MPa	MPa	
Clay brick	9	6.31	0.72	0.11	9	28.31	2.92	0.10
CS brick	6	2.74	0.16	0.06	6	13.26	1.71	0.13



## 14 Compression properties of masonry

The applicability of 100 mm diameter cores with one central bed joint and one head joint as well as 150 mm diameter cores with two bed joints and one central head joint are being investigated within this study. The compressive strength, Young's modulus and the fracture energy are evaluated using the core technique.

The compressive properties of masonry obtained by the tests on cores are correlated with the results obtained by companion tests on wallets.

### 14.1 Testing procedure

The applicability of 100 mm as well as 150 mm diameter cores is being investigated within this study, as shown in Figure 31. At least three samples for each type of core were tested.



Figure 31 – Type of cores adopted in this study: (a) T-shaped with 100mm diameter; (b) H-shaped with 150mm diameter.

In order to ensure that the loaded faces of the specimen are levelled and parallel to each other, a high-strength mortar capping is used. The high strength mortar has been selected to have a compressive strength higher than 60 MPa. More information regarding the compression and bending properties of capping mortar can be found in Appendix B.

The specimens were instrumented with six LVDTs (Figure 32). Two vertical LVDTs were glued to the brick along the vertical axis of symmetry of the sample (LVDT1, LVDT4). Two horizontal LVDTs were attached to brick along the horizontal axis of symmetry of the sample (LVTD2, LVTD5). Two external horizontal LVDTs were attached to record the transversal expansion of the core (LVTD3, LVTD6). The vertical LVDTs have a measuring range of 10 mm with an accuracy of 1.0% and the horizontal ones have a measuring range of 2 mm with an accuracy of 0.2%. The test was carried out using a displacement-controlled set-up to explore the post-peak behaviour. A testing machine including a hydraulic jack with 300-ton capacity was used. A displacement rate of 0.002mm/s was adopted. The compression test was performed either monotonic or cyclic. The cyclic test was performed as follows: the first stage was cyclic loading within the elastic range (from 5% to 20% of the maximum expected load) and the second stage included applying a monotonic displacement.

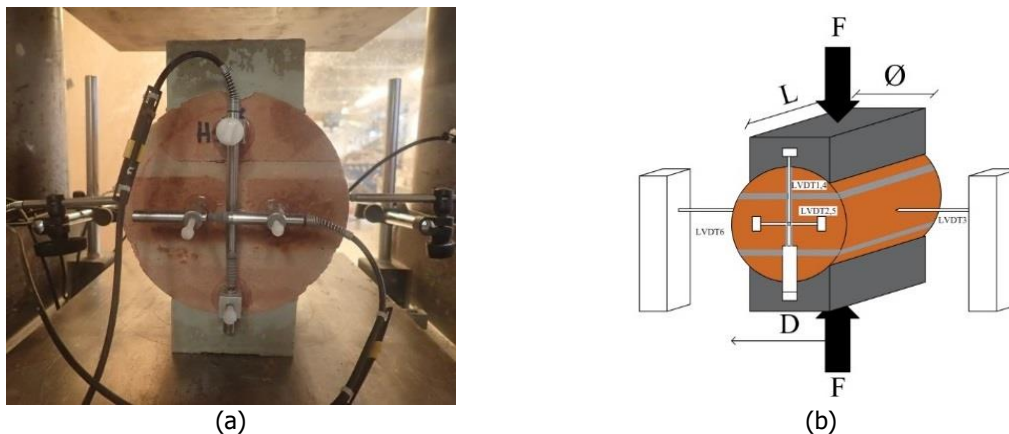


Figure 32 – Test set-up used to compress masonry cores.

## 14.2 Experimental results

The compressive strength of masonry core can be calculated either by considering the cross-section of the core or the cross-section of the cap, as suggested by Pelà et al. [24]. The two expressions introduced in the previous studies to find the compressive strength of the masonry cores are as follows:

$$f'_{m1,core} = \frac{F_{max}}{DL} \quad (1)$$

$$f'_{m2,core} = \frac{F_{max}}{\phi L} \quad (2)$$

where  $F_{max}$  is the maximum load,  $L$  is the length of cylindrical core,  $D$  is the core diameter and  $\phi$  is the cap width.

For the elastic modulus, three different estimates are adopted:

- $E_1$  is the secant elastic modulus evaluated at 1/3 of the maximum stress;
- $E_2$  is the secant elastic modulus evaluated at 1/10 of the maximum stress;
- $E_3$  is the chord Young's modulus evaluated between 1/10 or 1/5 and 1/3 of the maximum stress.

The stress state used to evaluate the elastic modulus is calculated by considering both the maximum cross-section of the core and the cross-section of the capping in order to obtain the best estimate.

The Poisson ratio  $\nu$  is determined in the elastic phase as the ratio between the lateral strains, which are evaluated in the direction perpendicular to the loading one, and the normal strains (Figure 33 b).

The displacement control procedure of the test allowed determining the post-peak behaviour of the material. The fracture energy in compression  $G_{fc}$  was determined as the area underneath the normal stress versus normal strain diagram, taking the height of the specimen into account. This concept was introduced by van Mier [35] for concrete material and subsequently applied to masonry by Lourenco [36].

The strain obtained by LVDTs' readings and by the jack's readings resulted similar in the post-peak phase. Consequently, the former were used to evaluate the pre-peak phase, while the latter were used to describe the post-peak phase, in which LVDTs may be detached from the specimen due to extensive cracking. The elastic modulus and the Poisson ratio were calculated based on the LVDTs readings, while the fracture energy was calculated based on the LVDTs' reading in the pre-peak and jack's reading in the post-peak phase.

The strain associated with peak strength, which is called peak strain,  $\epsilon_p$  is also reported.

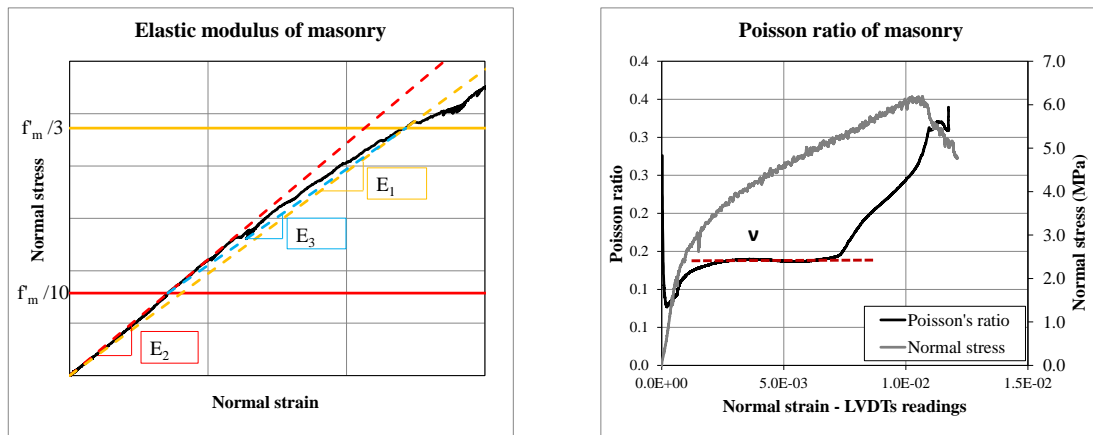


Figure 33 – Compression test on masonry: (a) three estimates of the elastic modulus; (b) evaluation of Poisson ratio.



### 14.2.1 Single wythe clay brick masonry

Figure 34 and Figure 35 show the stress-strain curve obtained from tests on T-shaped (diameter of 100 mm) and H-shaped (diameter of 150 mm) cores made of single wythe clay brick masonry, respectively. The graphs refer to the normal direction that is defined as the one parallel to the loading direction. The stress is calculated considering the cross-sectional area of the core. For both configurations, the stress-strain relationship in the normal direction presents a similar trend. The pre-peak stage was characterised by linear-elastic followed by an hardening behaviour until the peak. After reaching the peak stress, a linear softening behaviour was observed for both configurations.

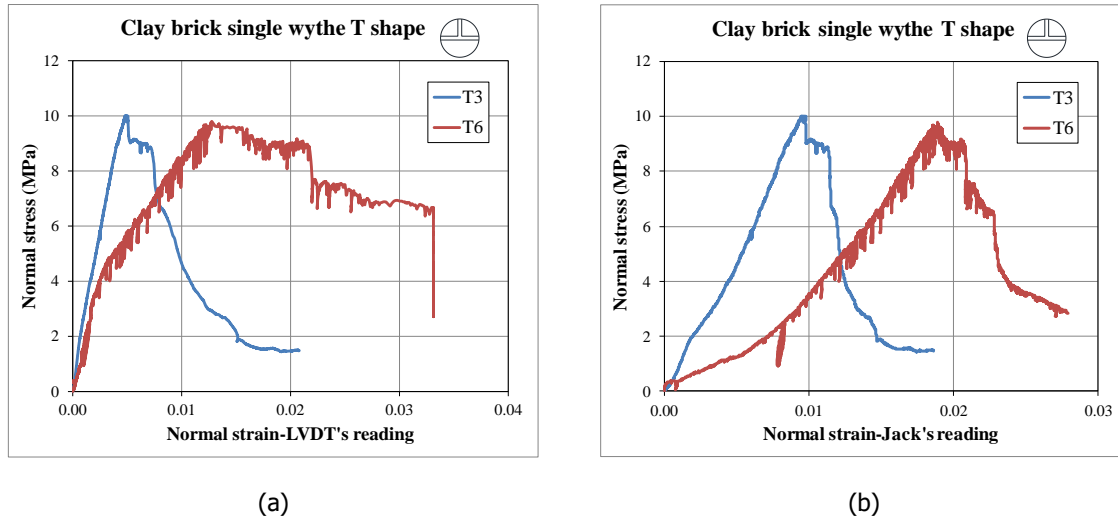


Figure 34 - Compression behaviour of T-shaped cores made of single wythe clay brick masonry: (a) normal strain obtained by LVDT's reading; (b) normal strain obtained by jack's reading.

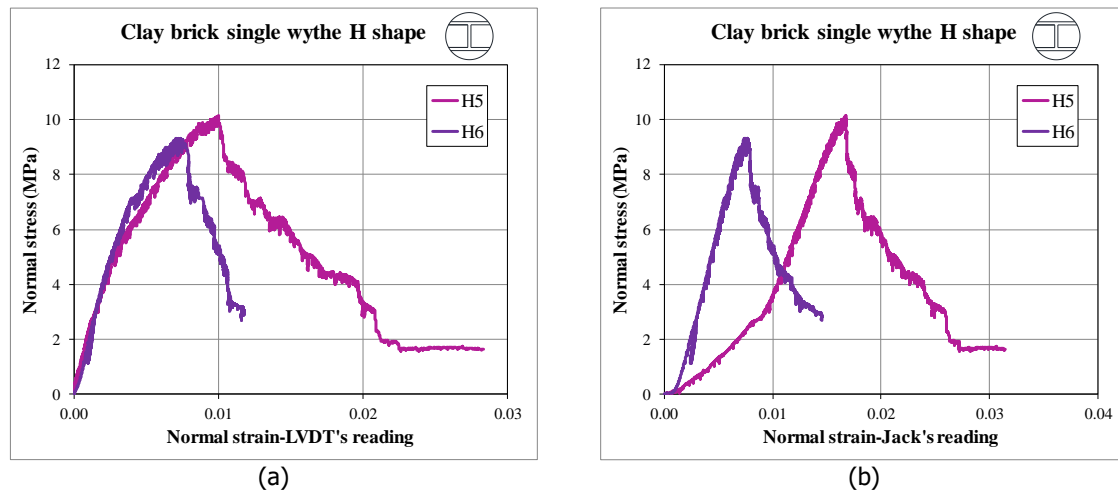


Figure 35 - Compression behaviour of H-shaped cores made of single wythe clay brick masonry: (a) normal strain obtained by LVDT's reading; (b) normal strain obtained by jack's reading.

Table 19 and Table 20 list the main experimental results obtained from tests on T-shaped and H-shaped cores made of single wythe clay brick masonry, respectively. The compression properties are evaluated both considering the cross-sectional area of the core and of the cap as a loaded area.

The crack pattern of the tested specimens is shown in Figure 36. The crack pattern was characterised by vertical cracks starting at the extremities of the regularisation cap and consequently spreading through the height of the specimens (Figure 37 and Figure 38). Consequently, it can be assumed that it is more appropriate to evaluate the compressive properties with respect to the cross-sectional area of the cap. It should be noted that during the test, damage in the cap was observed; this can affect the estimation of the fracture energy.

The compression properties of the cores evaluated with respect to the cross-sectional area of the cap, accordingly to the crack pattern, are shown in terms of histogram representation in Figure 39.

Table 19 – Compression properties of T-shaped cores made of single wythe clay brick masonry.

Specimen name (*)	Cross-section of core					Cross-section of cap					$\epsilon_{p,core}$	$\nu_{core}$
	$f'_{m,core}$	$E_{1,core}$	$E_{2,core}$	$E_{3,core}$	$G_{f-c,core}$	$f'_{m,cap}$	$E_{1,cap}$	$E_{2,cap}$	$E_{3,cap}$	$G_{f-c,cap}$		
	MPa	MPa	MPa	MPa	N/mm	MPa	MPa	MPa	MPa	N/mm	‰	-
T3	10.0	2643	2737	2599	7.82	13.1	3469	3592	3411	12.28	4.8	0.15
T6	9.8	1769	1368	2073	12.91	12.9	2322	1796	2721	16.95	13.0	0.11
<b>Avg.</b>	<b>9.9</b>	<b>2206</b>	<b>2053</b>	<b>2336</b>	<b>10.37</b>	<b>13.0</b>	<b>2896</b>	<b>2694</b>	<b>3066</b>	<b>14.62</b>	<b>8.90</b>	<b>0.13</b>
<b>St.dev.</b>	<b>0.14</b>	<b>618</b>	<b>968</b>	<b>372</b>	<b>3.60</b>	<b>0.19</b>	<b>811</b>	<b>1271</b>	<b>488</b>	<b>3.30</b>	<b>5.80</b>	<b>0.03</b>
<b>C.o.V.</b>	<b>0.01</b>	<b>0.28</b>	<b>0.47</b>	<b>0.16</b>	<b>0.35</b>	<b>0.02</b>	<b>0.28</b>	<b>0.47</b>	<b>0.16</b>	<b>0.23</b>	<b>0.65</b>	<b>0.22</b>

(\*) Complete specimen name starting with TUD-core-

Table 20 – Compression properties of H-shaped cores made of single wythe clay brick masonry.

Specimen name (*)	Cross-section of core					Cross-section of cap					$\epsilon_{p,core}$	$\nu_{core}$
	$f'_{m,core}$	$E_{1,core}$	$E_{2,core}$	$E_{3,core}$	$G_{f-c,core}$	$f'_{m,cap}$	$E_{1,cap}$	$E_{2,cap}$	$E_{3,cap}$	$G_{f-c,cap}$		
	MPa	MPa	MPa	MPa	N/mm	MPa	MPa	MPa	MPa	N/mm	‰	-
H5	10.13	2007	2556	1812	19.54	14.08	2787	3551	2517	27.14	10.0	0.19
H6	9.33	1965	1532	2287	10.59	13.99	2948	1744	4499	15.89	7.1	0.11
<b>Avg.</b>	<b>9.73</b>	<b>1986</b>	<b>2044</b>	<b>2049</b>	<b>15.07</b>	<b>14.04</b>	<b>2867</b>	<b>2647</b>	<b>3508</b>	<b>21.52</b>	<b>8.55</b>	<b>0.15</b>
<b>St.dev.</b>	<b>0.57</b>	<b>30</b>	<b>724</b>	<b>336</b>	<b>6.33</b>	<b>0.06</b>	<b>113</b>	<b>1277</b>	<b>1401</b>	<b>7.95</b>	<b>2.05</b>	<b>0.06</b>
<b>C.o.V.</b>	<b>0.06</b>	<b>0.01</b>	<b>0.35</b>	<b>0.16</b>	<b>0.42</b>	<b>0.004</b>	<b>0.04</b>	<b>0.48</b>	<b>0.40</b>	<b>0.37</b>	<b>0.24</b>	<b>0.38</b>

(\*) Complete specimen name starting with TUD-core-



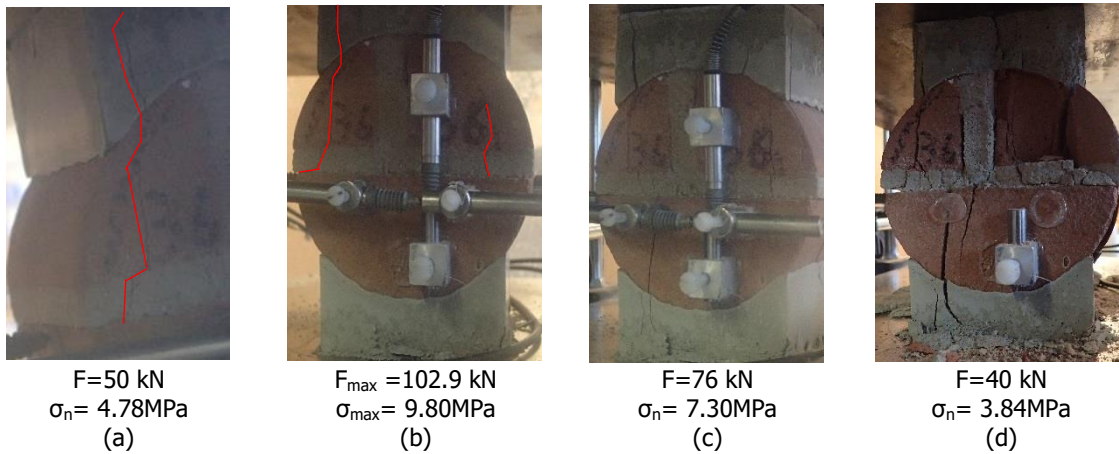
(a)

(b)

(c)

(d)

Figure 36 - Final crack pattern of T-shaped core made of single wythe clay brick masonry: (a) TUD-core-T3; (b) TUD-core-T6; (a) TUD-core-H5; (b) TUD-core-H6.



F=50 kN

$\sigma_n = 4.78 \text{ MPa}$

(a)

$F_{\max} = 102.9 \text{ kN}$

$\sigma_{\max} = 9.80 \text{ MPa}$

(b)

F=76 kN

$\sigma_n = 7.30 \text{ MPa}$

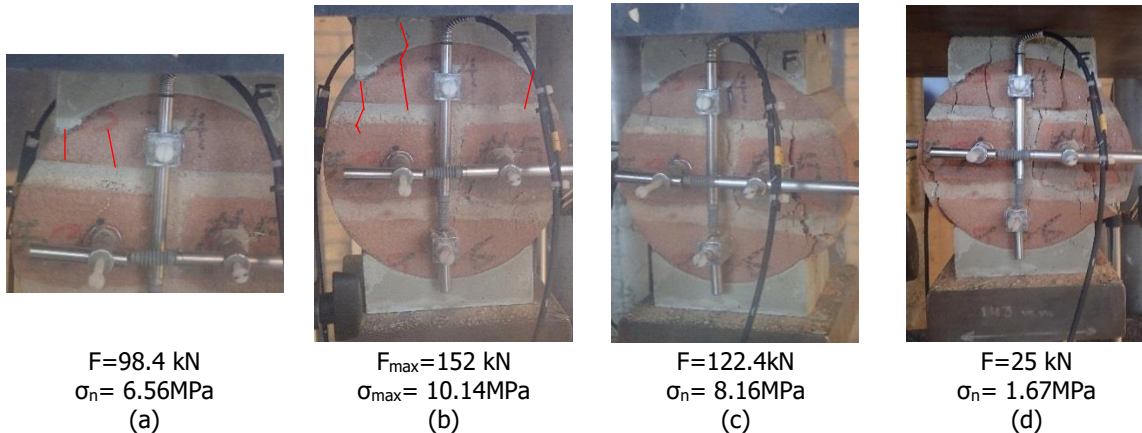
(c)

F=40 kN

$\sigma_n = 3.84 \text{ MPa}$

(d)

Figure 37 – Crack pattern of T-shaped core made of single wythe clay brick masonry showing vertical cracks aligned with the sides of the regularisation cap: (a) first crack; (b) maximum stress; (c) post peak phase; (d) end of the test.



F=98.4 kN

$\sigma_n = 6.56 \text{ MPa}$

(a)

$F_{\max} = 152 \text{ kN}$

$\sigma_{\max} = 10.14 \text{ MPa}$

(b)

F=122.4 kN

$\sigma_n = 8.16 \text{ MPa}$

(c)

F=25 kN

$\sigma_n = 1.67 \text{ MPa}$

(d)

Figure 38 – Crack pattern of H-shaped core made of single wythe clay brick masonry showing vertical cracks aligned with the sides of the regularisation cap TUD-core-H-5: (a) first crack; (b) maximum stress; (c) post peak phase; (d) end of the test.

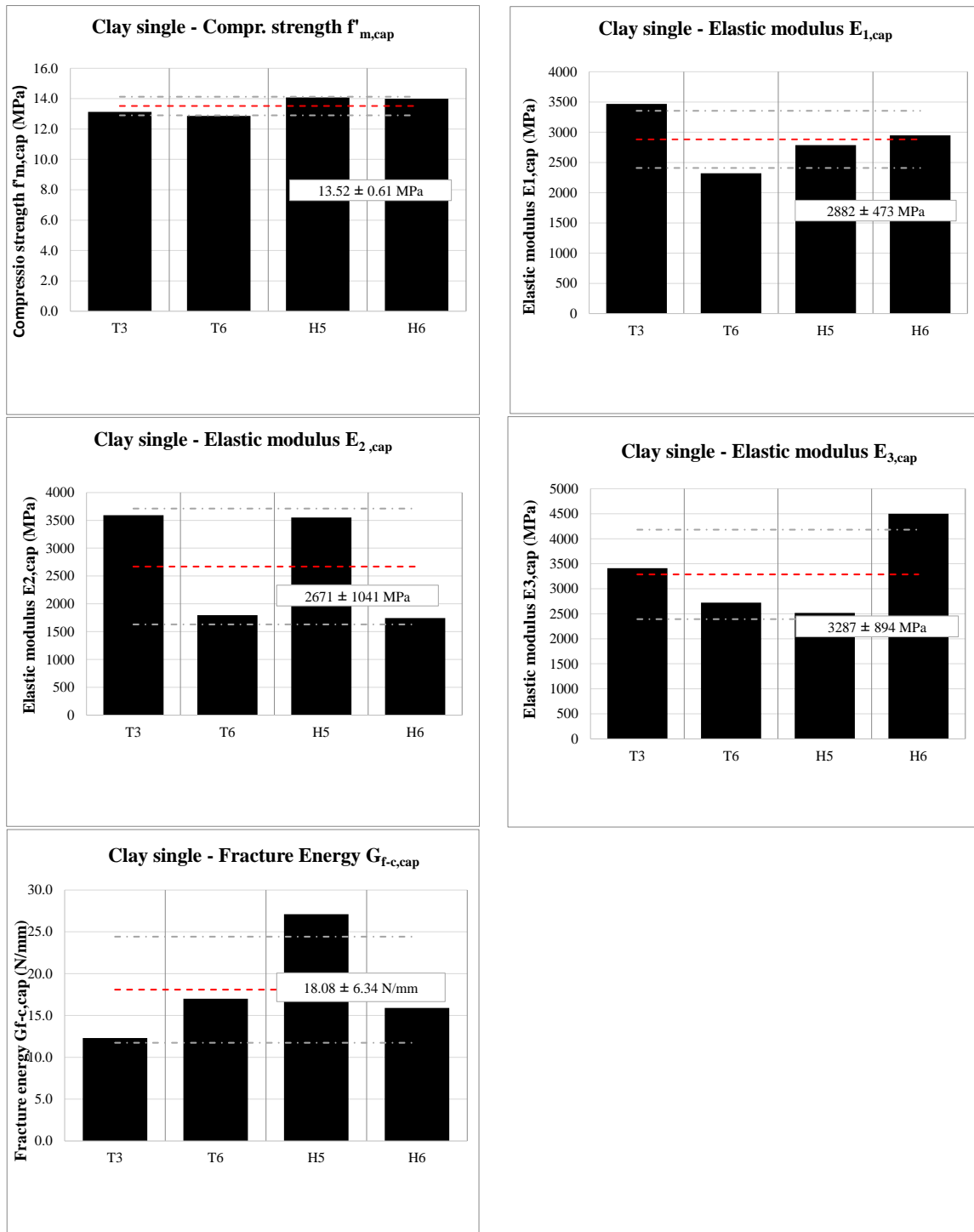


Figure 39 - Histogram representation of compression properties obtained by tests on T-shaped cores and H-shaped cores made of single wythe clay brick masonry. The properties are derived by considering the cross-sectional area of the cap as loaded area.

To validate the test on cores as a suitable in-situ test method, its results are correlated to the one obtained by standardised destructive tests. The vertical compression tests on the masonry wallets were performed according to EN 1052-1:1998 [17]. The dimensions of the adopted specimens and the testing set-up are shown in Figure 40. Totally, six specimens were tested. A summary of the compression properties of the single wythe clay specimens established from performing standardised test on the masonry wallets is listed in Table 21. More detailed information can be found in the dedicated report [37].

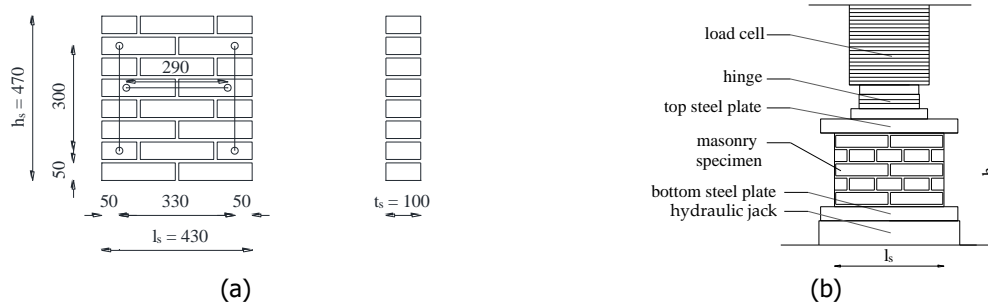


Figure 40 – (a) Dimensions of the single wythe clay brick masonry wallets; (b) compression test set-up.

Table 21 – Compression properties of single wythe clay brick masonry obtained by tests on wallets.

Standard test on masonry wallets	$f'_m$	$E_1$	$E_2$	$E_3$	$G_{f-c}$	$\epsilon_p$	$\nu$
	MPa	MPa	MPa	MPa	N/mm	‰	-
<b>Average</b>	<b>14.02</b>	<b>4380</b>	<b>4068</b>	<b>4590</b>	<b>28.52</b>	<b>4.3</b>	<b>0.14</b>
Standard deviation	0.56	605	783	603	3.40	0.4	0.02
Coefficient of variation	0.04	0.14	0.19	0.13	0.12	0.10	0.11

Table 22 shows the correlation between the compression properties obtained by tests on cores and companion tests on wallets. For the test on cores, the properties are evaluated both considering the stress evaluated with respect to (w.r.t.) the cross-section of the core and the one of the cap. By comparing the ratio between the properties obtained between the tests on cores and on wallets, the following conclusions can be drawn:

- The properties evaluated w.r.t. the cross-sectional area of the cap result closer to the properties of companion specimens.
- A good agreement is observed among the compressive strength of core samples and wallets for both 100 mm and 150 mm in diameter, considering the cross-sectional area of the cap.
- A ratio varying between 0.5 and 0.8 is found for the elastic moduli.
- A ratio varying between 0.4 and 0.8 is found for the fracture energy.
- A ratio between the strain corresponding to the peak strength of the core samples and the one of the wallets was found as 2, for both types of cores.
- A good agreement is observed among the Poisson ratio of core samples and wallets for both 100 mm and 150 mm cores in diameter.

The comparison of the compression properties of masonry obtained by tests on core and tests on masonry wallets for the single wythe clay brick masonry is given in terms of histogram in Figure 41.

Table 22 – Ratio between the compression properties obtained by tests on core and tests on wallets for single wythe clay brick masonry.

Ratio between properties obtained by core tests and tests on wallets	Stresses evaluated w.r.t. cross-sectional area of core					Stresses evaluated w.r.t. cross-sectional area of cap					$\epsilon_p$	$\nu$
	$f'_{m,core}/f'_m$	$E_{1,core}/E_1$	$E_{2,core}/E_2$	$E_{3,core}/E_3$	$G_{f-c,core}/G_{f-c}$	$f'_{m,cap}/f'_m$	$E_{1,cap}/E_1$	$E_{2,cap}/E_2$	$E_{3,cap}/E_3$	$G_{f-c,cap}/G_{f-c}$		
Ratio (Core $\phi=100$ mm /wallets)	0.71	0.50	0.50	0.51	0.36	0.93	0.66	0.66	0.67	0.51	2.1	1.1
Ratio (Core $\phi=150$ mm /wallets)	0.69	0.45	0.50	0.45	0.53	1.00	0.65	0.65	0.76	0.75	2.0	1.1

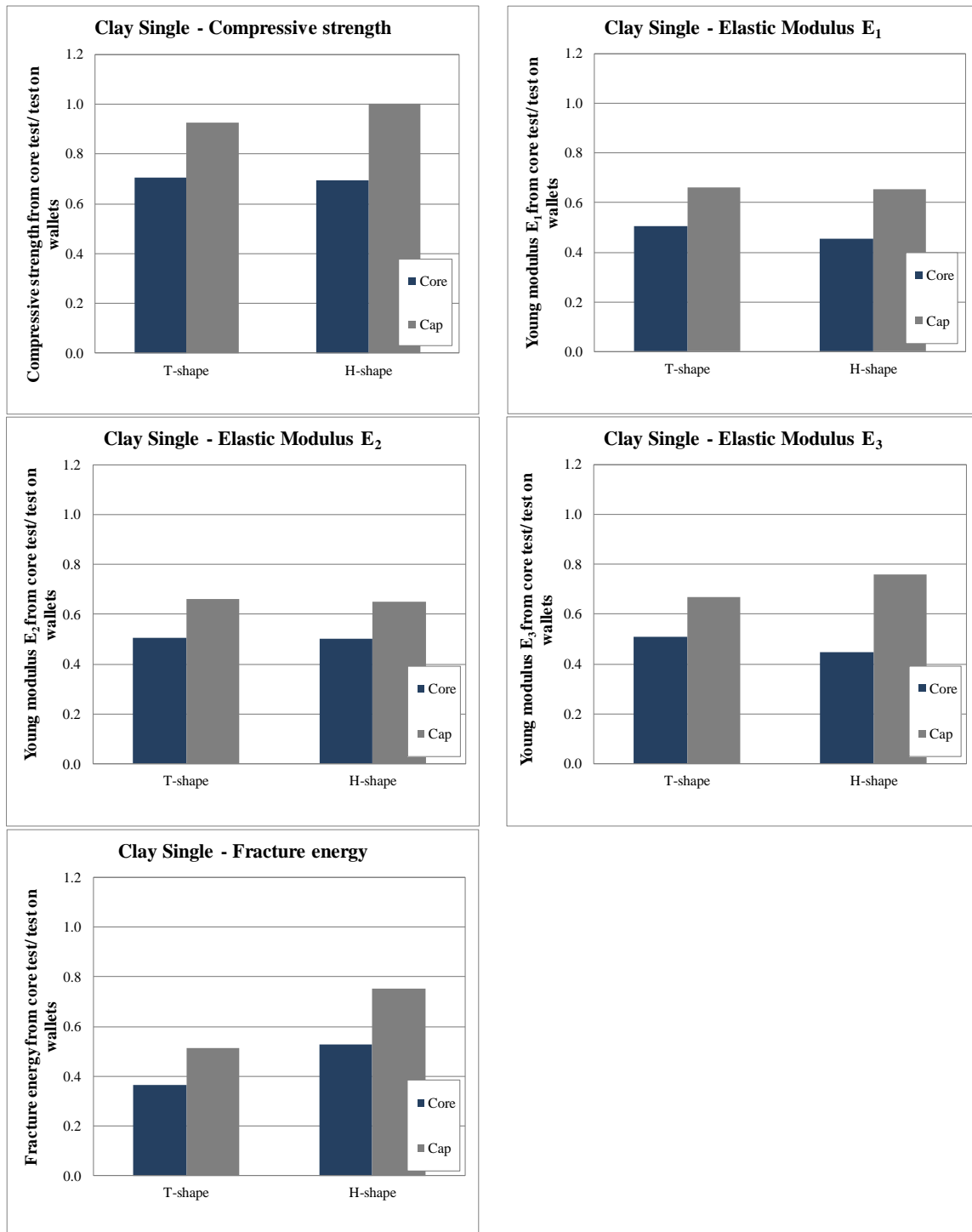


Figure 41 - Histogram representation of the ratio between the compression properties obtained by tests on cores and tests on wallets for the single wythe clay brick masonry.

### 14.2.2 Double wythe clay brick masonry

Figure 42 and Figure 43 show the stress-strain curve obtained from tests on T-shaped (diameter of 100 mm) and H-shaped (diameter of 150 mm) cores made of double wythe clay brick masonry, respectively. The graphs refer to the normal direction that is defined as the one parallel to the loading direction. The stress is calculated considering the cross-sectional area of the core. For both configurations, the stress-strain relationship in the normal direction presents a similar trend. The pre-peak stage was characterised by linear-elastic followed by an hardening behaviour until the peak. After reaching the peak stress, a linear softening behaviour was observed for both configurations.

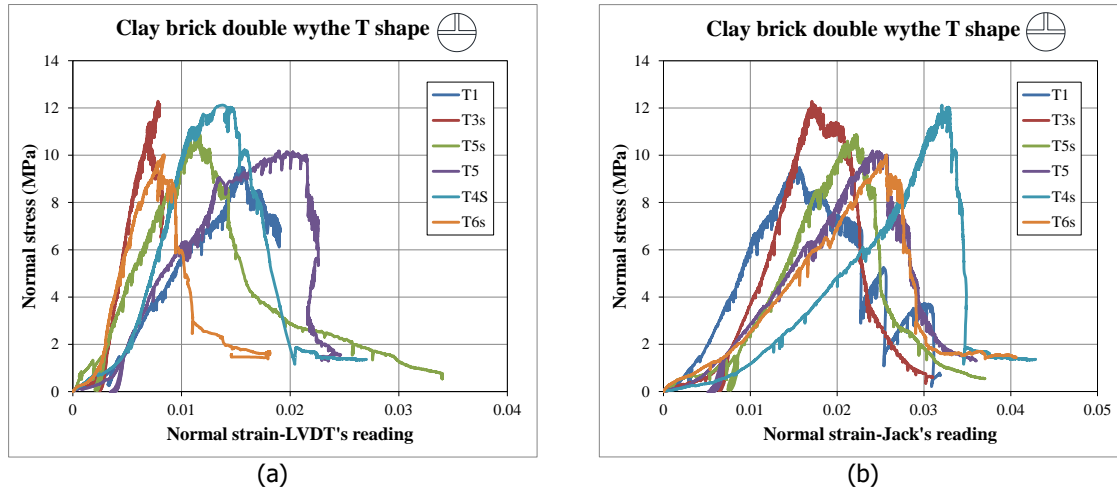


Figure 42 - Compression behaviour of T-shaped cores made of double wythe clay brick masonry: (a) normal strain obtained by LVDT's reading; (b) normal strain obtained by jack's reading.

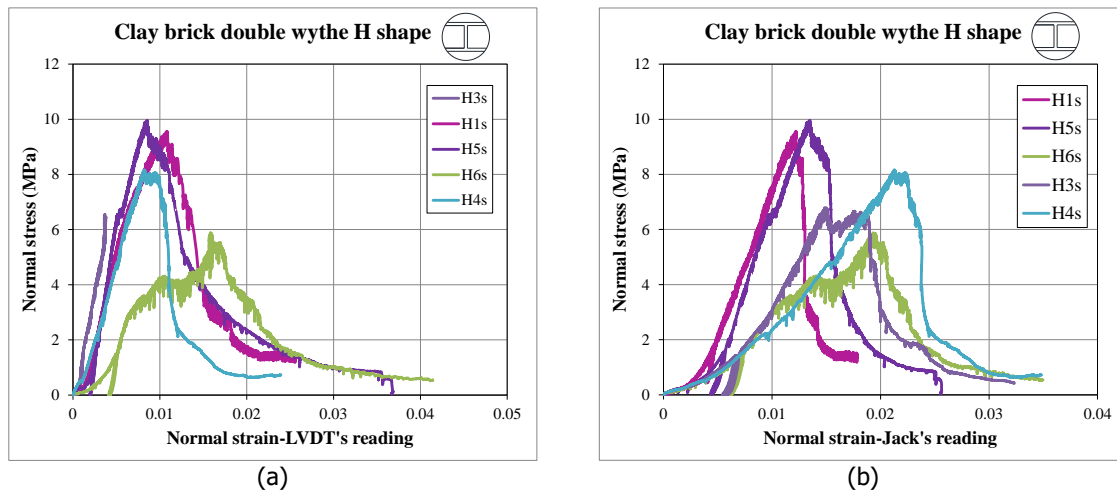


Figure 43 - Compression behaviour of H-shaped cores made of double wythe clay brick masonry: (a) normal strain obtained by LVDT's reading; (b) normal strain obtained by jack's reading.



Table 23 and Table 24 list the main experimental results obtained from tests on T-shaped and H-shaped cores made of double wythe clay brick masonry, respectively. The compression properties are evaluated both considering the cross-sectional area of the core and of the cap as a loaded area. The chord modulus  $E_3$  was calculated between the 20% and 30% of the maximum load, to exclude the initial start-up of the stress-strain diagram, which would unrealistically affects the estimation of the elastic moduli.

The crack pattern of the T-shaped cores with 100 mm in diameter and H-shaped cores with 150 mm in diameter is shown in Figure 44 and Figure 45, respectively. For the tested specimens, two different failure mechanisms were observed:

- (i) The specimens in which the first crack occurred in the brick aligned with the extremity of the regularisation cap. In the post-peak phase, the crack spread through the height of the core. For these specimens (e.g. specimens TUD-core-T3S, T4S, T5, H1S and H-4S) the cross-sectional area of the cap can be considered to evaluate the stress. The crack evolution for the specimen TUD-core-H-4S is shown in Figure 46.
- (ii) The specimens in which the first splitting crack (pre-peak phase) occurred in the brick or brick-mortar interface and not aligned with the extremities of the cap. In the post-peak phase, the crack spread through the height of the core. For these specimens (e.g. specimens TUD-core-T1, T5, T6S, H3S, H6S and H5S) the cross-sectional area of the core can be considered to evaluate the stress. The crack evolution for the specimen TUD-core-H-5S is shown in Figure 47.

Taking the cracks pattern into account, the properties of double wythe clay brick masonry are re-elaborating by separately defining the cross-sectional area for each specimen in agreement with the failure mode. The summary of the compression properties of the T-shaped and H-shaped cores re-elaborated by taking the crack pattern into account is listed in Table 25 and Table 26, respectively. The histogram representation of the compression properties is shown in Figure 48 and Figure 49, according to the observed crack pattern.

Table 23 – Compression properties of T-shaped cores made of double wythe clay brick masonry.

Specimen name (*)	Cross-section of core					Cross-section of cap					$\epsilon_{p,core}$	$\nu_{core}$
	$f'_{m,core}$	$E_{1,core}$	$E_{2,core}$	$E_{3,core}$	$G_{F-C,core}$	$f'_{m,cap}$	$E_{1,cap}$	$E_{2,cap}$	$E_{3,cap}$	$G_{F-C,cap}$		
	MPa	MPa	MPa	MPa	N/mm	MPa	MPa	MPa	MPa	N/mm	‰	-
T1	9.49	448	359	886	18.08	13.45	635	509	1256	25.64	16	0.10
T3S	12.29	945	709	2849	15.10	17.17	1321	990	3980	21.1	7.8	0.14
T5S	10.88	802	658	1423	15.66	15.2	1120	919	1988	21.88	12	0.16
T5	10.18	491	396	943	21.98	14.23	686	554	1317	30.71	19	0.14
T4S	12.12	565	436	1369	15.03	16.76	781	603	1892	20.78	14	0.15
T6S	10.02	906	660	3546	10.78	13.70	1239	903	4850	14.75	8.3	0.16
<b>Avg.</b>	<b>10.83</b>	<b>693</b>	<b>536</b>	<b>1836</b>	<b>16.1</b>	<b>15.09</b>	<b>964</b>	<b>746</b>	<b>2547</b>	<b>22.48</b>	<b>12.9</b>	<b>0.14</b>
<b>St.dev.</b>	<b>1.16</b>	<b>218</b>	<b>156</b>	<b>1099</b>	<b>3.7</b>	<b>1.58</b>	<b>299</b>	<b>213</b>	<b>1501</b>	<b>5.34</b>	<b>4.38</b>	<b>0.02</b>
<b>C.o.V.</b>	<b>0.11</b>	<b>0.31</b>	<b>0.29</b>	<b>0.60</b>	<b>0.2</b>	<b>0.10</b>	<b>0.31</b>	<b>0.29</b>	<b>0.59</b>	<b>0.24</b>	<b>0.34</b>	<b>0.16</b>

(\*) Complete specimen name starting with TUD-core-

Table 24 – Compression properties of H-shaped cores made of double wythe clay brick masonry.

Specimen name (*)	Cross-section of core					Cross-section of cap					$\epsilon_{p,core}$	$\nu_{core}$
	$f'_{m,core}$	$E_{1,core}$	$E_{2,core}$	$E_{3,core}$	$G_{F-C,core}$	$f'_{m,cap}$	$E_{1,cap}$	$E_{2,cap}$	$E_{3,cap}$	$G_{F-C,cap}$		
	MPa	MPa	MPa	MPa	N/mm	MPa	MPa	MPa	MPa	N/mm	‰	-
H1S	9.56	863	710	1520	13.19	16.29	1472	1210	2590	22.48	11	0.14
H5S	9.96	875	693	1840	15.83	16.98	1492	1182	3137	26.98	8.6	0.13
H6S	5.88	332	261	740	13.98	10.23	578	453	1286	24.30	16	0.12
H3S	6.79	1398	1209	2036	12.08	11.79	2408	2082	3506	20.81	3.1	0.13
H4S	8.17	799	739	955	13.95	13.61	1332	1231	1592	23.25	8.2	0.15
<b>Avg.</b>	<b>8.07</b>	<b>853</b>	<b>712</b>	<b>1418</b>	<b>13.81</b>	<b>13.78</b>	<b>1456</b>	<b>1232</b>	<b>2422</b>	<b>23.56</b>	<b>9.38</b>	<b>0.15</b>
<b>St.dev.</b>	<b>1.75</b>	<b>378</b>	<b>338</b>	<b>558</b>	<b>1.37</b>	<b>2.88</b>	<b>651</b>	<b>577</b>	<b>961</b>	<b>2.30</b>	<b>4.69</b>	<b>0.01</b>
<b>C.o.V.</b>	<b>0.22</b>	<b>0.44</b>	<b>0.47</b>	<b>0.39</b>	<b>0.10</b>	<b>0.21</b>	<b>0.45</b>	<b>0.47</b>	<b>0.40</b>	<b>0.10</b>	<b>0.50</b>	<b>0.09</b>



Table 25 – Re-elaboration of the compression properties of T-shaped cores made of double wythe clay brick masonry considering the cross-sectional area accordingly to the failure mode.

Specimen name (*)	Considered cross-sectional area accordingly to failure mode	Compression properties						
		$f'_m$	$E_1$	$E_2$	$E_3$	$G_{f-c}$	$\epsilon_p$	$\nu$
		MPa	MPa	MPa	MPa	N/mm	‰	-
T1	Core	9.49	448	359	886	18.08	16.0	0.10
T3S	Cap	17.17	1321	990	3980	21.10	7.8	0.14
T5S	Cap	15.20	1120	919	1988	21.88	12.0	0.16
T5	Core	10.18	491	396	943	21.98	19.0	0.14
T4S	Cap	16.76	781	603	1892	20.78	14.0	0.15
T6S	Core	10.02	906	660	3546	10.78	8.3	0.16
Avg.		13.14	845	655	2006	19.10	12.85	0.14
St.dev.		3.62	344	261	1298	4.32	4.38	0.02
C.o.V.		0.28	0.41	0.4	0.59	0.23	0.34	0.16

Table 26 – Re-elaboration of the compression properties of H-shaped cores made of double wythe clay brick masonry considering the cross-sectional area accordingly to the failure mode.

Specimen name (*)	Considered cross-sectional area accordingly to failure mode	Compression properties						
		$f'_m$	$E_1$	$E_2$	$E_3$	$G_{f-c}$	$\epsilon_p$	$\nu$
		MPa	MPa	MPa	MPa	N/mm	‰	-
H1S	Cap	16.29	1472	1210	2590	22.5	11.0	0.14
H5S	Cap	16.98	1492	1182	3137	27.0	8.6	0.13
H6S	Core	5.88	332	261	740	13.98	16.0	0.12
H3S	Core	6.79	1398	1209	2036	12.08	3.10	0.13
H4S	Core	8.17	799	739	955	13.95	8.20	0.15
Avg.		10.82	1098	920	1892	17.89	9.38	0.13
St.dev.		5.37	515	419	1032	6.49	4.69	0.01
C.o.V.		0.50	0.47	0.46	0.55	0.36	0.50	0.09



(a)



(b)



(c)



(d)



(e)



(f)

Figure 44 – Final crack pattern of T-shaped core made of double wythe clay brick masonry: (a) TUD-core-T1; (b) TUD-core-T3;(c) TUD-core-T5s; (d) TUD-core-T5;(e) TUD-core-T4s; (f) TUD-core-T6s.

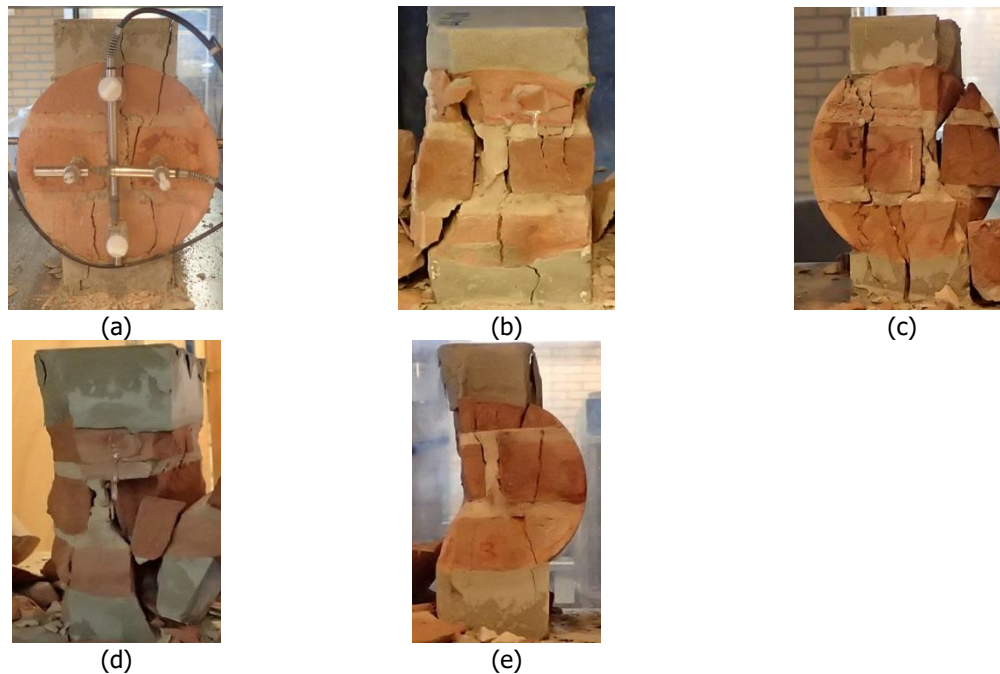


Figure 45 – Final crack pattern of H-shaped core made of double wythe clay brick masonry: (a) TUD-core-H1s; (b) TUD-core-H5s; (c) TUD-core-H6s; (d) TUD-core-H3s; (e) TUD-core-H4s.

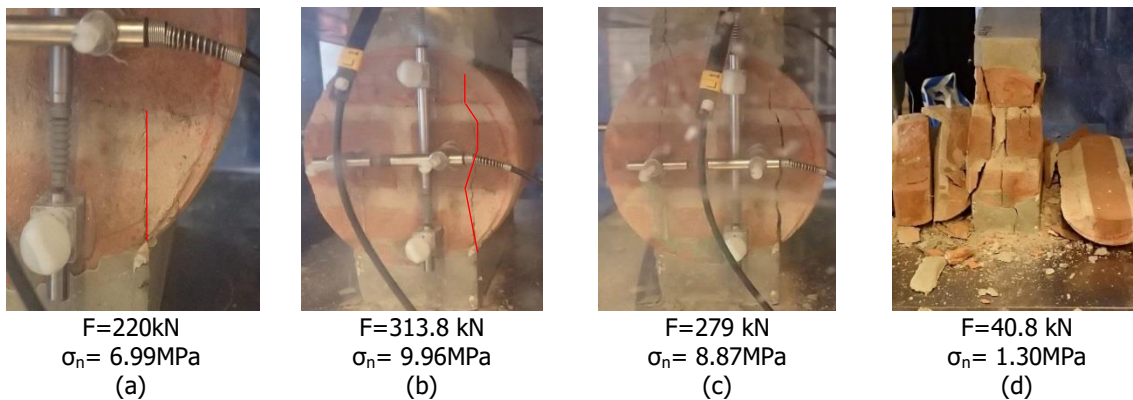


Figure 46 – Crack pattern of double wythe clay brick masonry core showing vertical cracks aligned with the sides of the regularisation cap (TUD-core-H-5S): (a) first crack; (b) maximum stress; (c) post-peak phase; (d) end of the test.

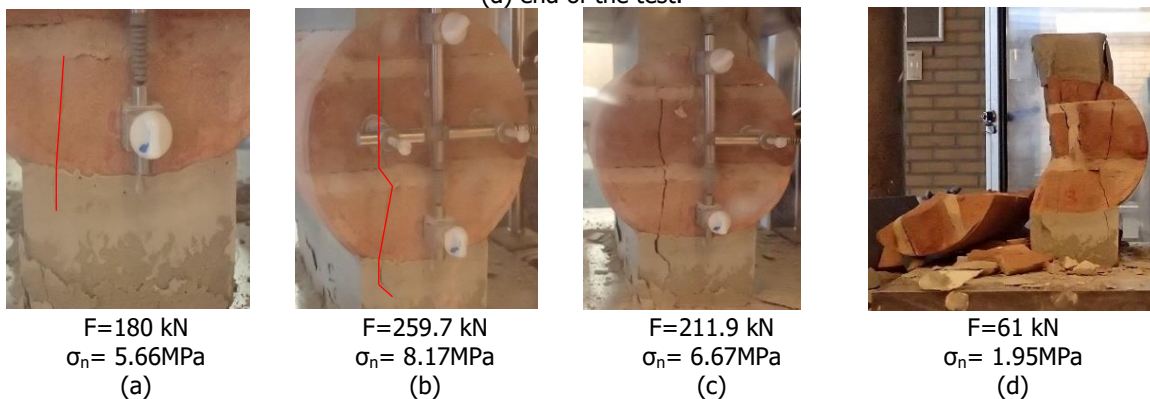


Figure 47 – Crack pattern of double wythe clay brick masonry core showing vertical cracks not aligned with the sides of the regularisation cap (TUD-core-H-4S): (a) first crack; (b) maximum stress; (c) post-peak phase; (d) end of the test.

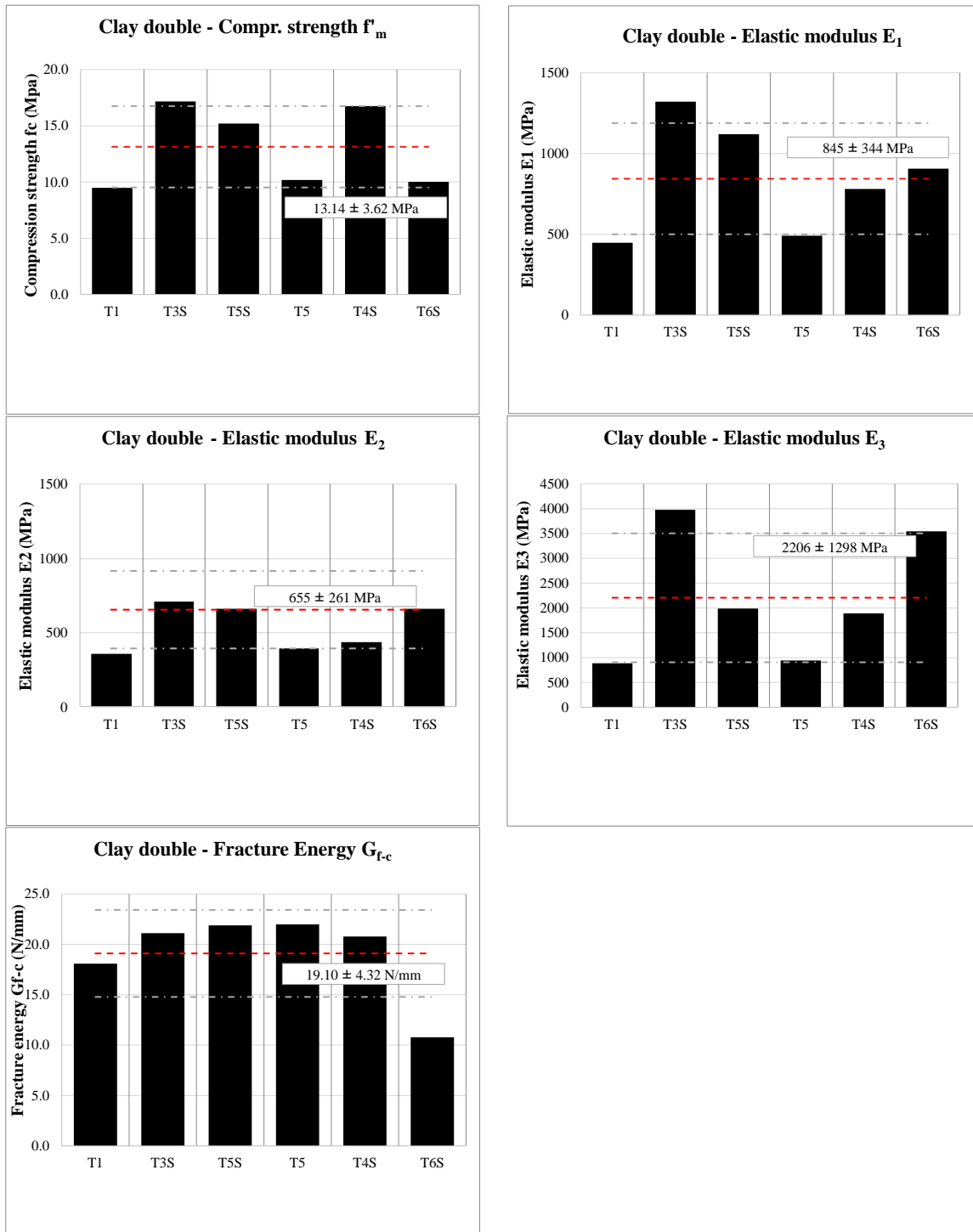


Figure 48 - Histogram representation of compression properties obtained by tests on T-shaped cores made of double wythe clay brick masonry. The properties are derived by considering the cross-sectional area of the cap or of the core accordingly to the failure mode.

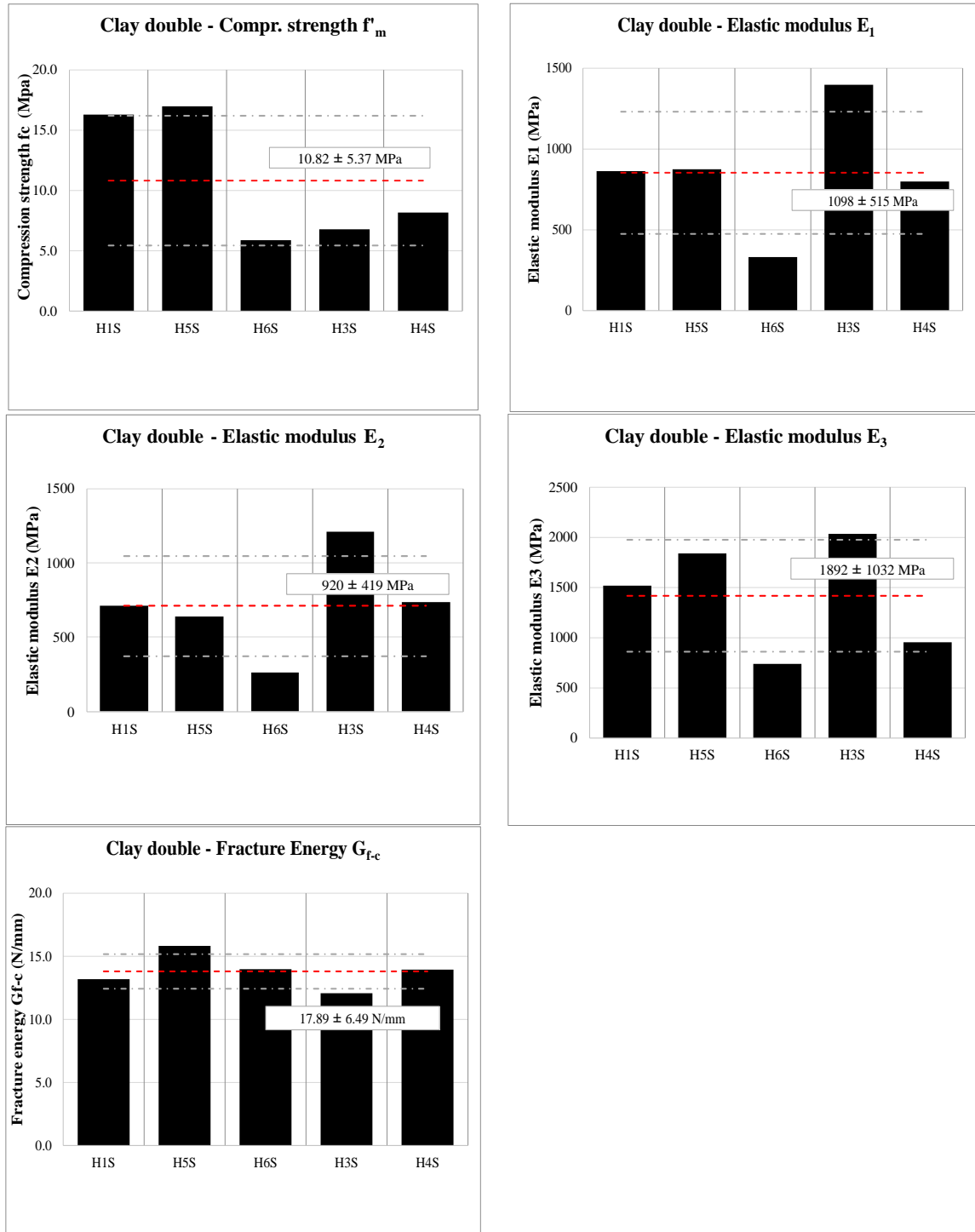


Figure 49 - Histogram representation of compression properties obtained by tests on H-shaped cores made of double wythe clay brick masonry. The properties are derived by considering the cross-sectional area of the cap or of the core accordingly to the failure mode.

To validate the test on core as a suitable in-situ test method, its results are correlated to the one obtained by standardised destructive tests. The vertical compression tests on the masonry wallets were performed according to EN 1052-1:1998 [17]. The dimensions of the adopted specimens and the testing set-up are shown in Figure 50. Totally, twelve specimens were tested. A summary of the compression properties of the double wythe clay brick masonry specimens determined by performing standardised tests on the masonry wallets is listed in Table 21. More detailed information can be found on the dedicated report [37].

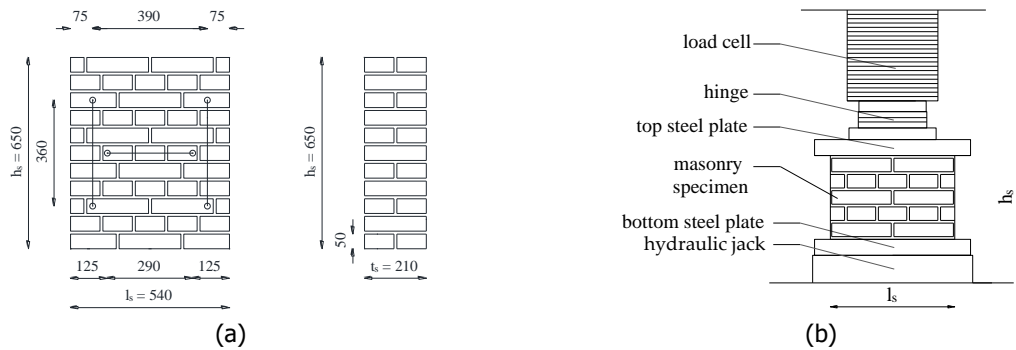


Figure 50 – (a) Dimensions of the double wythe clay brick masonry wallets; (b) compression test set-up.

Table 27 – Compression properties of double wythe clay brick masonry obtained by tests on wallets.

Standard test on masonry wallets	$f'_m$	$E_1$	$E_2$	$E_3$	$G_{f-c}$	$\epsilon_p$	$\nu$
	MPa	MPa	MPa	MPa	N/mm	‰	-
<b>Average</b>	<b>9.26</b>	<b>2771</b>	<b>2646</b>	<b>2951</b>	<b>34.8</b>	<b>4.1</b>	<b>0.12</b>
Standard deviation	1.26	496	970	431	8.1	0.76	0.02
Coefficient of variation	0.14	0.18	0.37	0.15	0.23	0.19	0.21

A ratio between the compression properties of masonry cores and those properties obtained from standardised tests on wallets is listed in Table 28 and Table 29; a histogram representation is given in Figure 51. The compression properties of masonry cores are first presented by considering for all the core samples either the cross-sectional area of the core or the cross-sectional area of the cap (Table 28). In a second step, the comparison is made by considering for each core sample the cross-sectional area accordingly to the failure mode (Table 29).

By considering the comparison in Table 29, the following conclusions can be drawn:

- The evaluation of the compressive strength depends on the considered cross-sectional area. In the case the cross-sectional area is defined in agreement with the failure mode, a good correlation between the compressive strength determined by the test on core and the test on wallets is found, especially considering H-shaped cores.
- A ratio between the chord elastic moduli of the cores and companion samples varies between 0.6 and 0.8.
- A ratio between the fracture energy of the core samples and companion samples is found as 0.5.
- The strain corresponding to the peak strength evaluated with tests on core is higher than the one evaluated with tests on wallets. A ratio equal to 3 and 2 is found for T-shaped and H-shaped cores, respectively
- A good agreement is observed for the Poisson ratio for both core's diameters.

Table 28 – Ratio between the compression properties obtained by tests on core and tests on wallets for double wythe clay brick masonry.

Ratio between properties obtained by core test and standardised test on wallets	Stresses evaluated w.r.t. cross-section of core					Stresses evaluated w.r.t. cross-section of cap					$\epsilon_p$	$\nu$
	$f'_{m,core}/f'_m$	$E_{1,core}/E_1$	$E_{2,core}/E_2$	$E_{3,core}/E_3$	$G_{f-c,core}/G_{f-c}$	$f'_{m,cap}/f'_m$	$E_{1,cap}/E_1$	$E_{2,cap}/E_2$	$E_{3,cap}/E_3$	$G_{f-c,cap}/G_{f-c}$		
Ratio (Core $D=100$ mm /wallets)	1.17	0.25	0.20	0.62	0.46	1.63	0.35	0.28	0.86	0.65	3.1	1.3
Ratio (Core $D=150$ mm /wallets)	0.87	0.31	0.27	0.48	0.40	1.49	0.53	0.47	0.82	0.68	2.3	1.2

Table 29 - Ratio between the compression properties obtained by test on cores and test on wallets for the double wythe clay brick masonry considering the cross-sectional area accordingly to the failure mode.

Ratio between properties obtained by core test and standardised test on wallets	Stresses evaluated w.r.t. the average				
	$\frac{f_{m,core}}{f_m}$	$\frac{E_{1,core}}{E_1}$	$\frac{E_{2,core}}{E_2}$	$\frac{E_{3,core}}{E_3}$	$\frac{G_{fc,core}}{G_{f-c}}$
Ratio (Core $D=100$ mm /wallets)	1.42	0.30	0.25	0.75	0.55
Ratio (Core $D=150$ mm /wallets)	1.17	0.40	0.35	0.64	0.51

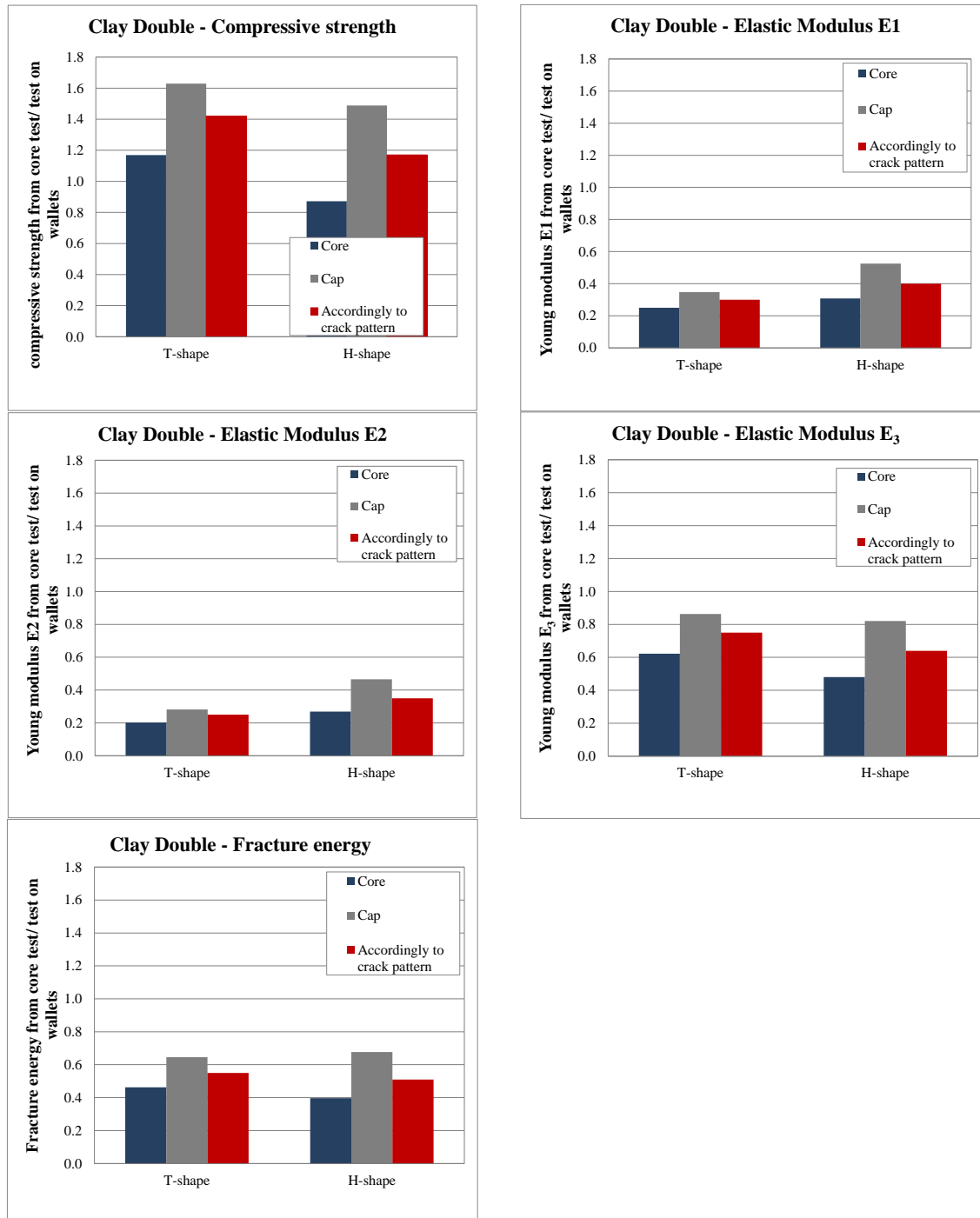


Figure 51 – Histogram representation of the ratio between the compression properties obtained by tests on core and tests on wallets for double wythe clay brick masonry.

### 14.2.3 Calcium silicate brick masonry

Figure 52 and Figure 53 show the stress-strain curve obtained from tests on T-shaped (diameter of 100 mm) and H-shaped (diameter of 150 mm) cores made of calcium silicate (CS) brick masonry, respectively. The graphs refer to the normal direction that is defined as the one parallel to the loading direction. The stress is calculated considering the cross-sectional area of the core. For both configurations, the stress-strain relationship in the normal direction presents a similar trend. The pre-peak stage was characterised by linear-elastic followed by an hardening behaviour until the peak. After reaching the peak stress, a linear softening behaviour was observed for both configurations.

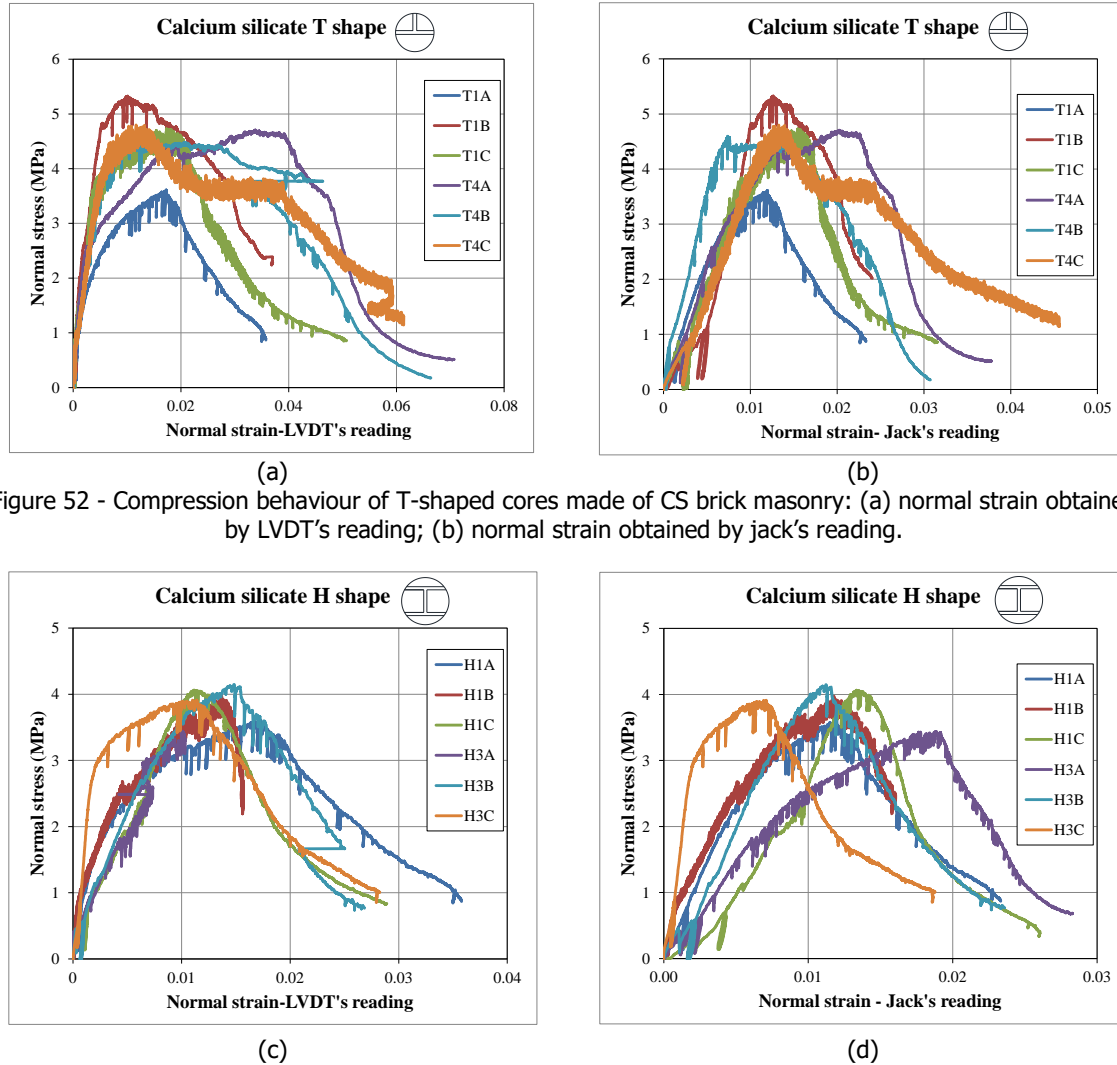


Figure 52 - Compression behaviour of T-shaped cores made of CS brick masonry: (a) normal strain obtained by LVDT's reading; (b) normal strain obtained by jack's reading.

Figure 53 - Compression behaviour of H-shaped cores made of CS brick masonry: (a) normal strain obtained by LVDT's reading; (b) normal strain obtained by jack's reading.



Table 30 and Table 31 list the main experimental results obtained from tests on T-shaped and H-shaped cores made of CS brick masonry, respectively. The compression properties are evaluated both considering the cross-sectional area of the core and of the cap as a loaded area.

The crack pattern of the tested specimen is shown in Figure 54 and Figure 55. The crack pattern was characterised by vertical cracks starting at the extremities of the regularisation cap and subsequently spreading through the height of the specimen leading to the splitting of the brick (Figure 56 and Figure 57). Consequently, it can be assumed that it is more appropriate to evaluate the compressive properties with respect to the cross-sectional area of the cap. It should be noted that during the test, damage in the cap was observed; this can affect the estimation of the fracture energy.

The compression properties of the cores evaluated with respect to the cross-sectional area of the cap, accordingly to the crack pattern, are shown in terms of histogram representation in Figure 58 and Figure 59.

Table 30 – Compression properties of T-shaped cores made of calcium silicate brick masonry.

Specimen name (*)	Cross-section of core					Cross-section of cap					$\epsilon_{p,core}$	$\nu_{core}$
	$f'_{m,core}$	$E_{1,core}$	$E_{2,core}$	$E_{3,core}$	$G_{F-C,core}$	$f'_{m,cap}$	$E_{1,cap}$	$E_{2,cap}$	$E_{3,cap}$	$G_{F-C,cap}$		
	MPa	MPa	MPa	MPa	N/mm	MPa	MPa	MPa	MPa	N/mm	‰	-
T1A	4.01	1633	3359	1300	20.1	5.44	2217	4559	1764	27.3	29	0.12
T1B	5.32	1760	1823	1731	12.4	7.07	2339	2423	2299	16.5	10	0.16
T1C	4.73	1796	1513	1982	12.9	6.11	2320	1954	2560	17.0	17	0.19
T4A	4.71	1455	3559	1123	24.5	6.10	1886	4612	1456	31.0	34	0.14
T4B	4.60	1030	2873	780	15.5	6.02	1349	3763	1022	20.3	11	0.19
T4C	4.80	959	2882	720	19.8	6.29	1257	3748	943	25.9	12	0.17
<b>Avg.</b>	<b>4.70</b>	<b>1439</b>	<b>2665</b>	<b>1272</b>	<b>17.55</b>	<b>6.17</b>	<b>1895</b>	<b>3510</b>	<b>1674</b>	<b>23.00</b>	<b>18.8</b>	<b>0.16</b>
<b>St.dev.</b>	<b>0.42</b>	<b>365</b>	<b>825</b>	<b>507</b>	<b>4.74</b>	<b>0.53</b>	<b>487</b>	<b>1099</b>	<b>662</b>	<b>5.94</b>	<b>10.2</b>	<b>0.03</b>
<b>C.o.V.</b>	<b>0.09</b>	<b>0.25</b>	<b>0.31</b>	<b>0.40</b>	<b>0.27</b>	<b>0.09</b>	<b>0.26</b>	<b>0.31</b>	<b>0.40</b>	<b>0.26</b>	<b>0.54</b>	<b>0.17</b>

(\*) Complete specimen name starting with TUD-core-

Table 31 – Compression properties of H-shaped cores made of calcium silicate brick masonry.

Specimen name (*)	Cross-section of core					Cross-section of cap					$\epsilon_{p,core}$	$\nu_{core}$
	$f'_{m,core}$	$E_{1,core}$	$E_{2,core}$	$E_{3,core}$	$G_{F-C,core}$	$f'_{m,cap}$	$E_{1,cap}$	$E_{2,cap}$	$E_{3,cap}$	$G_{F-C,cap}$		
	MPa	MPa	MPa	MPa	N/mm	MPa	MPa	MPa	MPa	N/mm	‰	-
H1A	3.61	879	1547	723	13.7	5.95	1441	2534	1185	22.6	17	-
H1B	3.97	1210	2220	986	13.2	6.34	1931	3542	1573	21.0	14	0.20
H1C	4.06	461	651	402	9.4	6.37	722	1020	630	14.7	11	0.15
H3A	3.40	488	6099	357	7.1	5.42	770	9623	563	11.1	10	0.20
H3B	4.15	491	1864	3630	12.6	6.69	794	3008	581	20.4	15	0.16
H3C	3.91	1408	1187	1551	11.7	6.30	2268	1913	2500	18.8	11	-
<b>Avg.</b>	<b>3.85</b>	<b>823</b>	<b>2261</b>	<b>730</b>	<b>11.27</b>	<b>6.18</b>	<b>1321</b>	<b>3607</b>	<b>1172</b>	<b>18.10</b>	<b>13.0</b>	<b>0.18</b>
<b>St.dev.</b>	<b>0.29</b>	<b>412</b>	<b>1957</b>	<b>474</b>	<b>2.57</b>	<b>0.44</b>	<b>667</b>	<b>3075</b>	<b>767</b>	<b>4.36</b>	<b>2.76</b>	<b>0.03</b>
<b>C.o.V.</b>	<b>0.07</b>	<b>0.50</b>	<b>0.87</b>	<b>0.65</b>	<b>0.23</b>	<b>0.07</b>	<b>0.50</b>	<b>0.85</b>	<b>0.65</b>	<b>0.24</b>	<b>0.21</b>	<b>0.15</b>

(\*) Complete specimen name starting with TUD-core-



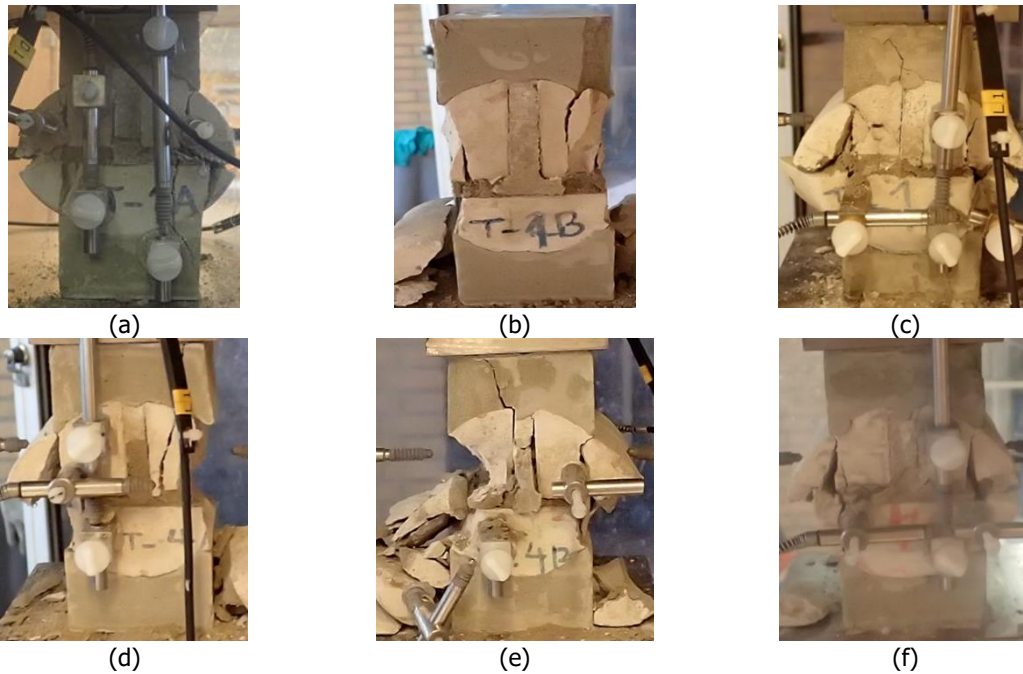


Figure 54 – Final crack pattern of T-shaped cores made of calcium silicate brick masonry: (a) TUD-core-T1A; (b) TUD-core-T1B; (c) TUD-core-T1C; (d) TUD-core-T4A; (e) TUD-core-T4B; (f) TUD-core-T4C.

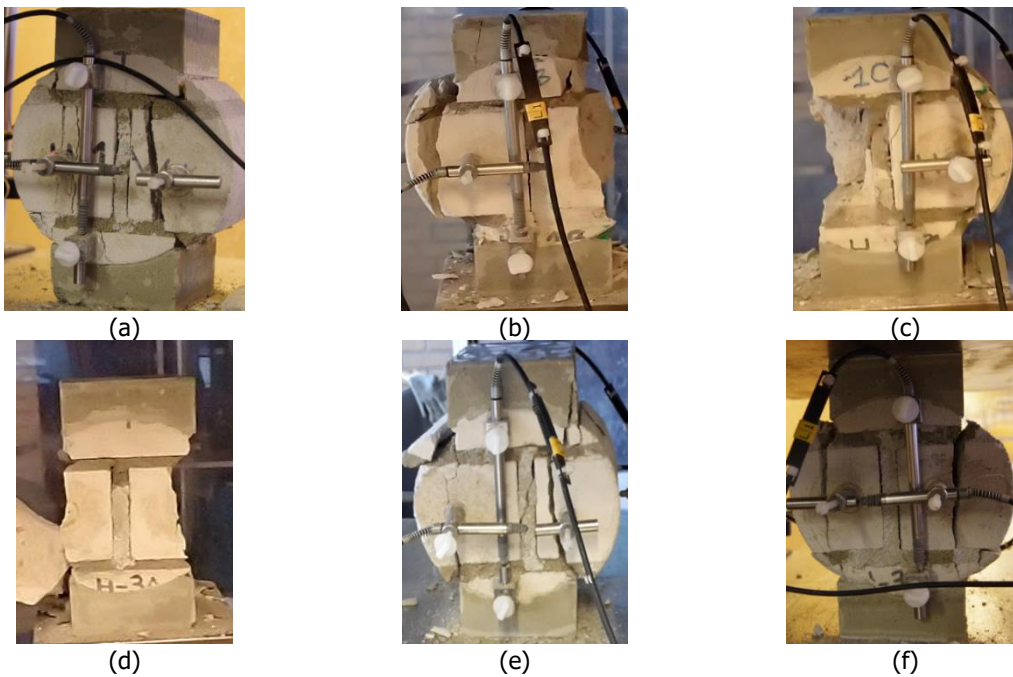


Figure 55 – Final crack pattern of H-shaped cores made of calcium silicate brick masonry: (a) TUD-core-H1A; (b) TUD-core-H1B; (c) TUD-core-H1C; (d) TUD-core-H3A; (e) TUD-core-H3B; (f) TUD-core-H3C.

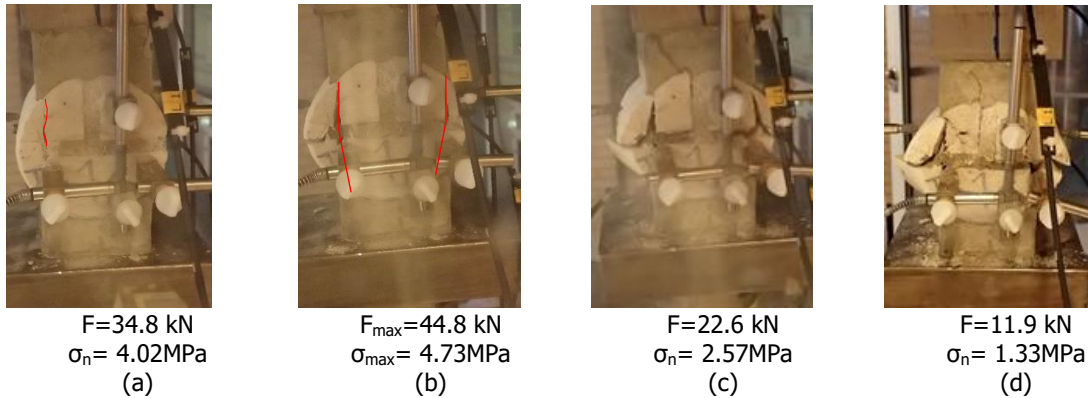


Figure 56 – Crack pattern of T-shaped core (TUD-Core-T-1B): made of calcium silicate brick masonry showing vertical cracks aligned with the sides of the regularisation cap: (a) first crack; (b) maximum stress; (c) post peak phase; (d) end of the test.

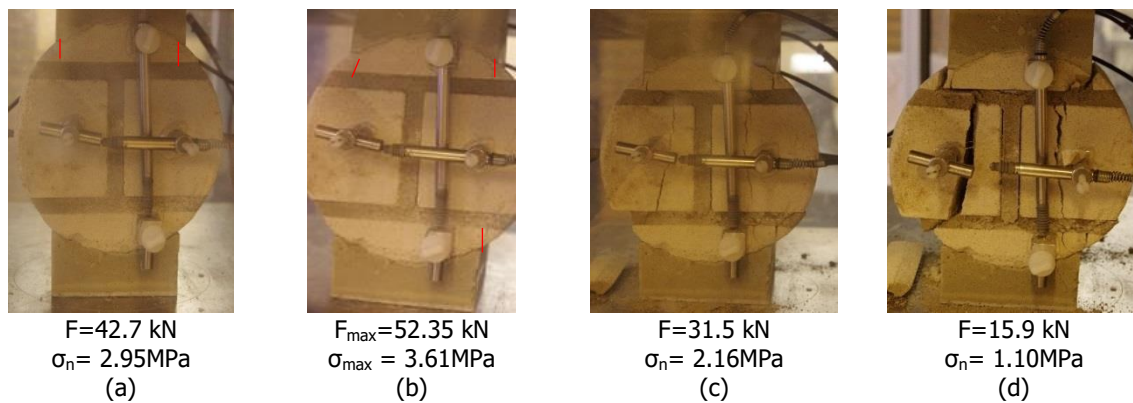


Figure 57 – Crack pattern of H-shaped core (TUD-Core-H-1A) made of calcium silicate brick masonry showing vertical cracks aligned with the sides of the regularisation cap: (a) first crack; (b) maximum stress; (c) post peak phase; (d) end of the test.

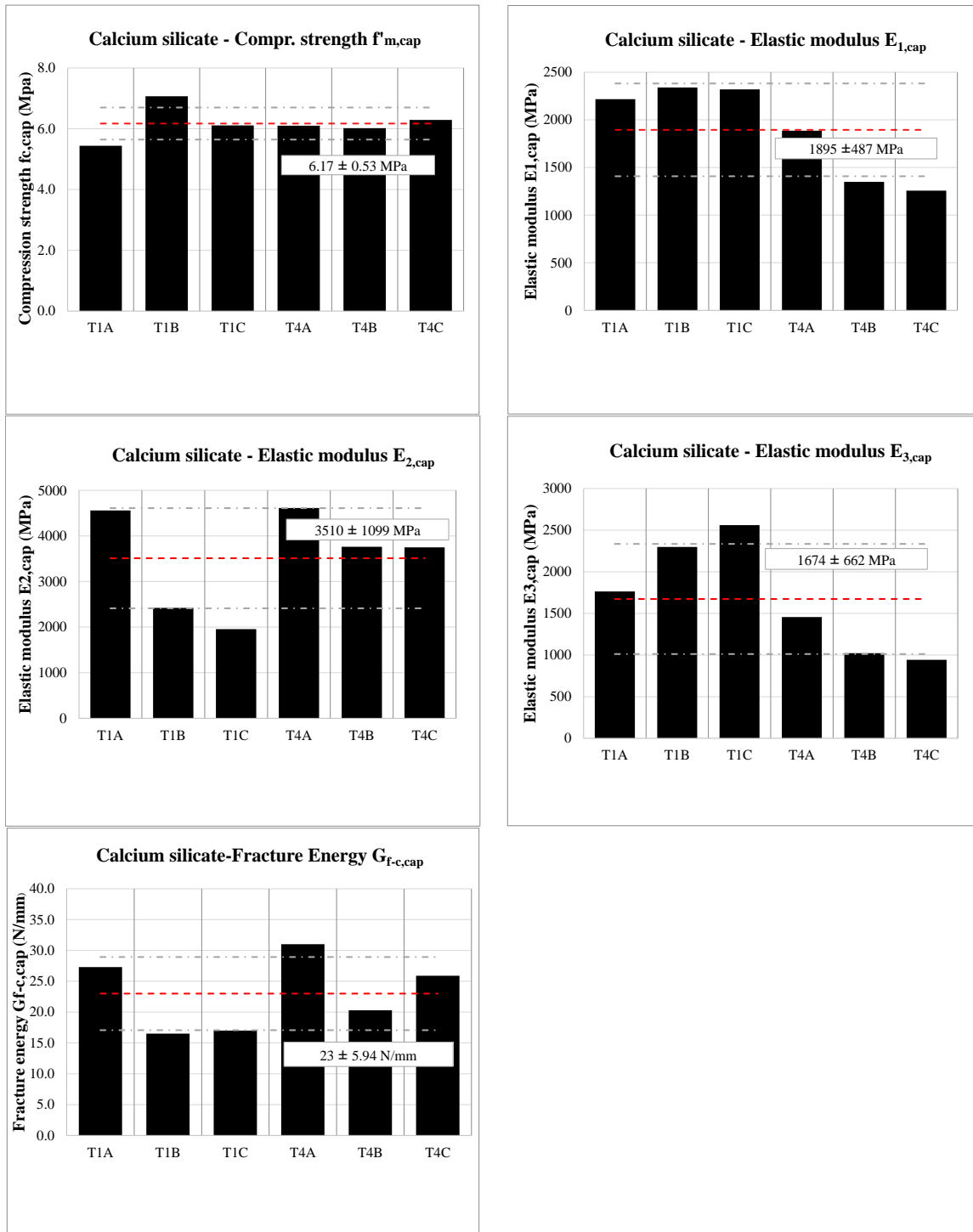


Figure 58 - Histogram representation of compression properties obtained by tests on T-shaped cores made of calcium silicate brick masonry. The properties are derived by considering the cross-sectional area of the cap as loaded area.

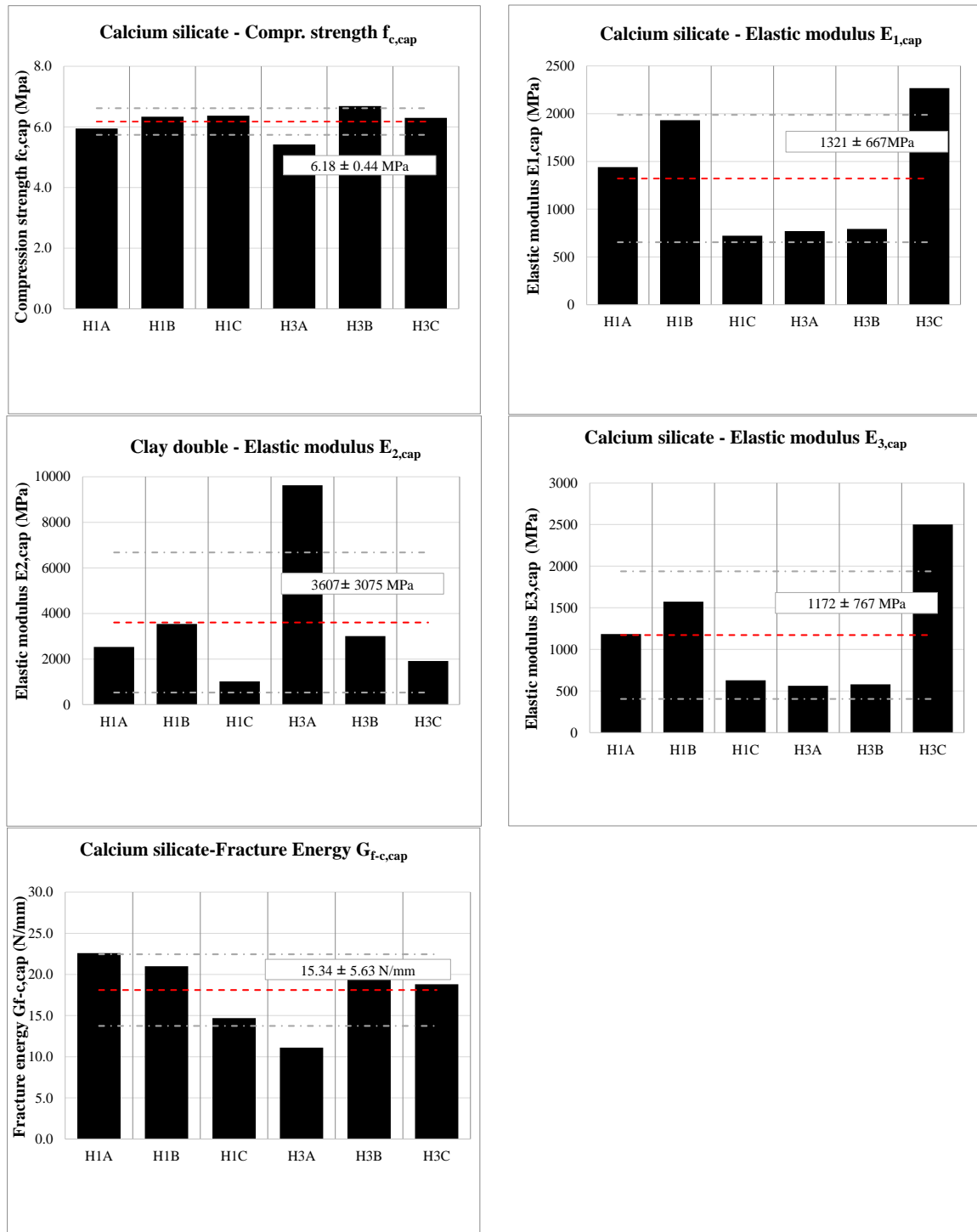


Figure 59 - Histogram representation of compression properties obtained by tests on H-shaped cores made of calcium silicate brick masonry. The properties are derived by considering the cross-sectional area of the cap as loaded area.

To validate the test on cores as a suitable in-situ test method, its results are correlated with the one obtained by standardised destructive tests. The vertical compression tests on the masonry wallets were performed according to EN 1052-1:1998. The dimensions of the adopted specimens and the testing set-up are shown in Figure 60. Totally, six specimens were tested. A summary of the compression properties of the CS brick masonry specimens determined by performing standardised tests on the masonry wallets is listed in Table 32. More detailed information regarding the testing procedure and testing results can be found on the dedicated report [38].

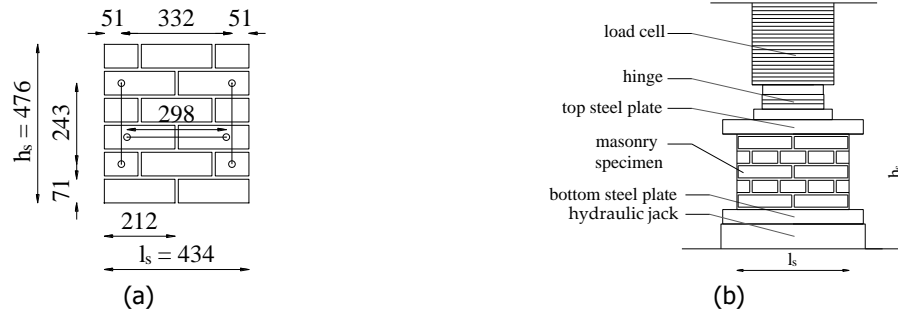


Figure 60 – (a) Dimensions of the calcium silicate brick masonry wallets; (b) compression test set-up.

Table 32 – Compression properties of calcium silicate brick masonry obtained by tests on wallets.

Standard test on masonry wallets	$f'_m$	$E_1$	$E_2$	$E_3$	$G_{f-c}$	$\epsilon_p$	$\nu$
	MPa	MPa	MPa	MPa	N/mm	‰	-
Average	6.35	4972	8206	4265	20.0	5.9	0.16
Standard deviation	0.32	568	1008	527	3.43	1.21	0.03
Coefficient of variation	0.05	0.11	0.12	0.12	0.17	0.2	0.19

A ratio between the compression properties obtained by tests on cores and tests on wallets is given in Table 33; an histogram representation is given in Figure 61. The compression properties of masonry cores are given both considering the cross-sectional area of the core and of the cap. The comparison leads to the following conclusions:

- The evaluation of the compressive strength depends on the considered cross-sectional area. In the case the cross-sectional area is defined in agreement with the failure mode (cross-sectional area of the cap), a good correlation between the compressive strength determined by the test on cores and the test on wallets is found for both cores' diameter.
- The ratio obtained by test on cores and test of wallets for the chord elastic modulus varies between 0.2 and 0.4.
- A good agreement in terms of fracture energy is found between the two test methods considering the cross-sectional area of the core.
- The strain corresponding to the peak strength evaluated with test on cores is higher than the one evaluated with tests on wallets. A ratio equal to 3 and 2 is found for T-shaped and H-shaped cores, respectively.
- For both T-shaped and H-shaped cores, a good agreement is observed between the two test methods in terms of Poisson ratio.

Table 33 – Ratio between the compression properties obtained by test on cores and test on wallets for calcium silicate brick masonry.

Ratio between properties obtained by core test and standardised test on wallets	Stresses evaluated w.r.t. cross-section of core					Stresses evaluated w.r.t. cross-section of cap					$\epsilon_p$	$\nu$
	$f'_{m,core}/f'_m$	$E_{1,core}/E_1$	$E_{2,core}/E_2$	$E_{3,core}/E_3$	$G_{f-c,core}/G_{f-c}$	$f'_{m,cap}/f'_m$	$E_{1,cap}/E_1$	$E_{2,cap}/E_2$	$E_{3,cap}/E_3$	$G_{f-c,cap}/G_{f-c}$		
Ratio (Core $D=100$ mm /wallets)	0.74	0.29	0.33	0.30	1.01	0.97	0.38	0.43	0.39	1.37	3.2	1.0
Ratio (Core $D=150$ mm /wallets)	0.61	0.17	0.27	0.17	0.56	0.97	0.27	0.44	0.28	0.90	2.2	1.1

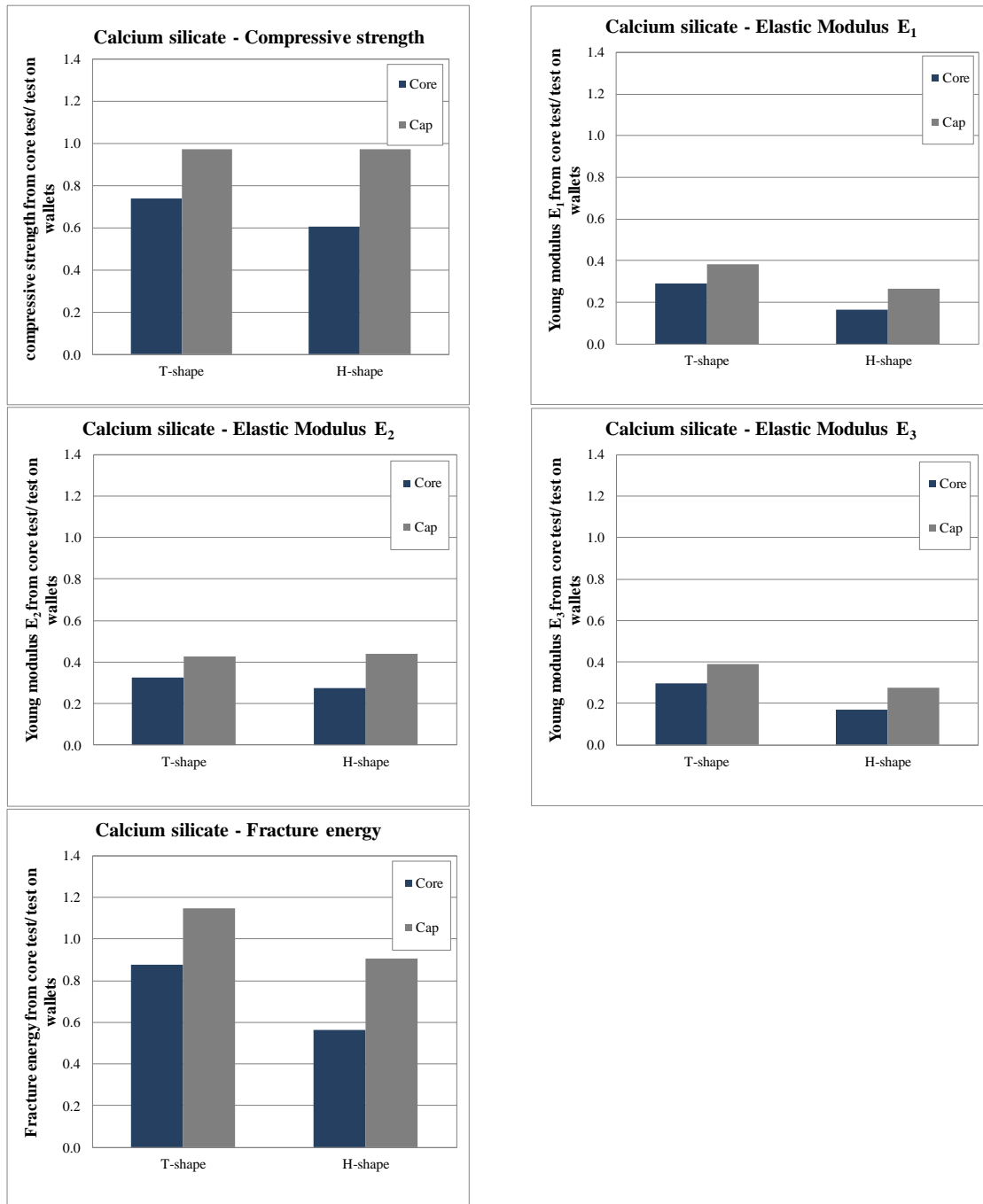


Figure 61 – Histogram representation of the ratio between the compression properties obtained by tests on core and tests on wallets for the calcium silicate brick masonry.

#### 14.2.4 Summary of the compression properties

The applicability of the core technique, both T-shaped cores (diameter of 100 mm) and H-shaped cores (diameter of 150 mm), to evaluate the compression properties of masonry was validated by comparing the obtained results with the results of standardised tests on wallets.

Figure 62 shows the comparison for single wythe clay brick masonry, double wythe clay brick masonry and calcium silicate brick masonry in terms of ratio between the compression properties obtained by tests on cores and on wallets. Considering the obtained results the following conclusions can be drawn:

- The compressive properties obtained by tests on cores adopting T-shaped and H-shaped cores relate in a similar proportion to the properties obtained by tests on wallets. Consequently, both core types are adequate for the in-situ investigations.
- A good correlation between the compressive strength obtained by tests on cores and tests on wallets is reported if the maximum stress is evaluated in agreement with the crack pattern. In the majority of the cases, the crack pattern at maximum load consisted of vertical crack located at the extremities of the regularisation cap, with the exception of some cores made of double wythe clay brick masonry. In the case of double wythe clay brick masonry, it should be noted that the presence of the joint in the thickness could influence the failure mode. Additionally, the crack pattern can be governed by the relative stiffness between the cap and the masonry.
- The ratio between the chord elastic modulus obtained by tests on cores and tests on wallets results less than the unitary value for both core types, ranging around 0.5. However, low values are reported for the calcium silicate brick masonry.
- The fracture energy in compression was calculated for the tests on core. However, high variability was observed in the comparison with the value obtained by tests on wallets (ratio varies between 0.5 and 1.3) indicating a poor correlation. This can be influenced by the cracking observed in the cap during the test.

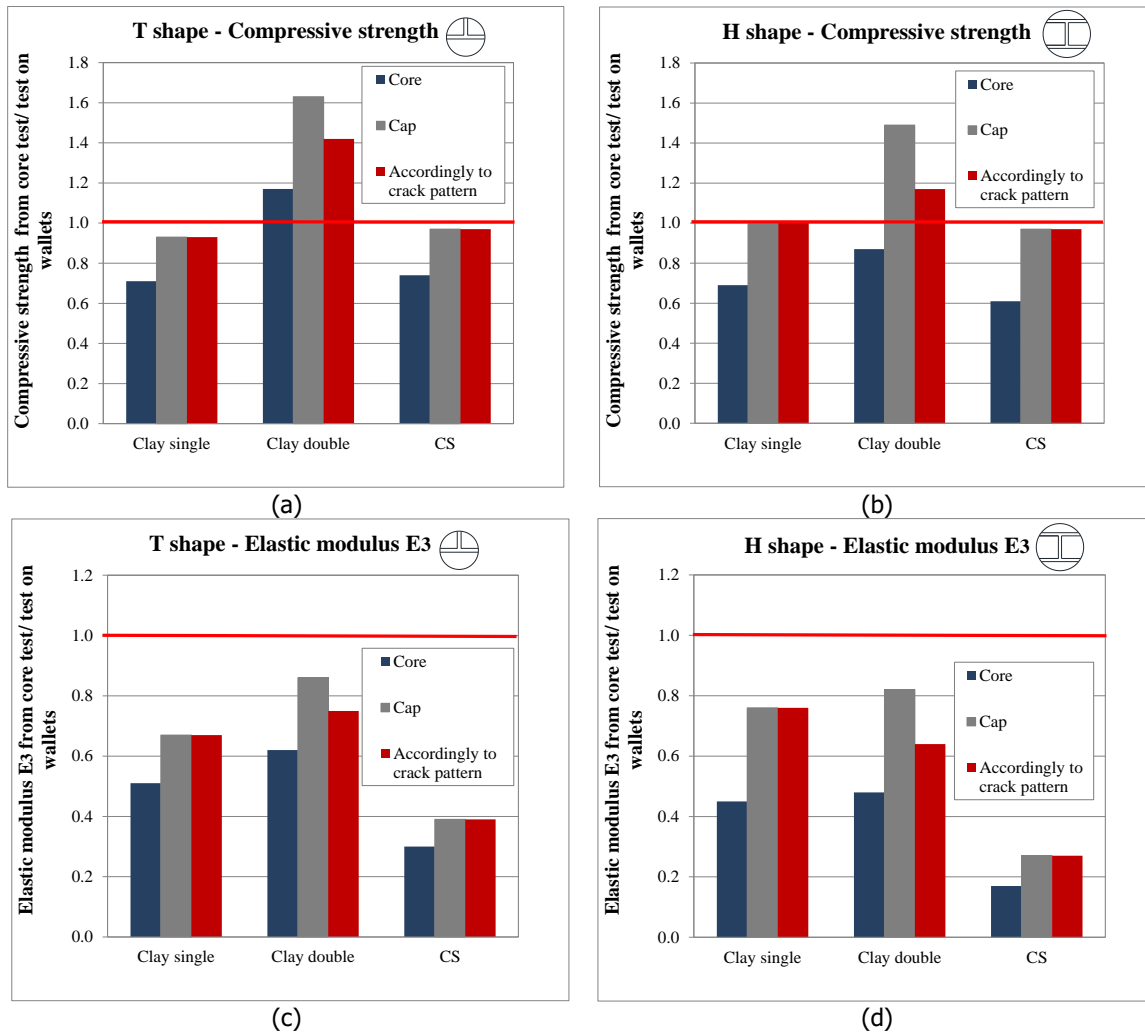


Figure 62 - Histogram representation of the ratio between the compression properties obtained by tests on T-shaped and H-shaped cores and tests on wallets: (a)-(b) compressive strength; (c)-(d) chord modulus. (Note: for single wythe clay brick masonry and CS brick masonry the failure was always in correspondence of the sides of the regularisation cap).



## 15 Evaluation of shear properties

As reported in literature, masonry cores subjected to splitting test were able to reproduce the masonry shear properties in terms of initial shear strength and coefficient of friction. In the current research program, similar tests are carried out to evaluate the shear properties.

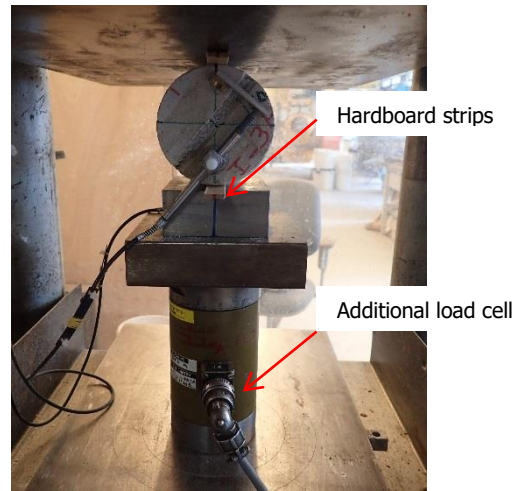
### 15.1 Testing procedure

Splitting tests on cores having a diameter of 100 mm were carried out inclining the mortar layer 40°, 45°, 50° and 55° with respect to its original position. The test allows inducing a mixed compression-shear stress state at the centre of the mortar joint.

The test was carried out by a displacement-controlled apparatus including a hydraulic jack with 300-ton capacity. Being the maximum splitting load was lower than the resolution of the hydraulic jack, an additional load cell was employed to register accurately the applied splitting load. Two hardboard strips, with density of 1099 kg/m<sup>3</sup> and dimension of 194x15x2-mm, were inserted between the loading plates and the sample to distribute the load. The relative sliding displacement between the two bricks was measured using one LVDT on each face. The LVDTs had a measuring range of 2 mm with an accuracy of 0.02%. A displacement rate of 0.5µm/s was adopted.



(a)



(b)

Figure 63 – Evaluation of shear properties with test on core: (a) specimen; (b) splitting test set-up.

### 15.2 Experimental results

The axial stress at failure and the shear strength are determined as:

$$f_{p,core} = \frac{F_{max}}{A} \cos \alpha \quad (3)$$

$$f_{v,core} = \frac{F_{max}}{A} \sin \alpha \quad (4)$$

where  $F_{max}$  is the maximum force,  $A$  is the area of the mortar layer, and  $\alpha$  is the mortar layer inclination, with respect to the horizontal reference.

By considering the Coulomb friction criterion, the value of the initial shear strength  $f_{v0,core}$  and the coefficient of friction  $\mu_{core}$  are evaluated by a linear regression of the shear and compressive stresses obtained by tests on cores with different mortar layer inclinations. In literature, two methods are reported for the evaluation of the shear properties of masonry. Following Pelà et al.[30], the properties are defined by considering the regression line approximating all the data obtained by tests on core with different inclinations. Following Mazzotti et al. [29], first the average of the shear and compression stress is made for each mortar inclination and subsequently the linear approximation is made to evaluate the properties of masonry. In this report, both methods are applied for comparison.

### 15.2.1 Single wythe clay brick masonry

Figure 64 shows the force versus the joint relative displacement measured between the two portions of bricks for cores made of single wythe clay brick masonry. Thanks to the displacement-controlled test set-up, the post-peak behaviour was recorded for some samples. However, in general a brittle failure was reported.

Table 34 to Table 37 show the main results for the splitting tests on cores made of single wythe clay brick masonry. Each table shows the maximum failure load, the corresponding compressive and the shear stress and the observed failure mode for each specimen. The splitting tests were performed at inclination angle between 40° to 55°. The observed failure modes for the core samples can be summarised as follows:

- Sliding along the brick-mortar interface (e.g. samples TUD-C-I7, TUD-C-I2). This type of failure in the current document is denoted as "SL".
- Sliding along the brick-mortar interface with cracking of the mortar joint and sliding at both sides of the joint. This failure mode can include also cracking of the brick near the loading point. This type of failure is denoted as "SL+SP". This type of failure usually exhibited higher load resistance with respect to pure sliding failure "SL".

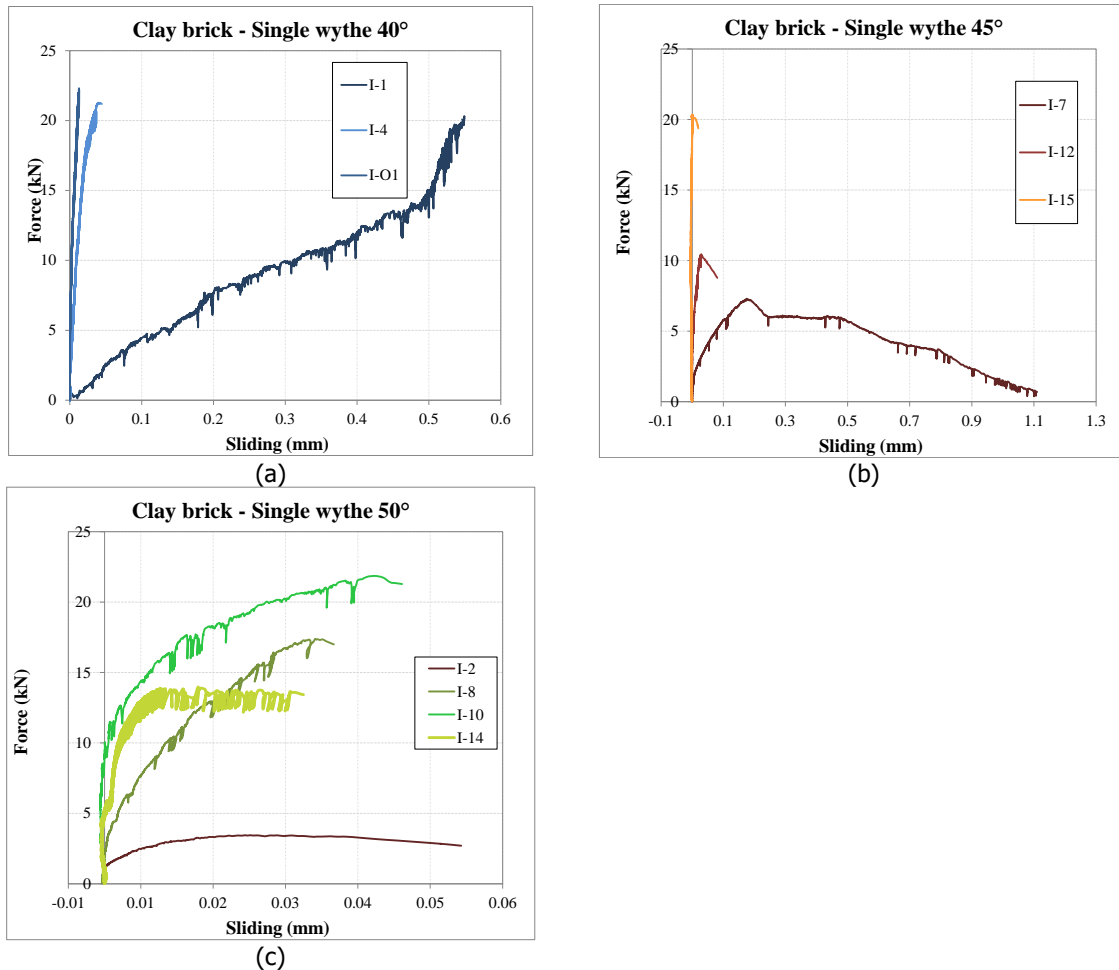


Figure 64 – Splitting load versus joint relative displacement for different mortar layer inclinations obtained by tests on cores made of single wythe clay brick masonry: (a)  $\alpha = 40^\circ$ ; (b)  $\alpha = 45^\circ$ ; (c)  $\alpha = 50^\circ$ .

Table 34 – Experimental results of splitting tests on core made of single wythe clay brick masonry tested with mortar layer inclination of  $\alpha = 40^\circ$ .


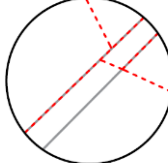
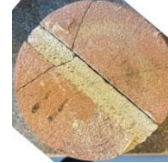
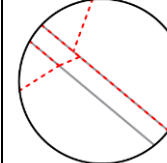

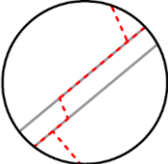

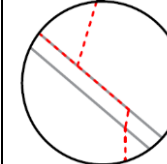

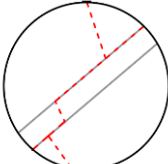

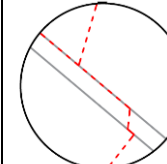
Test					Crack pattern			
ID	$F_{max}$ kN	$f_{p,c}$ MPa	$f_{v,c}$ MPa	Failure	Front		Back	
I-1	20.32	1.48	1.24	SL+SP				
I-4	21.28	1.55	1.30	SL+SP				
I-O1	22.37	1.71	1.44	SL+SP				

Table 35 – Experimental results of splitting tests on core made of single wythe clay brick masonry tested with mortar layer inclination  $\alpha = 45^\circ$ .


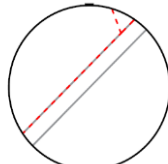

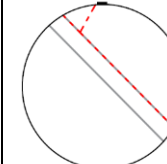
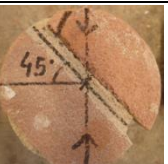
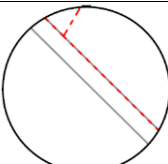

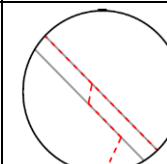

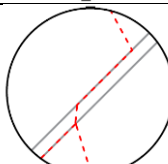

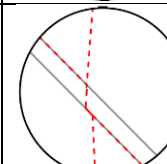
Test					Crack pattern			
ID	$F_{max}$ kN	$f_{p,c}$ MPa	$f_{v,c}$ MPa	Failure	Front		Back	
I-7	7.30	0.49	0.49	SL				
I-12	10.45	0.70	0.70	SL+SP				
I-15	20.51	1.38	1.38	SL+SP				

Table 36 – Experimental results of splitting tests on core made of single wythe clay brick masonry tested with mortar layer inclination  $\alpha = 50^\circ$ .

Test					Crack pattern			
ID	$F_{max}$ kN	$f_{p,c}$ MPa	$f_{v,c}$ MPa	Failure	Front		Back	
I-2	3.45	0.21	0.25	SL				
I-8	17.38	1.06	1.27	SL+SP				
I-10	21.86	1.34	1.59	SL+SP				
I-14	13.96	0.85	1.02	SL+SP				

Table 37 – Experimental results of splitting tests on core made of single wythe clay brick masonry tested with mortar layer inclination  $\alpha = 55^\circ$ .

Test					Crack pattern			
ID	$F_{max}$ kN	$f_{p,c}$ MPa	$f_{v,c}$ MPa	Failure	Front		Back	
I-13	13.62	0.74	1.06	SL				

Table 38 – Results of splitting tests on cores made of single wythe clay brick masonry.

$\alpha=40^\circ$			$\alpha=45^\circ$			$\alpha=50^\circ$			$\alpha=55^\circ$		
Cores name(*)	$f_p$ MPa	$f_v$ MPa	Cores name(*)	$f_p$ MPa	$f_v$ MPa	Cores name(*)	$f_p$ MPa	$f_v$ MPa	Cores name(*)	$f_p$ MPa	$f_v$ MPa
I-1	1.48	1.24	I-7	0.49	0.49	I-2	0.21	0.25	I-13	0.74	1.06
I-4	1.55	1.30	I-12	0.70	0.70	I-8	1.06	1.27			
I-01	1.71	1.44	I-15	1.38	1.38	I-10	1.34	1.59			
						I-14	0.85	1.02			
<b>Avg.</b>	<b>1.58</b>	<b>1.32</b>	<b>Avg.</b>	<b>0.86</b>	<b>0.86</b>	<b>Avg.</b>	<b>0.87</b>	<b>1.03</b>	<b>Avg.</b>	<b>0.74</b>	<b>1.06</b>
<b>St. dev.</b>	0.12	0.10	<b>St. dev.</b>	0.46	0.46	<b>St. dev.</b>	0.48	0.57	<b>St. dev.</b>	-	-
<b>C.o.V.</b>	0.07	0.08	<b>C.o.V.</b>	0.54	0.54	<b>C.o.V.</b>	0.56	0.55	<b>C.o.V.</b>	-	-

(\*) Complete specimen name starting with TUD-Core-

Table 38 lists the main results of splitting tests on core made of single wythe clay brick masonry. Increasing the mortar layer inclination results, as expected, in an increase of the shear component and a decrease of the normal component. The results of splitting tests on the cores tested at inclination angle of 40° is less scattered than any other inclination. Scattering of the results in the splitting tests is predictable, since the local conditions of the material components play a significant role on the results. However, the method based on the average results for each mortar inclination can be largely affected by the dispersion of the data obtained for each inclination, which in some cases can reach a variation of 50%.

Figure 65 shows the failure envelope in terms of shear stress versus compression stress relationship. First, the failure envelope is reported for each inclination (Figure 65a). Secondly, the two methods proposed by Pelà et al. [30] and Mazzotti et al. [29] are adopted considering all the results (Figure 65b) or the average results for each inclination (see Figure 65c). By adopting the two methods, similar results are obtained.

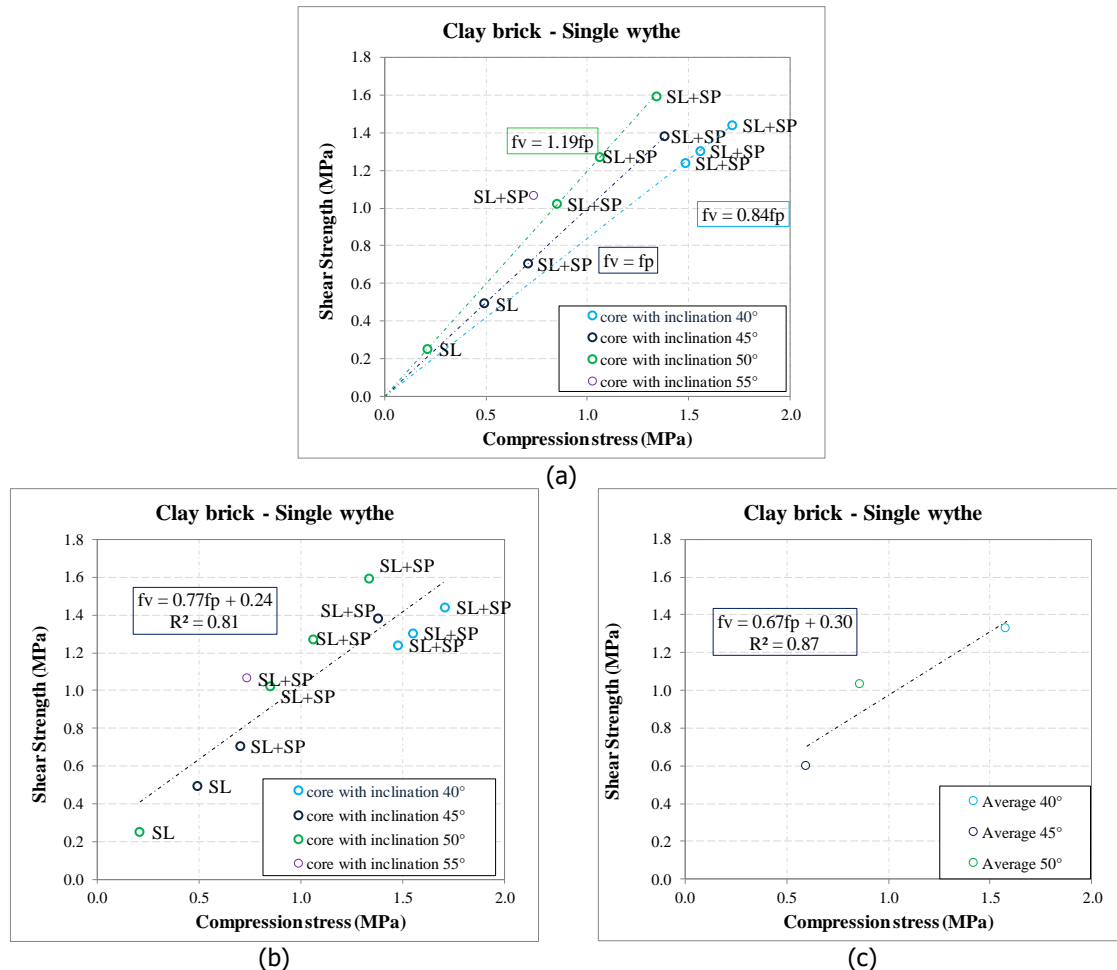


Figure 65 – Splitting tests on core made of single wythe clay brick masonry: (a) failure envelope for each inclination; (b) failure envelope obtained by using all the results; (c) failure envelope obtained by using the average result for each inclination.

To validate the test on core as a suitable in-situ test method, its results are correlated to the one obtained by standardised destructive tests. The shear properties of the brick-mortar interface can be investigated by shear-compressive on at least nine masonry triplets (EN 1052-3:2002 [18]). The shear properties of masonry, including the initial shear strength and coefficient of friction can be derived using the Coulomb friction criterion. Following the standard prescription, a three-stacked bonded brick specimen can be adopted, as shown in Figure 66. More detailed information regarding the testing set-up, testing procedure and the outcome of these tests can be found on Ref. [37].

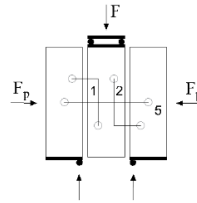


Figure 66 – Standard triplet adopted for shear-compression test.

Figure 67 and Table 39 give the comparison between the test results obtained by splitting tests on cores and triplet tests. For the test on cores, results are reported both considering each single result and considering the average value for each mortar layer inclination. Comparing the shear properties obtained from splitting tests on the cores extracted from the single wythe clay brick masonry wall with the results of tests on the companion samples, the following conclusions can be drawn:

- A good agreement between the results obtained by tests on core and triplet tests can be observed in terms of friction coefficient.
- Differently than the friction coefficient, the initial shear strength determined by tests on cores depends on the method adopted for the evaluation of the core results. In comparison with the triplet test, the method considering the average value for each mortar layer inclination gives the closest results. However, as previously remarked this method can be affected by the dispersion of the data for each mortar inclination.

It is worth noting that the obtained results from the core samples should be treated more carefully, since these samples were extracted from the wall previously subjected to in-plane loading.

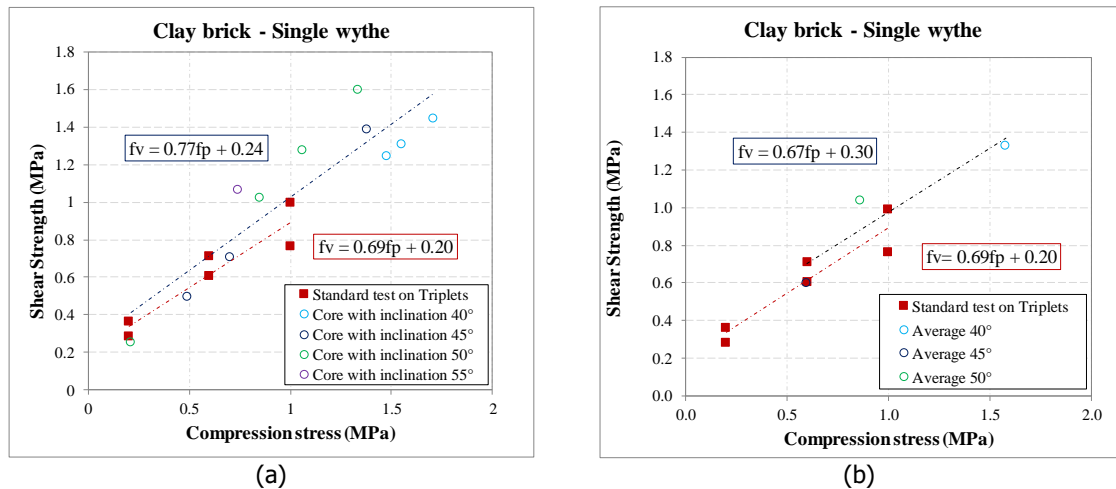


Figure 67 - Comparison between the results of tests on core and tests on triplets for single wythe clay brick masonry: (a) considering all the results of each inclination; (b) considering the average values for each inclination.

Table 39 – Comparison between the results of tests on cores and on triplets for single wythe clay brick masonry.

Shear properties		Initial shear strength	Coefficient of friction
		$f_{v0}$ MPa	$\mu$
Triplets		0.20	0.69
Core	All the results	0.24	0.77
	Average of the results	0.30	0.67
Ratio Core/ Triplets	All the results	1.20	1.12
	Average of the results	1.50	0.97



### 15.2.2 Double wythe clay brick masonry

Figure 68 shows the force versus the joint relative displacement measured between the two portions of bricks for cores made of double wythe clay brick masonry. Thanks to the displacement-controlled test set-up, the post-peak behaviour was recorded for some samples. However, in general a brittle failure was reported.

Table 40 to Table 43 show the main results for the splitting tests on core made of double wythe clay brick masonry. It should be mentioned that the extracted cores were cut in half in the thickness in correspondence of a head joint (Figure 69). Each table shows the maximum failure load, the corresponding compressive and the shear stress and the observed failure mode for each specimen. The splitting tests were performed at inclination angle between  $40^\circ$  to  $55^\circ$ . The observed failure modes for the core samples can be summarised as follows:

- Sliding along the brick-mortar interface ("SL", e.g. TUD-C- I-8S, TUD-C-I9).
- Sliding along the brick-mortar interface including cracking of the mortar joint and of the bricks, resulting in the formation of a brick wedge. This type of failure usually exhibited higher load resistance ("SL+SP", e.g. TUD-C- I2B, TUD-C-I1).

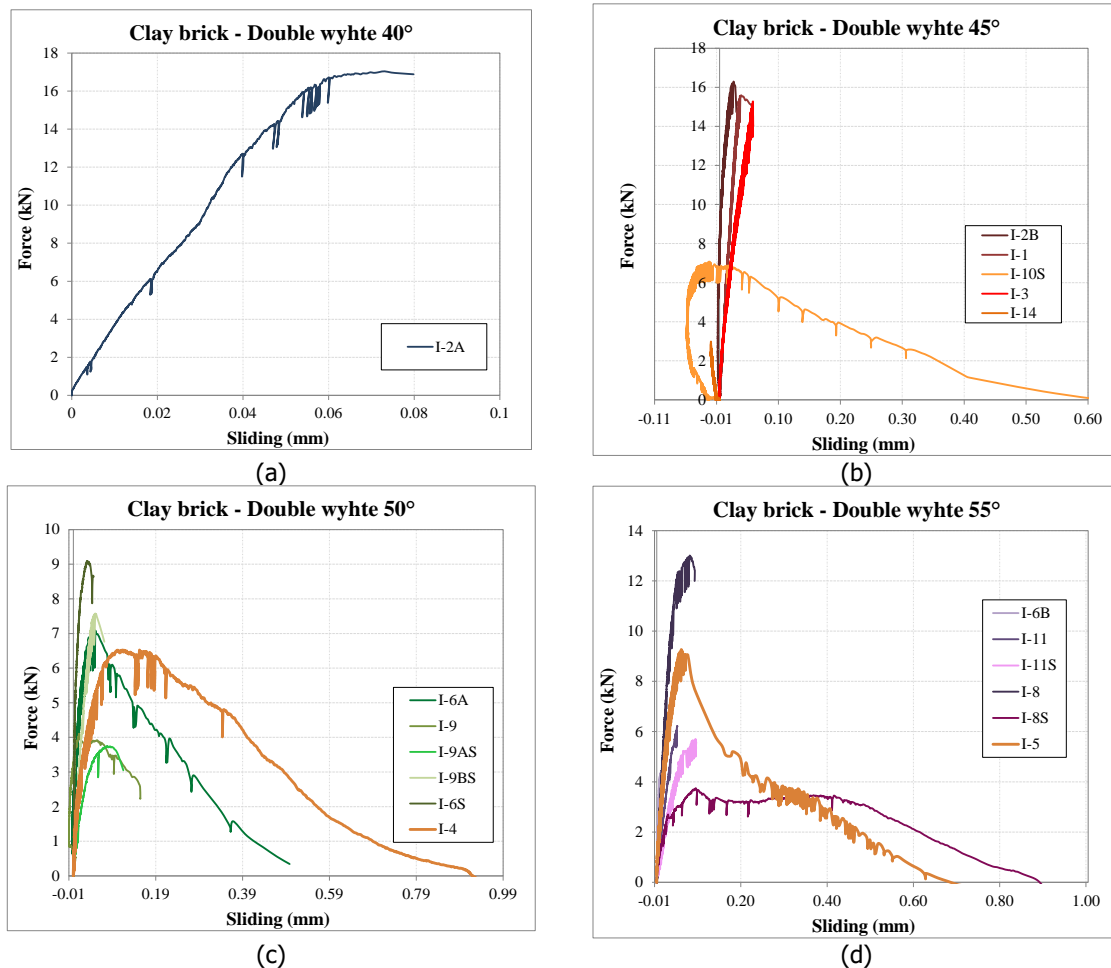


Figure 68 - Splitting load versus joint relative displacement for different mortar layer inclinations obtained by tests on cores cut from double wythe clay brick masonry: (a)  $\alpha = 40^\circ$ ; (b)  $\alpha = 45^\circ$ ; (c)  $\alpha = 50^\circ$ ; (d)  $\alpha = 55^\circ$ .



(a)



(b)

Figure 69 – Core samples extracted from the double wythe wall.

Table 40 - Experimental results of splitting tests on core samples with  $\alpha = 40^\circ$ .


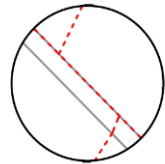

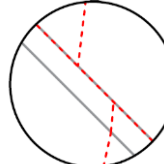

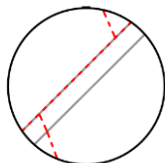

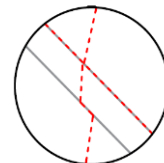

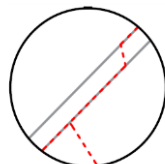

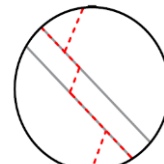

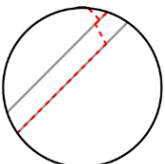

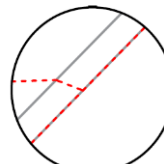

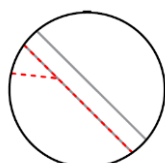

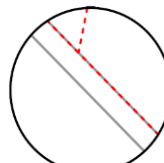
Test					Crack pattern			
ID	$F_{max}$ kN	$f_{p,c}$ MPa	$f_{v,c}$ MPa	Failure	Front		Back	
I-2A	17.04	1.37	1.15	SL+SP				

Table 41 - Experimental results of splitting tests on core samples with  $\alpha = 45^\circ$ .

Test					Crack pattern			
ID	$F_{max}$ kN	$f_{p,c}$ MPa	$f_{v,c}$ MPa	Failure	Front		Back	
I-2B	16.3	1.21	1.21	SL+SP				
I-1	15.6	1.17	1.17	SL+SP				
I-10S	7.08	0.52	0.52	SL+SP				
I-3	15.3	1.12	1.12	SL+SP				




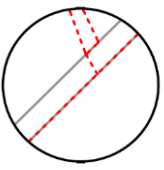

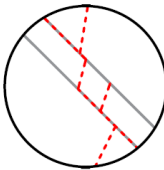
I-14S	20.7	1.47	1.47	SL+SP				
-------	------	------	------	-------	---	--	---	---

Table 42 - Experimental results of splitting tests on core samples with  $\alpha = 50^\circ$ .

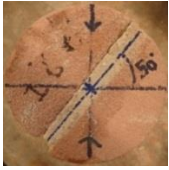
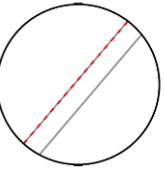

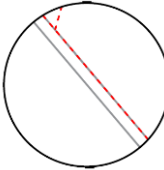

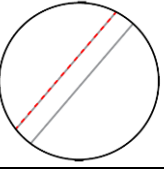

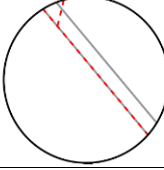

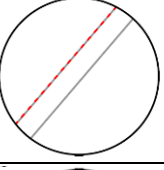

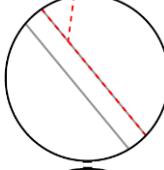

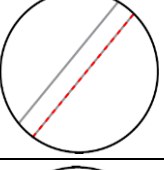

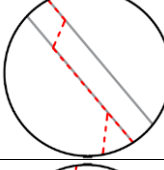

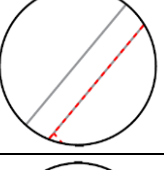
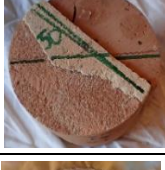
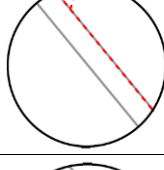

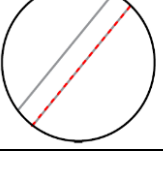

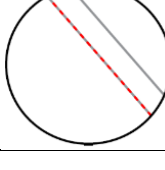
Test					Crack pattern			
ID	$F_{max}$ kN	$f_{p,c}$ MPa	$f_{v,c}$ MPa	Failure	Front		Back	
I-6A	7.08	0.48	0.57	SL				
I-9	4.10	0.27	0.32	SL				
I-9SA	3.74	0.25	0.30	SL				
I-9SB	7.58	0.51	0.61	SL+SP				
I-6S	9.09	0.6	0.71	SL+SP				
I-4	6.52	0.45	0.53	SL				

Table 43 - Experimental results of splitting tests on core samples with  $\alpha = 55^\circ$ .


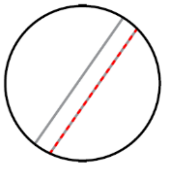
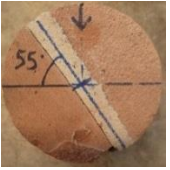
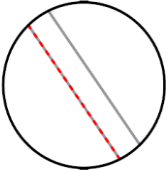

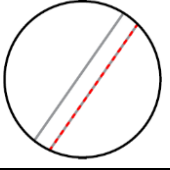

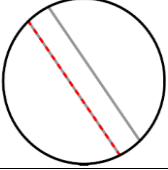

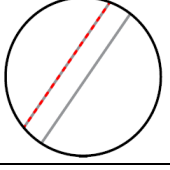

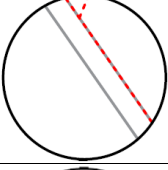

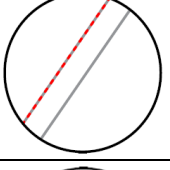

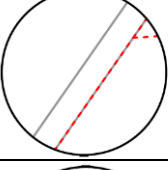

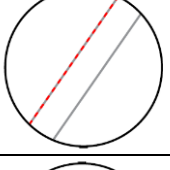
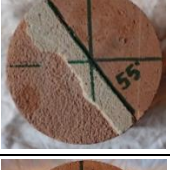
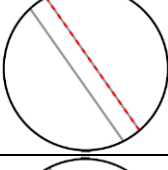

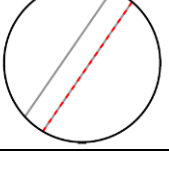

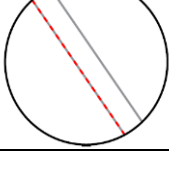
Test					Crack pattern			
ID	$F_{max}$ kN	$f_{p,c}$ MPa	$f_{v,c}$ MPa	Failure	Front		Back	
I-6B	4.38	0.26	0.38	SL				
I-11	7.34	0.45	0.60	SL				
I-11S	6.06	0.37	0.53	SL				
I-8	13.01	0.76	1.08	SL+SP				
I-8S	3.75	0.22	0.32	SL				
I-5	9.27	0.55	0.78	SL				

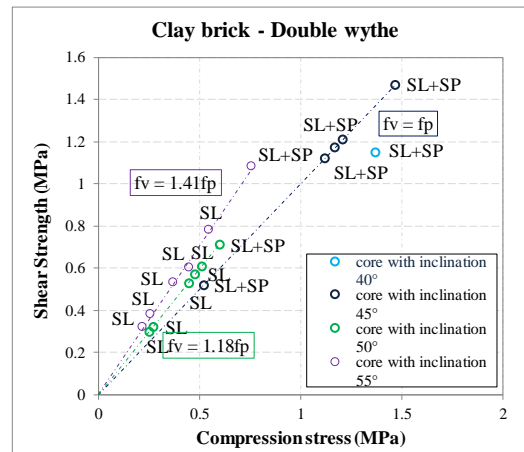
Table 44 lists the main results of splitting tests on core made of double wythe clay brick masonry. As expected, increasing the mortar layer inclination results in an increase in the shear component and a decrease in the normal component. The wide dispersion of the results from the splitting tests is observed for the double wythe clay brick masonry specimens as observed by other authors ([29]-[30]). Scattering of the results in the splitting tests is predictable, since the local conditions of the material components play a significant role on the results.

Figure 70 shows the failure envelope in terms of shear versus compression stress relationship. First, the failure envelope is reported for each inclination (Figure 70a). Secondly, the two methods proposed by Pelà et al. [30] and Mazzotti et al. [29] are adopted considering all the results (Figure 70b) or the average results for each inclination (see Figure 70c). By comparing the two methods, a lower value of initial shear strength and an higher value of friction coefficient is found when the average values for each inclination are considered. However, this method can be influenced by the scatter of the results obtained for each inclination.

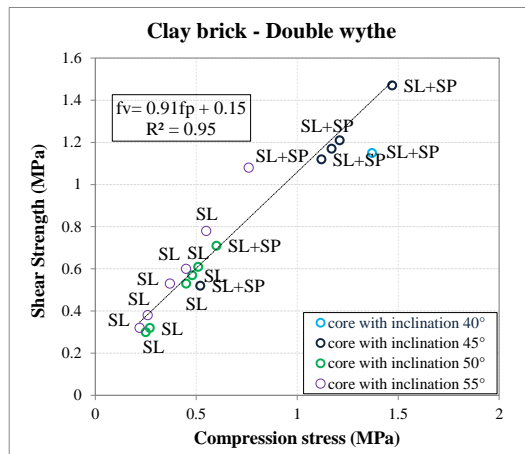
Table 44 - Results of splitting tests on cores made of double wythe clay brick masonry.

$\alpha=40^\circ$			$\alpha=45^\circ$			$\alpha=50^\circ$			$\alpha=55^\circ$		
Cores name(*)	$f_p$ MPa	$f_v$ MPa	Cores name(*)	$f_p$ MPa	$f_v$ MPa	Cores name(*)	$f_p$ MPa	$f_v$ MPa	Cores name(*)	$f_p$ MPa	$f_v$ MPa
I-2A	1.37	1.15	I-2B	1.21	1.21	I-6A	0.48	0.57	I-6B	0.26	0.38
			I-1	1.17	1.17	I-9	0.27	0.32	I-11	0.45	0.60
			I-10S	0.52	0.52	I-9SA	0.25	0.30	I-11s	0.37	0.53
			I-3	1.12	1.12	I-9SB	0.51	0.61	I-8	0.76	1.08
			I-14S	1.47	1.47	I-6S	0.60	0.71	I-8S	0.22	0.32
<b>Avg.</b>	<b>1.37</b>	<b>1.15</b>	<b>Avg.</b>	<b>1.09</b>	<b>1.09</b>	<b>Avg.</b>	<b>0.43</b>	<b>0.51</b>	<b>Avg.</b>	<b>0.44</b>	<b>0.62</b>
<b>St. dev.</b>	-	-	<b>St. dev.</b>	0.35	0.35	<b>St. dev.</b>	0.14	0.16	<b>St. dev.</b>	0.20	0.28
<b>C.o.V.</b>	-	-	<b>C.o.V.</b>	0.32	0.32	<b>C.o.V.</b>	0.32	0.32	<b>C.o.V.</b>	0.46	0.46

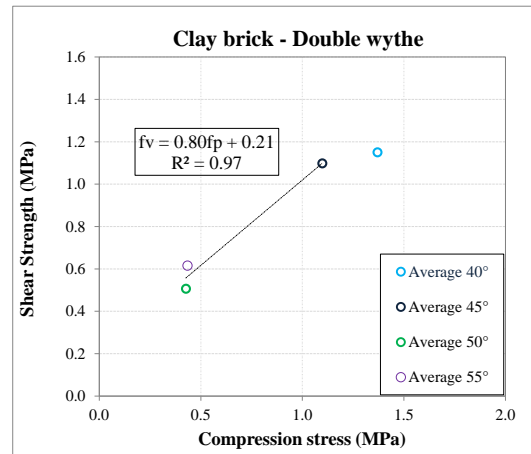
(\*) Complete specimen name starting with TUD-C-



(a)



(b)



(c)

Figure 70 – Interpretation of splitting tests: (a) failure envelope for each type of inclination; (b) failure envelope obtained by using all the results; (c) failure envelope obtained by using the average result for each inclination.

To validate the test on core as a suitable in-situ test method, its results are correlated to the one obtained by standardised destructive tests (Figure 66). Figure 71 and Table 45 give the comparison between the test results obtained by splitting tests on core and triplet tests. For the test on cores, results are reported both considering each single result and considering the average value for each mortar layer inclination. Comparing the shear properties obtained from splitting tests on the cores extracted from the double wythe clay brick masonry wall with the results of tests on the companion samples, it can be concluded that both the initial shear strength and the friction coefficient determined by tests on cores depends on the method adopted for the evaluation of the core results. In comparison with the triplet test, the method considering the average value for each mortar layer inclination gives the closest results. However, as previously remarked this method can be affected by the dispersion of the data for each mortar inclination.

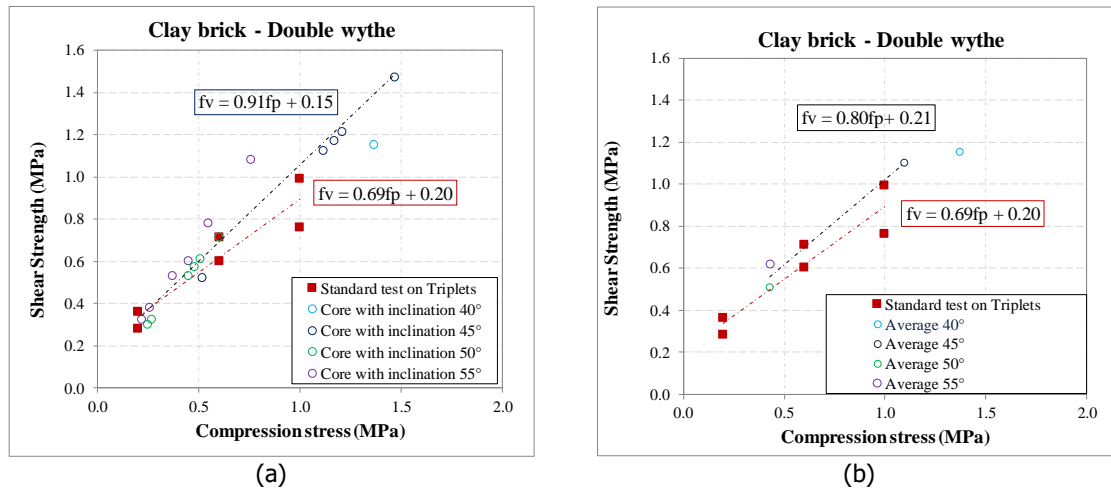


Figure 71 - Comparison between the results of double wythe clay brick masonry cores and tests on triplets: (a) considering all the results of each inclination; (b) considering the mean values for each inclination.

Table 45 – Shear properties of cores sawn-cut from the double wythe clay brick masonry and triplets.

Test method		Initial shear strength	Coefficient of friction
		$f_{v0}$ MPa	$\mu$
Triplets		0.20	0.69
Core	All the results	0.15	0.91
	Average of the results	0.21	0.80
Ratio Core/ Triplets	All the results	0.75	1.32
	Average of the results	1.05	1.16

### 15.2.3 Calcium silicate brick masonry

Figure 72 shows the force versus the joint relative displacement measured between the two portions of bricks for cores made of CS brick masonry. Thanks to the displacement-controlled test set-up, the post-peak behaviour was recorded for some samples. However, in general a brittle failure was reported.

Table 46 to Table 49 show the main results for the splitting tests on core made of CS brick masonry. Each table shows the maximum failure load, the corresponding compressive and the shear stress and the observed failure mode for each specimen. The splitting tests were performed at inclination angle between 40° to 55°. The observed failure modes for the core samples can be summarised as follows:

- Sliding along the brick-mortar interface, corresponding to low value of the ultimate load ("SL", e.g. TUD-C-I7C, TUD-C-I7A).
- Sliding along the brick-mortar interface including cracking of the mortar joint and of the bricks, resulting in the formation of a brick wedge. The crack mostly involves with splitting of a brick wedge. This type of failure usually exhibited higher load resistance ("SL+SP", e.g. TUD-C-I5B).

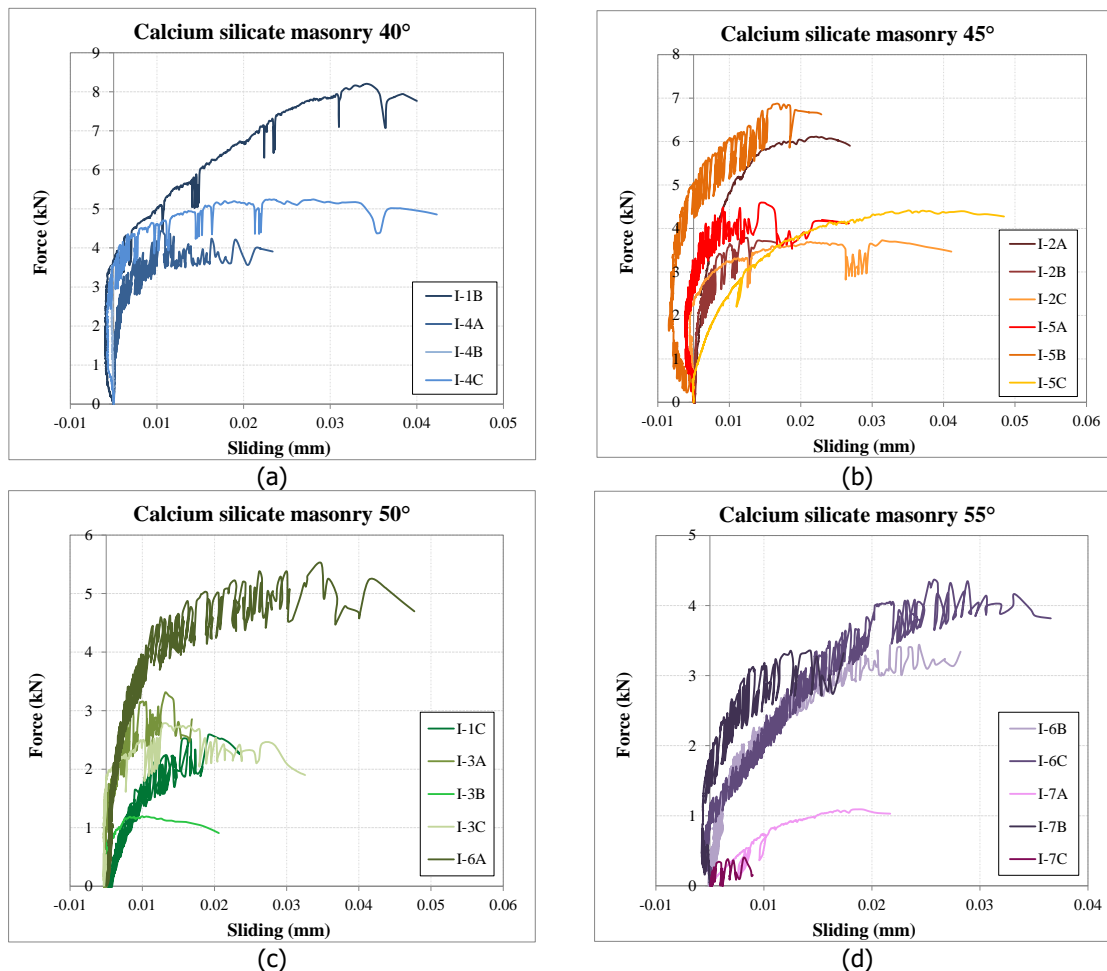


Figure 72 - Splitting load versus joint relative displacement for different mortar layer inclinations obtained by tests on cores made of CS brick masonry: (a)  $\alpha = 40^\circ$ ; (b)  $\alpha = 45^\circ$ ; (c)  $\alpha = 50^\circ$ ; (d)  $\alpha = 55^\circ$ .

Table 46 - Experimental results of splitting tests on core samples with  $\alpha = 40^\circ$ .


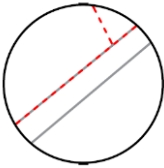

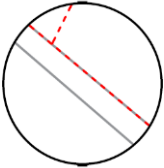

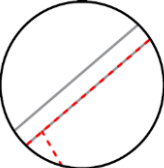

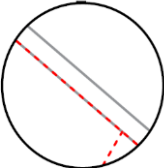

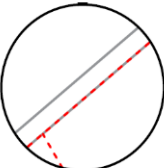

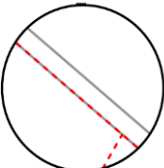

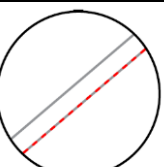

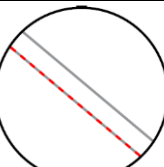
Test					Crack pattern			
ID	$F_{max}$ kN	$f_{p,c}$ MPa	$f_{v,c}$ MPa	Failure	Front		Back	
I-1B	8.20	0.66	0.56	SL+SP				
I-4A	4.45	0.36	0.30	SL+SP				
I-4B	3.53	0.28	0.24	SL+SP				
I-4C	5.24	0.42	0.25	SL				



Table 47 - Experimental results of splitting tests on core samples with  $\alpha = 45^\circ$ .


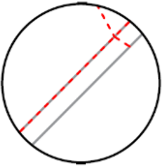

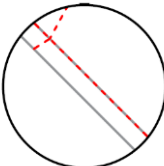
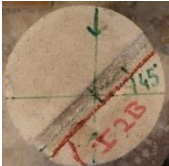
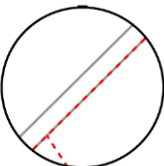

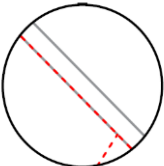

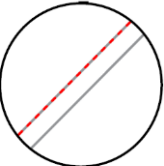

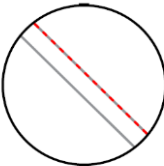

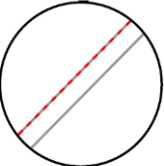

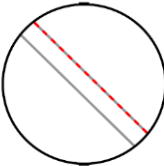

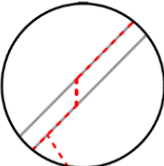

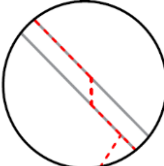

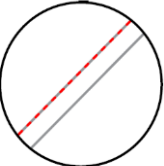

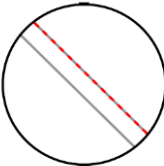
Test					Crack pattern			
ID	$F_{max}$ kN	$f_{p,c}$ MPa	$f_{v,c}$ MPa	Failure	Front		Back	
I-2A	6.11	0.46	0.46	SL+SP				
I-2B	3.80	0.28	0.28	SL+SP				
I-2C	3.73	0.28	0.28	SL				
I-5A	4.59	0.34	0.34	SL				
I-5B	6.87	0.51	0.51	SL+SP				
I-5C	4.77	0.35	0.35	SL				

Table 48 - Experimental results of splitting tests on core samples with  $\alpha = 50^\circ$ .


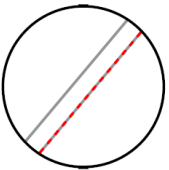

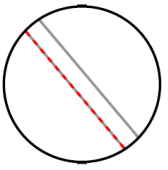

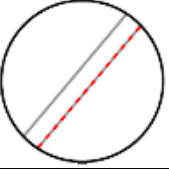

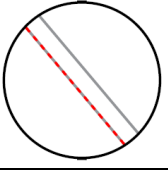

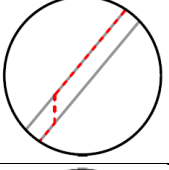

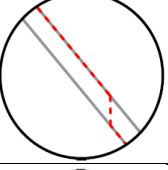

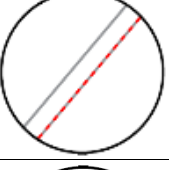

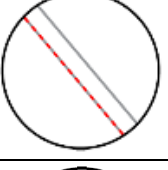
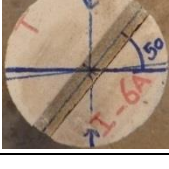
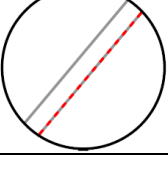

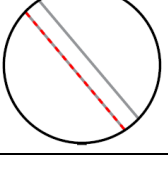
Test					Crack pattern			
ID	$F_{max}$ kN	$f_{p,c}$ MPa	$f_{v,c}$ MPa	Failure	Front		Back	
I-1C	2.58	0.17	0.21	SL				
I-3A	3.31	0.22	0.27	SL				
I-3B	1.20	0.08	0.10	SL				
I-3C	2.79	0.19	0.22	SL				
I-6A	5.52	0.37	0.45	SL				



Table 49 - Experimental results of splitting tests on core samples with  $\alpha = 55^\circ$ .


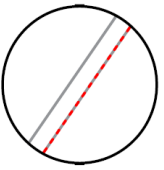
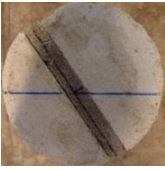
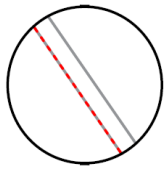

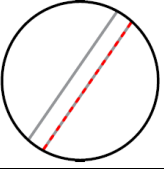

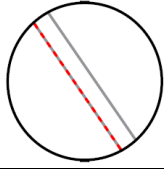

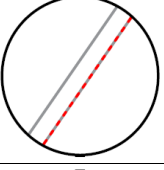

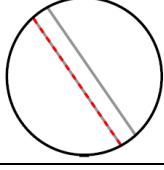
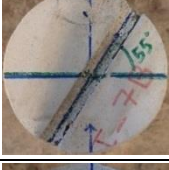
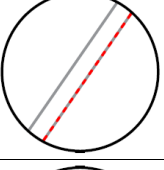

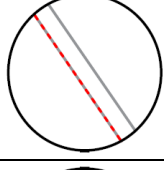

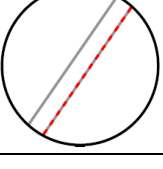

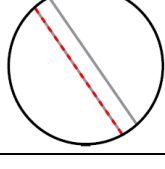
Test					Crack pattern			
ID	$F_{max}$ kN	$f_{p,c}$ MPa	$f_{v,c}$ MPa	Failure	Front		Back	
I-6B	3.44	0.21	0.30	SL				
I-6C	4.37	0.26	0.38	SL				
I-7A	1.09	0.07	0.09	SL				
I-7B	3.35	0.20	0.29	SL				
I-7C	0.40	0.02	0.03	SL				

Table 50 lists the results of splitting tests for each type of inclination for the CS brick masonry. Increasing the mortar layer inclination results, as expected, in an increase of the shear component and a decrease of the normal component. For each inclination, the results show a coefficient of variation between 40 to 50%. The wide dispersion of the results from the splitting tests is observed for the CS brick masonry specimens as observed by other authors ([29]-[30]). Scattering of the results in the splitting tests is predictable, since the local conditions of the material components play a significant role on the results.

Table 50 - Results of splitting tests on cores made of calcium silicate brick masonry.

$\alpha=40^\circ$			$\alpha=45^\circ$			$\alpha=50^\circ$			$\alpha=55^\circ$		
Cores name(*)	$f_p$	$f_v$	Cores name(*)	$f_p$	$f_v$	Cores name(*)	$f_p$	$f_v$	Cores name(*)	$f_p$	$f_v$
	MPa	MPa		MPa	MPa		MPa	MPa		MPa	MPa
I-1B	0.66	0.56	I-2A	0.46	0.46	I-1C	0.17	0.21	I-7A	0.07	0.09
I-4A	0.36	0.30	I-2B	0.28	0.28	I-3A	0.22	0.27	I-7B	0.20	0.29
I-4B	0.28	0.24	I-2C	0.28	0.28	I-3B	0.08	0.10	I-7C	0.02	0.03
I-4C	0.42	0.35	I-5A	0.34	0.34	I-3C	0.19	0.22	I-6B	0.21	0.30
			I-5B	0.51	0.51	I-6A	0.37	0.45	I-6C	0.26	0.38
			I-5C	0.35	0.35						
<b>Avg.</b>	<b>0.43</b>	<b>0.38</b>	<b>Avg.</b>	<b>0.37</b>	<b>0.37</b>	<b>Avg.</b>	<b>0.21</b>	<b>0.25</b>	<b>Avg.</b>	<b>0.15</b>	<b>0.22</b>
<b>St. dev.</b>	0.16	0.14	<b>St. dev.</b>	0.11	0.11	<b>St. dev.</b>	0.11	0.13	<b>St. dev.</b>	0.10	0.15
<b>C.o.V.</b>	0.38	0.37	<b>C.o.V.</b>	0.29	0.29	<b>C.o.V.</b>	0.51	0.51	<b>C.o.V.</b>	0.67	0.67

(\*) Complete specimen name starting with TUD-Core-

Figure 73 shows the failure envelope in terms of shear versus compression stress relationship. First, the failure envelope is reported for each inclination (Figure 73a). Secondly, the two methods proposed by Pelà et al. [30] and Mazzotti et al. [29] are adopted considering all the results (Figure 73b) or the average results for each inclination (see Figure 73c). By comparing the two methods, a lower value of initial shear strength and an higher value of friction coefficient is found when the linear regression considers the average value for each inclination. However, this method can be influenced by the scatter of the results obtained for each inclination.

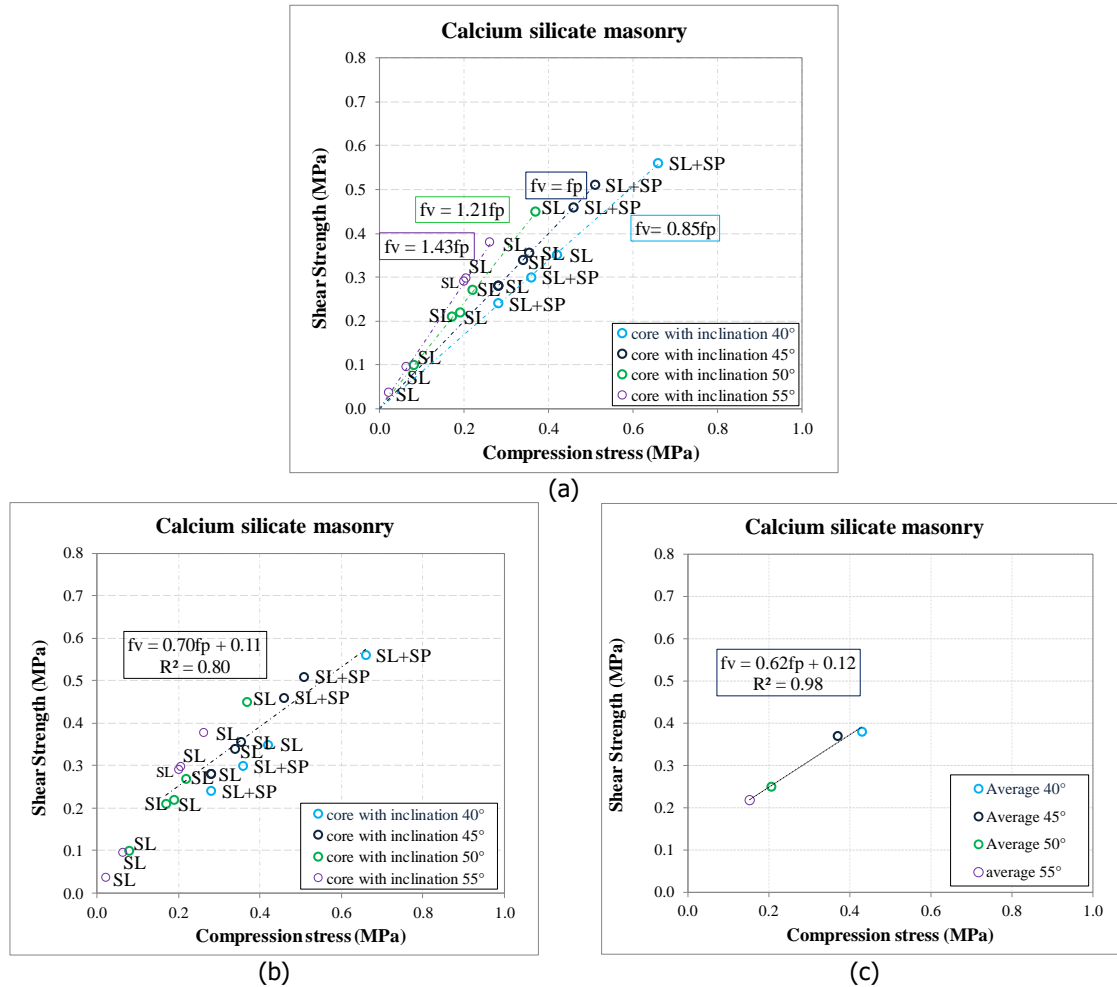


Figure 73 – Interpretation of splitting tests: (a) failure envelope for each type of inclination; (b) failure envelope obtained by using all the results; (c) failure envelope obtained by using the average result for each inclination.

To validate the test on core as suitable in-situ test method, its results are correlated to the one obtained by standardised destructive tests (Figure 66). Figure 74 and Table 51 give the comparison between the test results obtained by splitting tests on core and triplet test. For the test on core, results are reported both considering each single result and considering the average value for each mortar layer inclination. Comparing the shear properties obtained from splitting tests on the cores extracted from the CS brick masonry wall with the results of tests on the companion samples, it can be concluded that:

- A good agreement between the results obtained by tests on core and triplet tests can be observed in terms of initial shear strength.
- Differently than initial shear strength, the friction coefficient determined by tests on cores depends on the method adopted for the evaluation of the core results. In comparison with the triplet test, the method considering the average value for each mortar layer inclination gives the closest results. However, as previously remarked this method can be affected by the dispersion of the data for each mortar inclination.

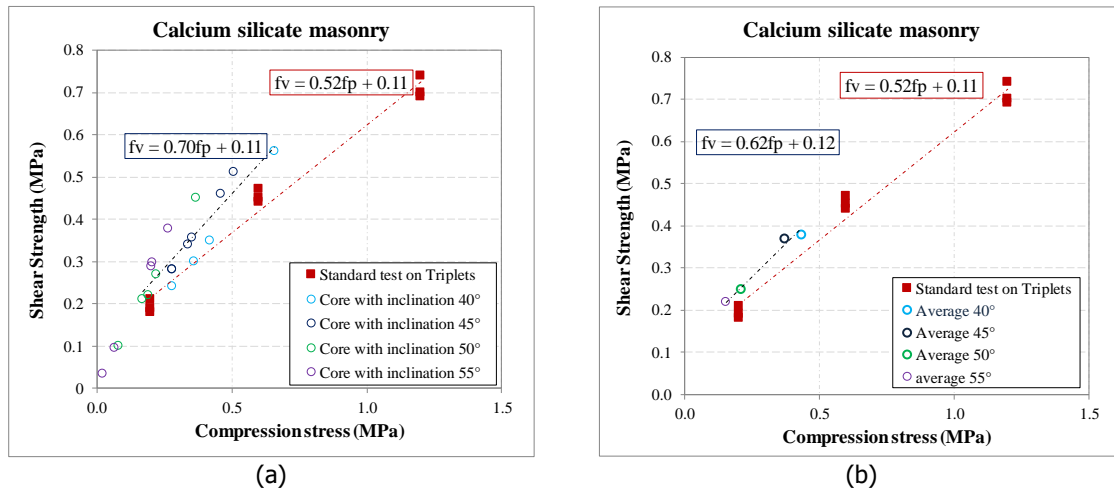


Figure 74 - Comparison between the results of calcium silicate core samples and tests on triplets: (a) considering all the results of each inclination; (b) considering the mean values for each inclination.

Table 51 – Shear properties of calcium silicate masonry cores and triplets.

Test method		Initial shear strength	Coefficient of friction
		$f_{v0}$ MPa	$\mu$
Triplet		0.11	0.52
Core	All the results	0.11	0.70
	Average of the results	0.12	0.62
Ratio Core/ Triplets	All the results	1.00	1.35
	Average of the results	1.09	1.19

### 15.2.4 Summary of the shear properties

The applicability of the core technique to evaluate the shear properties of masonry was validated by comparing the obtained results with the results of standardised tests on triplets. To describe the shear failure of the brick-mortar interface, the Mohr-Coulomb failure criterion is adopted. The value of the initial shear strength  $f_{v0,core}$  and the coefficient of friction  $\mu_{core}$  are evaluated by a linear regression of the shear and compressive stresses obtained by tests on cores with different mortar layer inclinations. In literature, two methods are reported for the evaluation of the shear properties of masonry. Following Pelà et al.[30], the properties are defined by considering the regression line approximating all the data obtained by tests on cores with different inclinations. Following Mazzotti et al. [29], first the average of the shear and compression stress is made for each mortar inclination and subsequently the linear approximation is made to evaluate the shear properties of masonry. In this report, both methods are applied for comparison.

Figure 75 shows the comparison for single wythe clay brick masonry, double wythe clay brick masonry and calcium silicate brick masonry in terms of ratio between the shear properties obtained by tests on cores and on wallets. Considering the obtained results the following conclusions can be drawn:

- Both the initial shear strength and the friction coefficient determined by tests on cores depend on the methods adopted for the evaluation of the shear properties of cores.
- The ratio between the initial shear strength obtained by tests on triplets and tests on core for clay brick masonry deviates from the unitary value. Differently, for the calcium silicate brick masonry a good agreement is reported.
- The ratio between the friction coefficient obtained by tests on triplets and tests on cores for the three type of brick masonry tested ranges between 1.0 and 1.3.

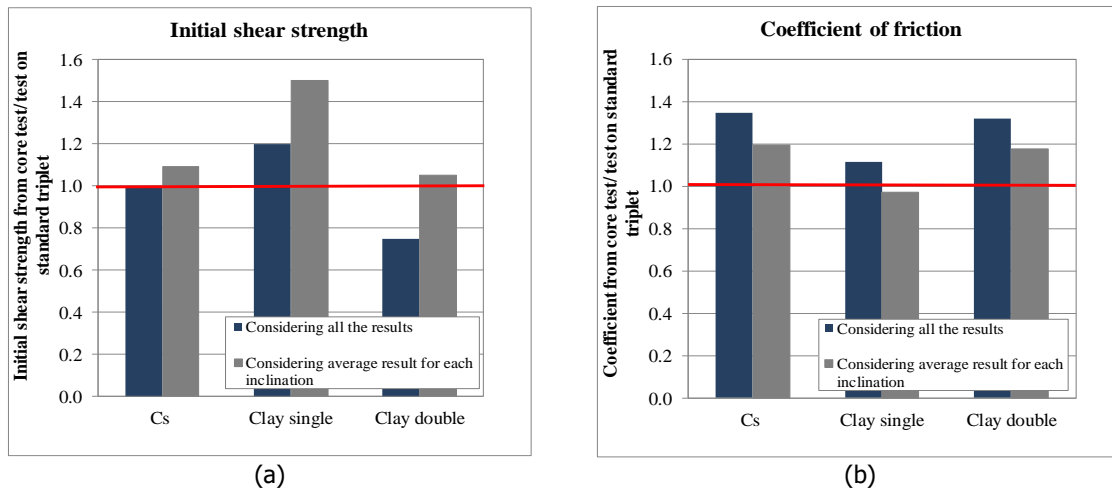


Figure 75 - Histogram representation of the ratio between the shear properties obtained by tests on cores and tests on triplets: (a) initial shear strength; (b) coefficient of friction.

## 16 Spatial variability of the properties across the height of wall

The degree of spatial variability in material properties of unreinforced masonry (URM) is much higher than the other structural materials, such as steel or concrete [39]. To investigate the possible spatial variability of the masonry properties across the height of wall, a sampling strategy was defined aiming to extract the cores at different locations.

Figure 76 to Figure 78 show the variability of the compressive strength, the chord elastic modulus and the shear strength for double wythe clay brick masonry and CS brick masonry. The properties are normalised with respect to the average values; the average value and the standard deviation are given. The obtained results did not show a correlation between the variability of the properties and the location of the extraction. Please note that these results have been obtained for core extracted by replicated masonry walls built in controlled environmental conditions. Additionally, it is possible to note that the CS brick masonry shows a lower variability of the compressive strength and the shear strength with respect to the double wythe clay brick masonry. On the contrary, a similar variability is obtained for the chord Young's modulus.

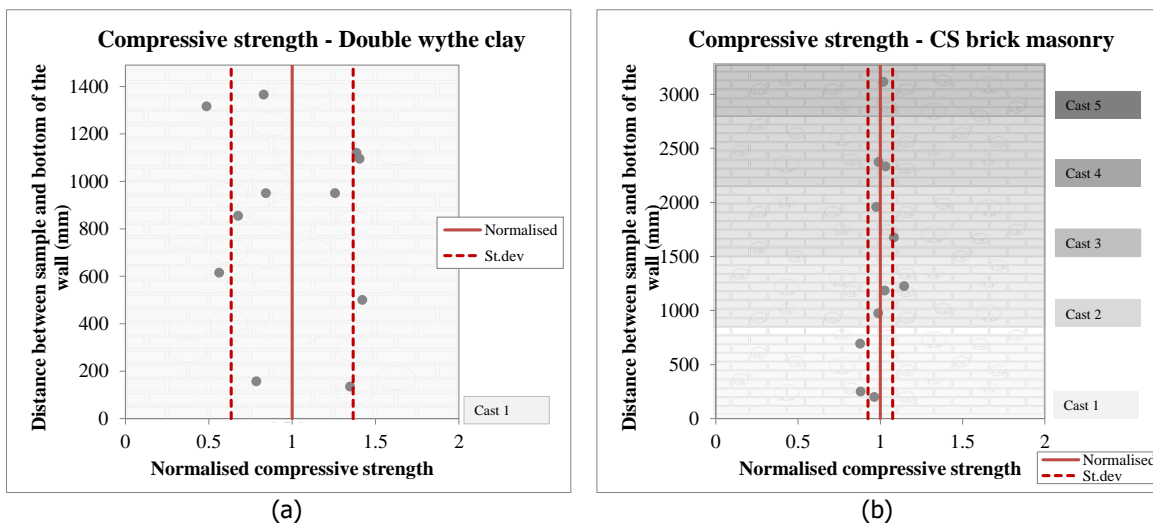


Figure 76 – Spatial variability of the compressive strength: (a) double wythe clay brick masonry; (b) calcium silicate brick masonry.

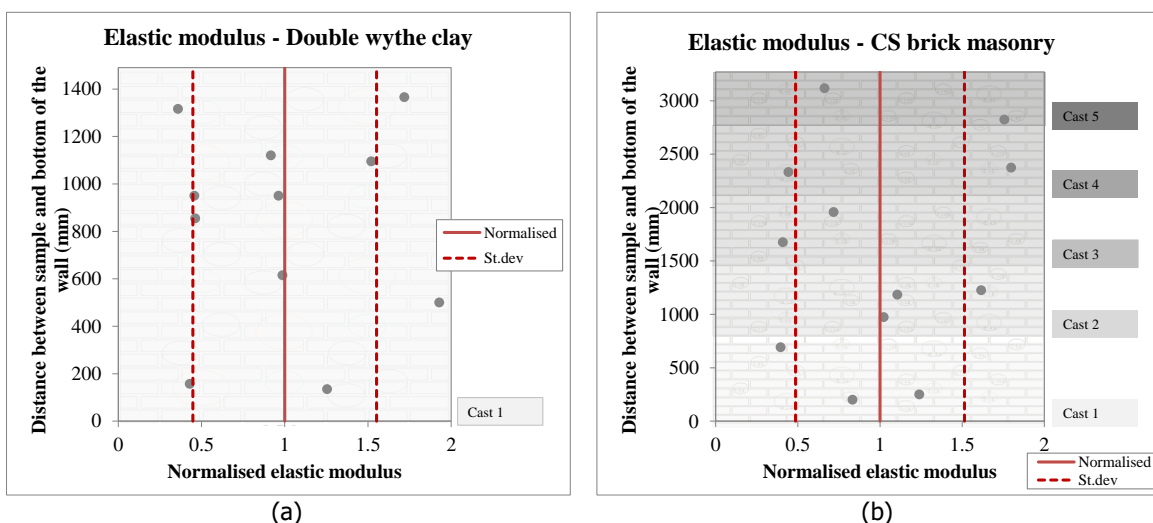


Figure 77 – Spatial variability of the Young's modulus: (a) double wythe clay brick masonry; (b) calcium silicate brick masonry.

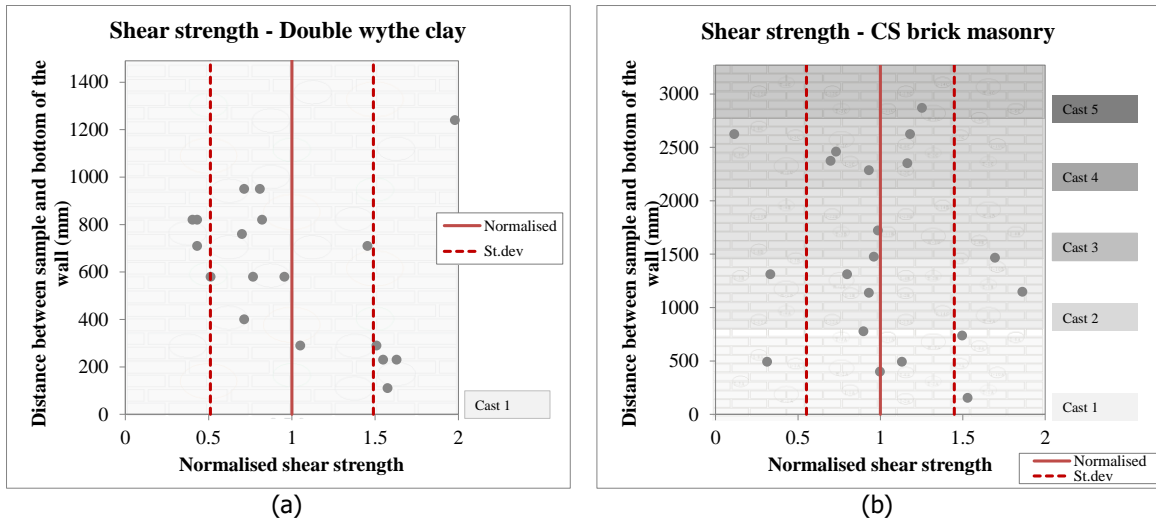


Figure 78 – Spatial variability of maximum shear strength: (a) double wythe clay brick masonry; (b) calcium silicate brick masonry.

## 17 Meta-analysis

In order to provide correlations between the material properties obtained by tests on cores and the one obtained by standardised destructive tests a meta-analysis is performed. The studies carried out by Pelà et al. ([24]-[30]), Sassoni et al. ([25]-[26]) and Mazzotti et al. [29] are combined with the one obtained in the current research. It should be pointed out that the results of the studies conducted by Brencich et al. [22] and Ispir et al. [23] are not taken into consideration, since different testing procedure was adopted by them.

Figure 79 shows the correlation between the tests on core and the tests on wallets in terms of compressive strength and chord elastic modulus. In this analysis, the compressive properties have been evaluated considering the cross-sectional area accordingly to the failure mode. This procedure has also been applied to the literature data by considering loaded area as the cross-sectional area of the cap for the data by Pelà et al. [24] and cross-sectional area of the core for the data by Sassoni et al. [25].

The analysis shows a good correlation ( $R^2 = 0.74$ ) in terms of compressive strength independently from the masonry type and the size of the core (Figure 79a). The following formulation is proposed for the evaluation of the compressive strength from tests on core:

$$f'_m = 0.89 f'_{m,core} \quad (5)$$

If all the available data are considered for the chord Young's modulus, a negative coefficient of determination is obtained, which denotes the absence of a correlation (red line in Figure 79b). This outcome is mainly governed by the data on CS masonry core, which are outliers with respect to the rest of the data. Consequently, it can be concluded that the relationship obtained for the chord Young's modulus depends on the masonry type. By analysing only the data of clay brick masonry, a good correlation ( $R^2 = 0.76$ ) in terms of chord Young's modulus is found. The following formulation is proposed for the evaluation of the chord Young's modulus from tests on clay brick masonry cores:

$$E_3 = 1.4 E_{3,core} \text{ for clay brick masonry} \quad (6)$$

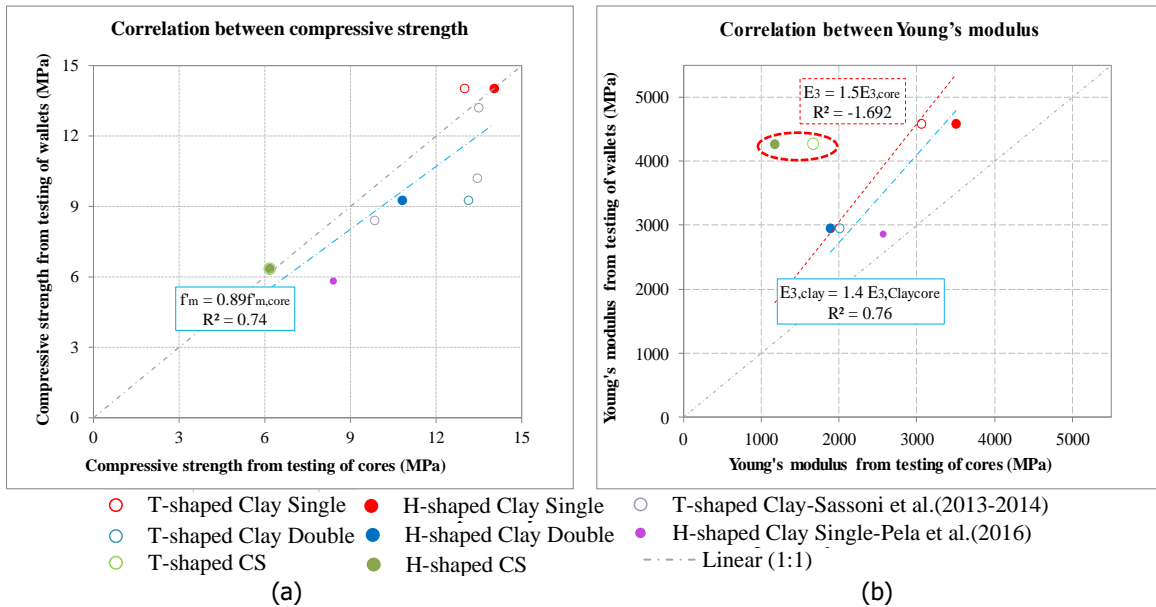


Figure 79 – Analysis of compression properties: (a) compressive strength; (b) chord Young's modulus.

Figure 80 shows the correlation between the tests on core and the tests on triplets in terms of the initial shear strength and the coefficient of friction. The failure envelope accordingly to the Coulomb friction criterion is derived considering the regression line approximating all the results (blue line), as suggested by Pelà et al. [30], and the regression line fitting the average value obtained for each inclination (green line), as suggested by Mazzotti et al. [29]. The best approximation for the initial shear strength is obtained by considering the regression line approximating all the results. On the contrary, considering the regression line fitting the average value obtained for each inclination a better approximation of the coefficient of friction can be provided. It can be concluded that the following formulation can be adopted to evaluate the initial shear properties of masonry:

$$f_{v0} = 0.98 f_{v0,core} \quad (\text{based on all the results}) \quad (7)$$

$$\mu = 0.94 \mu_{core} \quad (\text{based on average results for inclination}) \quad (8)$$

It should be noted that these formulation approximate the experimental results with a coefficient of determination ( $R^2$ ) equal to 0.66 and 0.44 for the initial shear strength and the coefficient of friction, respectively. To increase the accuracy of these formulations, additional testing results are required.

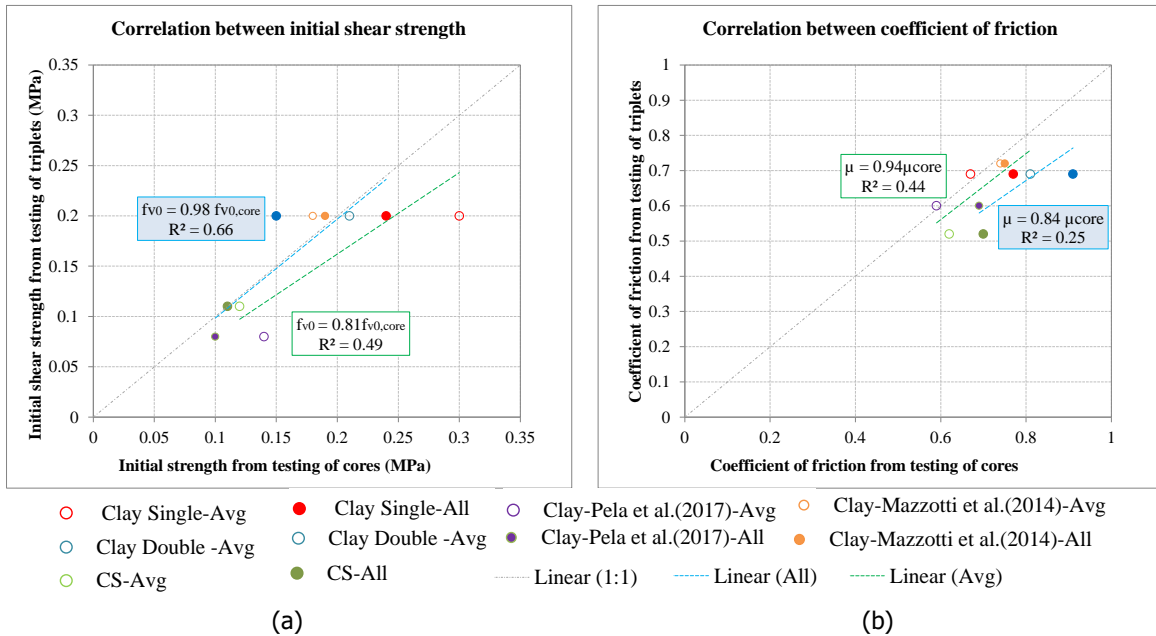


Figure 80 – Analysis of shear properties: (a) initial shear strength; (b) initial coefficient of friction.



## 18 Conclusions

The suitability of using cores for assessing the compression and shear properties of masonry was investigated by few authors. It was concluded that tests on the masonry cores seem promising, since an acceptable correspondence between the results of cores samples and those results obtained from standardised tests on the companion samples was reported in the literature.

In order to provide a quick and efficient testing method for in-situ investigation, the core method was investigated in the testing program developed at TU Delft in 2016/2017. Compression and splitting tests on the masonry cores were carried out on single wythe clay brick masonry, double wythe clay brick masonry and calcium silicate brick masonry. The outcomes of the tests on the cores were compared with the experimental results obtained from standardized destructive tests on companion specimens. The masonry cores were extracted perpendicular to the surface of replicated masonry walls built in controlled laboratory environment. Moreover, a sampling strategy to extract the cores was specifically defined aiming to investigate the possible spatial variability of the masonry properties across the height of the wall.

The suitability of using small diameter cores, both cores with 100 mm in diameter (T-shaped) and 150 mm in diameter (H-shaped), for assessing the compression properties of masonry are investigated in the current document. Prior to testing, the masonry cores were completed with high-strength mortar aiming to uniformly distribute the axial load and to prevent any possible stress concentration that might be raised due to uneven faces loaded. Having the advantage of using a displacement-controlled set-up, the post-peak behaviour of masonry was recorded. The compressive strength, Young's modulus, Poisson ratio and the fracture energy are evaluated. For each masonry type, between 3 to 6 specimens were tested for both sizes. The applicability of the core technique to evaluate the compression properties of masonry is validated by comparing the obtained results with the results of standardised tests on the companion samples. In view of the results achieved in the current study, it is possible to draw the following conclusions:

- It is suggested to evaluate the compressive properties from tests on core by considering the loaded cross-sectional area in agreement with the failure mode. The failure mode can be evaluated in the pre-peak phase. If vertical cracks start at the sides of the regularisation cap, then the cross-sectional area of the cap should be considered as loaded area. If vertical cracks occurred within the entire section of the masonry, then the cross-sectional area of the core should be considered as loaded area. More information are necessary to identify the cause for the different failure modes; however it is reasonable to assume that this difference is governed by the ratio between the stiffness of the masonry and the stiffness of the capping material. Consequently, in experimental parametric investigation is suggested.
- Both T-shaped core with a diameter of 100 mm and H-shaped core with a diameter of 150 mm can be used to obtain the compressive properties of masonry.
- The compressive strength of masonry obtained by tests on core resulted independently on the masonry type and the size of the core. The compressive strength of masonry can be evaluated as 0.89 times the compressive strength obtained by tests on masonry cores ( $R^2 = 0.74$ ).
- The relationship between the chord Young's modulus obtained from tests on core and companion samples depends on the masonry type. The chord Young's modulus of clay brick masonry can be evaluated as 1.4 times the chord Young's modulus obtained by tests on masonry cores ( $R^2 = 0.76$ ). To extrapolate the same formulation for the CS brick masonry, it is recommended to perform more tests on more CS brick masonry objects.
- The fracture energy in compression was calculated for the tests on core. However, high variability was observed in the comparison with the value obtained by tests on wallets (ratio varies between 0.5 and 1.3) indicating a poor correlation. This can be influenced by the cracking observed in the cap during the test.
- The variability of the compression properties was not correlated to the location of extraction for the tested specimens. It should be noted that these results have been obtained for core extracted by replicated masonry walls built in controlled environmental conditions.
- The results obtained in this study are based on a limited number of tests. To improve the correlation with standard destructive tests in terms of compressive properties additional studies are suggested.

The suitability of using small diameter core with one central bed joint (100 mm in diameter) to assess the shear properties of the brick-mortar interface is investigated in the current document. The splitting load was applied while the masonry cores were rotated with respect to the original position. The masonry cores were tested at mortar layer inclination of 40°, 45°, 50° and 55°. For each inclination 3 to 5 tests were performed. The initial shear strength and coefficient of friction can be derived considering the regression line accordingly to the Coulomb friction criterion by plotting the shear strength versus compression stress and, subsequently performing a linear regression line. The estimation of the regression line can be provided as follows: 1) approximating all the results as suggested by Pelà et al. [30] and 2) using the regression line fitting the average value obtained for each inclination, as suggested by Mazzotti et al. [29]. Comparing the shear properties of the brick-mortar interface found from core testing with those of the triplets, the following conclusions could be drawn:

- The best approximation of the initial shear strength is obtained by considering the regression line approximating all the results. The initial shear strength of the brick-mortar interface obtained by triplet tests can be evaluated as 0.98 times of the one obtained by test on cores ( $R^2 = 0.66$ ), independently from the masonry types.
- The best approximation of the coefficient of friction is obtained by considering the regression line fitting the average value obtained for each inclination. The coefficient of friction of the brick-mortar interface of masonry can be obtained by triplet tests can be evaluated as 0.94 times of the one obtained by test on cores ( $R^2 = 0.44$ ), independently from the masonry types.
- The accuracy of the proposed formulation in the current study can be improved upon performing more tests on the different masonry types.
- The variability of the maximum shear stress was not correlated to the location of extraction for the tested specimens. It should be noted that these results have been obtained for core extracted by replicated masonry walls built in controlled environmental conditions.
- The results obtained in this study are based on a limited number of tests and to improve the correlation with standard destructive tests in terms of shear properties additional studies are suggested.

## References

- [15] ASTM C 1197-04. Standard test method for in-situ measurement of masonry deformability properties using the flat jack method. 2004.
- [16] ASTM C 1531-03. Standard Test Method for in situ measurement of masonry mortar joint shear strength index. 2004.
- [17] EN 1052-1. Method of test masonry – Part 1: Determination of compressive strength. Nederlands Normalisatie-instituut (NEN), 1998.
- [18] EN 1052-3: Method of test masonry – Part 3: Determination of initial shear strength. Nederlands Normalisatie-instituut (NEN), 2002.
- [19] Jafari, S., Esposito, R. tests on masonry cores: Background document and testing protocol. Delft University of Technology. Report number C31B67WP1-5, version 01, 19 July 2016.
- [20] EN 1996-1-1+A1 (2013). Eurocode 6 – Design of masonry structures – Part 1-1: General rules for reinforced and unreinforced masonry structures. Nederlands Normalisatie-instituut (NEN).
- [21] Jafari S, Esposito R, Rots JG, (2017). Literature review on the assessment of masonry properties by tests on cores samples. Proceedings of the 4th WTA International PhD Symposium, 14-16 September; Delft, The Netherlands.
- [22] Brencich A, Sterpi E. Compressive strength of solid clay brick masonry: calibration of experimental tests and theoretical issues. Structural Analysis of Historical Constructions. 2006.
- [23] Ispir M, Demir C, Ilki A, Kumbasar N. Material characterization of the historical unreinforced masonry Akaretler Row Houses in Istanbul. Materials in civil engineering. 2010;22 (7):702-13.
- [24] Pelà L, Canella E, Aprile A, Roca P. Compression test of masonry core samples extracted from existing brickwork. Construction and Building Materials. 2016.
- [25] Sassoni E, Mazzotti C. The use of small cores for assessing the compressive strength of clay brick masonries. Cultural Heritage. 2013;14(3): e95-e101
- [26] Sassoni E, Mazzotti C, Pagliai G. Comparison between experimental methods for evaluating the compressive strength of existing masonry buildings. Construction and Building Materials. 2014;68:206-19.
- [27] UIC – International Union of Railways: UIC 778-3R. Recommendations for the assessment of the load carrying capacity of the existing masonry and mass-concrete arch bridges. Paris: UIC; 1995.
- [28] Benedetti A, Pelà L, editors. Experimental characterization of mortar by testing on small specimens. 15th IB2MaC: developing the future of masonry; 2012: IB2MaC.
- [29] Mazzotti C, Sassoni E, Pagliai G. Determination of shear strength of historic masonries by moderately destructive testing of masonry cores. Construction and Building Materials. 2014;54:421-31.
- [30] Pelà L, Kasioumi K, Roca P. Experimental evaluation of the shear strength of aerial lime mortar brickwork by standard tests on triplets and non-standard tests on core samples. Engineering Structures. 2017;136:441-53.
- [31] Protocol for the construction of masonry, ver. 18-03-2015
- [32] EN 1015-11 (1999). Method of test for mortar for masonry – Part 11: Determination of flexural strength of hardened mortar. Nederlands Normalisatie-instituut (NEN).
- [33] EN 772-1 (2000). Methods of test for masonry units - Part 1: Determination of compressive strength. Nederlands Normalisatie-instituut (NEN).
- [34] NEN 6790 (2005). Technical principles for building structures - TGB 1990 - Masonry structures - Basic requirements and calculation methods. Nederlands Normalisatie-instituut (NEN).
- [35] Van Mier, J.G.M. (1984) Strain Softening of concrete under multiaxial loading conditions, PhD thesis, Eindhoven University of Technology.
- [36] Lourenco, P.B., De Borst, R. and Rots, J.G. (1997). A plane stress softening plasticity model for orthotropic materials. International Journal for Numerical Methods in Engineering 40(21), 4033-4057.
- [37] Jafari, S., Esposito, R. Material tests for the characterisation of replicated solid clay brick masonry. Delft University of Technology. Final report 16 August 2017.
- [38] Jafari, S., Esposito, R. Material tests for the characterisation of replicated calcium silicate brick masonry. Delft University of Technology. Final report 14 November 2016.
- [39] Li J, Stewart MG, Masia MJ et al. (2016) Spatial correlation of material properties and structural strength of masonry in horizontal bending. Journal of Structural Engineering.
- [40] EN 13412 (2002). Products and systems for the protection and repair of concrete structures - Test methods - Determination of modulus of elasticity in compression (NEN).

## Appendix A

This appendix reports the declaration of performance for the construction materials used to build the masonry wall.

Table A. 3 - Declaration of performance of calcium silicate bricks.


Wanddikte in mm	Type steen	Afmetingen (BxHxL) mm	Gewicht per stuk in kg	Druksterkte N/mm <sup>2</sup>	Aantal per m <sup>2</sup> (incl. voeg)	Kg Metselfix per m <sup>2</sup> excl. morsverlies
55 (klamp)	Waalformaat	102x55x214	2	16	39,9	12,3
72 (klamp)	Amstelformaat	102x72x214	3	16	39,9	16,1
82 (klamp)	Maasformaat	102x82x214	3	16	39,9	18,4
102	Waalformaat	102x55x214	2	16	68,7	33,7
102	Amstelformaat	102x72x214	3	16	54,4	28,3
102	Maasformaat	102x82x214	3	16	48,5	26,1
150	Dubbel amstelformaat	150x72x214	4	16	54,4	42,5
150	Dubbel maasformaat	150x82x214	5	16	48,5	39,2

Table A. 4 - Declaration of performance for calcium silicate masonry mortar.

1. Unieke identificatie	Sakrete Brickfix	Nr. RV001 – 2013-11-05
2. Aanduiding	M5 type G (voor algemene toepassing) conform NEN-EN 998-2: 2010	
3. Toepassing	Metselmortel voor binnen- en buitentoepassing	
4. Naam en contactadres fabrikant	Remix Droge Mortel BV Hoofdstraat 41 NL-9531 AB Borger Postbus 3 NL-9530 AA Borger	
5. Naam en contactadres gemachtigde	geen	
6. Systeem voor de beoordeling en verificatie van de prestatiebestendigheid	systeem 2+	
7. Activiteit van de aangemelde certificatie-instantie zoals vereist in de geharmoniseerde norm	De aangemelde certificatie-instantie Kiwa BMC B.V. (identificatienummer 0620) heeft onder systeem 2+ de initiële inspectie van de productie-installatie en van de productiecontrole in de fabriek uitgevoerd en zal tevens de permanente bewaking, beoordeling en evaluatie van de productiecontrole op zich nemen. Op basis daarvan is het conformiteitscertificaat voor de productiecontrole in de fabriek verstrekt.	
8. Europese Technische beoordeling	niet van toepassing	
9. Aangegeven prestaties		
<b>Essentiële kenmerken (NEN-EN 998-2)</b>	<b>Prestaties</b>	<b>Europees beoordelingsdocument</b>
5.4.1 druksterkte	M5	NEN-EN 998-2:2010
5.4.2 Hechtsterkte (kruisproef)	$\geq 0,3 \text{ N/mm}^2$ (tabelwaarde)	
5.2.2 chloridegehalte	$< 0,1 \text{ M.-%}$	
5.6 brandklasse	A1	
5.3.3 waterabsorptie	$\leq 0,40 \text{ kg/(m}^2 \cdot \text{min}^{0,5})$	
5.4.4 waterdampdoorlaatbaarheid	15/35 (tabelwaarde)	
5.4.6 warmtegeleidbaarheid	$\leq 0,82 \text{ W/(m} \cdot \text{K)}$ P = 50% $\leq 0,89 \text{ W/(m} \cdot \text{K)}$ P = 90% (tabelwaarden)	
5.4.7 duurzaamheid	NPD	
vrijkomende gevaarlijke bestanddelen	NPD	
<p>10. De prestaties van het in de punten 1 en 2 omschreven product zijn conform de in punt 9 aangegeven prestaties. Deze prestatieverklaring wordt verstrekt onder de exclusieve verantwoordelijkheid van de in punt 4 vermelde fabrikant.</p> <p>Borger, 5 November 2013</p> <p style="text-align: right;">Getekend: AGAR Holding BV</p> <div style="text-align: right;">               Mr. R.M.P.P. Reef              Algemeen directeur         </div> <div style="text-align: left;">              Remix Droge Mortel BV is een              werkmaatschappij van Agar Holding BV.         </div>		




Table A. 5 - Declaration of performance of clay bricks.



### Euroa VB WF

Euroa is een vormbak-sortering van Wienerberger Erlecom. Deze sortering is leverbaar in WF (exacte maten volgens fabrieksopgave). De precieze kleur van de steen kan afwijken van de getoonde afbeelding. Terca gevelbakstenen: kwalitatief hoogwaardige gevelbakstenen die bijdragen aan het creëren van een prettige, mooie en duurzame leefomgeving.

 [Bestel monster](#)

☐ Dit product selecteren voor vergelijking

#### Technische informatie ×

Gemiddelde maat	+/- 211 x 101 x 50 mm
Maattolerantie	T2
Maatspreiding	R1
Gemiddelde druksterkte $\geq$ (N/mm <sup>2</sup> )	35
Klasse vorstbestendigheid	F2 [D]
Initiële wateropzuigingscategorie	IW3 (normaal zuigend)
Bruto droge volumieke massa (kg/m <sup>3</sup> )	1700
Vrijwillige wateropneming (Massa %)	20
Keurmerk	KOMO kwaliteitsverklaring en NL BSB productcertificaat
Toepassingsvoorwaarden	Dient te worden verwerkt overeenkomstig de geldende richtlijnen van Wienerberger.

Table A. 6 - Composition of clay brick masonry mortar.

Raw material	Unit	Quantity
Cement CEM1 42.5R	kg	60
Limestone filler 0.09 mm	kg	40
Hydrated lime CL80S	kg	90
Sand (0.00-1.20 mm)	kg	630
Sand (1.20-3.55 mm)	kg	180
air entrained	kg	0.05

## Appendix B

### Evaluation of properties of capping material

In the previous studies, the masonry sample was completed prior to compression tests by using the high-strength mortar. The compression and bending properties of the capping material is characterised in this section. The compressive strength, Young's modulus and the flexural strength are found from testing of mortar samples collected and cast during the preparation of the samples.

#### Preparation of bars

The mortar bars have a length of  $l_m = 160$  mm, a height of  $h_m = 40$  mm and thickness of  $t_m = 40$  mm. The mortar was prepared with fixed water content per bag of mix (20 kg): 2.5 l/bag.

Cement and water have been mixed together continuously with a mixing machine for 3 minutes, as shown in Figure 81. The mould was filled in two approximately equal layers, each layer being compacted by 25 strokes of the tamper. Subsequently, the mortar surface was levelled. The mortar samples were kept in a laboratory-controlled environment. The tests were performed after at least 3, 7, 10 and 28 days from the construction day.



(a)



(b)

Figure 81 – Preparation of capping material.

#### Testing procedure

The secant modulus of the mortar bars has been determined following the prescriptions of NEN-EN 13412 [40]. A mortar bar was subjected to cyclic compressive load while it was tested in the linear elastic phase. The mortar bar is instrumented with four LVDT placed on each face of the sample, as shown in Figure 82. The secant modulus is evaluated between 1/10 and 1/3 of the maximum stress.

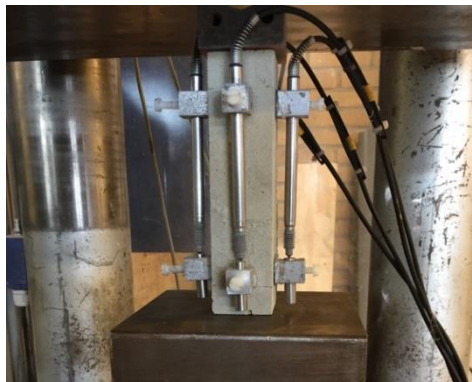


Figure 82 - Cyclic compression test on mortar bar.



The flexural strength was determined by three-point bending test (Figure 83a). The test set-up is composed by two steel bearing rollers having a diameter of  $10 \pm 0.5$  mm and spaced  $d_l = 100 \pm 0.5$  mm. A third roller is centrally placed on top of the sample to apply the load. The load was applied at a constant rate of 50 N/s so that failure occurred within a period of 30 to 90 s.

The compression test was performed on the broken pieces obtained from the flexural test, which have at least a length of 40 mm. The specimen is placed between two steel plates with a length of  $l_p = 40$  mm. For the interpretation of the results the specimen is considered to be 40x40x40-mm (Figure 83b). The load was applied at a constant rate of 1.5 kN/s so that failure occurred within a period of 30 to 90 s.

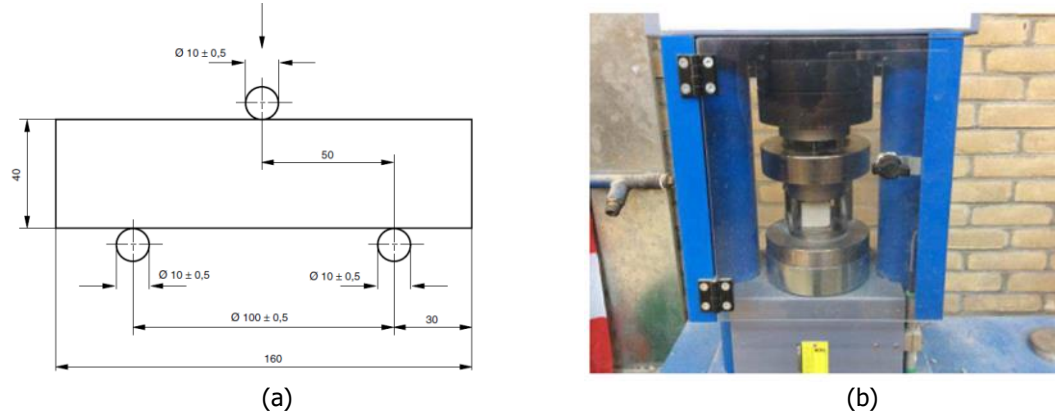


Figure 83 - Test on mortar specimens: (a) three-point bending test; (b) compression test.

## Experimental results

The flexural strength  $f_{mt}$  of the mortar bar was calculated as:

$$f_{mt} = \frac{3 F_{max} d_l}{2 t_m h_m^2} \quad (9)$$

where  $F_{max}$  is the maximum load,  $d_l$  is the distance between the supports ( $100 \text{ mm} \pm 0.5 \text{ mm}$ ),  $h_m$  is the height of the mortar specimen (40 mm) and  $t_m$  is the thickness of the mortar specimen (40 mm).

The compressive strength  $f_m$  of the mortar was calculated as [32]:

$$f_m = \frac{F_{max}}{t_m l_p} \quad (10)$$

where  $F_{max}$  is the maximum load,  $t_m$  is the thickness of the mortar specimen (40 mm) and  $l_p$  is the length of the loading plate (40 mm).

A summary of the results of tests on the mortar bars used for the capping is listed in Table 52.

Table 52 – Compression and flexural properties of mortar bars used for capping.

Day	Compressive strength $f_m$			Flexural strength $f_{mt}$			Young's modulus $E_m$		
	Mean	St.dev.	C.o.V.	Mean	St.dev.	C.o.V.	Mean	St.dev.	C.o.V.
	(MPa)	(MPa)	-	(MPa)	(MPa)	-	(MPa)	(MPa)	-
3	60.58	1.06	0.018	4.28	0.35	0.082	33979	2904	0.085
7	58.67	0.94	0.016	5.33	0.18	0.034	36969	1587	0.043
10	63.35	1.64	0.026	5.54	0.34	0.061	37721	1209	0.032
28	63.26	1.13	0.018	5.57	0.37	0.066	34778	363	0.010